

Mean field and beyond in α -decay chains of superheavy elements^{B+G}

P.-G. Reinhard¹, P. Fleischer¹, M. Bender²,

¹ Institut für Theoretische Physik, Universität Erlangen, Staudtstr. 7, D-91058 Erlangen

² Gesellschaft für Schwerionenforschung, Planckstr. 1, D-64291 Darmstadt

Recent experiments at GSI [1] and JINR Dubna [2] brought evidence for the synthesis of new superheavy elements. One of the key observable in these experiments is the Q_α value along the α -decay chains. In this contribution, we want to investigate this observable within self-consistent mean-field models.

We consider two different models, the Skyrme-Hartree-Fock approach (SHF) and the relativistic mean-field model (RMF), for a most recent review see [3]. From the world of different parametrisations we confine the discussion to a few well adjusted, typical and recent sets. For SHF we consider the parametrisations SkP, SkI3, SkI4, and SLy6. The force SkP uses effective mass $m^*/m = 1$ and is designed to allow a self-consistent treatment of pairing. The other forces all have smaller effective masses around $m^*/m = 0.7-0.8$. The force SLy6 stem from an attempt to cover properties of pure neutron matter together with normal nuclear ground-state properties. The forces SkI3/4 employ a spin-orbit force with isovector freedom to simulate the relativistic spin-orbit structure. SkI3 contains a fixed isovector part exactly analogous to the RMF, whereas SkI4 is adjusted allowing free variation of the isovector spin-orbit force. The modified spin-orbit force has a strong effect on the spectral distribution in heavy nuclei and thus for the predictions of superheavy elements. For the RMF we consider the parametrisations NL-Z2 and NL3. The force NL-Z2 comes from fits much similar to those of SkI3 and SkI4. NL3 is fitted without looking at the electron-scattering formfactor but with taking more care about the isovector trends. We ought to remind here that these different parametrisations produce much different predictions for the magic shell closure in SHE [4, 5].

Fig. 1 compares calculated and experimental α energies for the new isotopes. Most models make similar predictions at the lower end of the chains and these agree

very nicely with the available new data for both chains. Larger differences among the forces show up when going to heavier systems. This is mainly due to differently pronounced shell closures which produce these curious kinks. Having a closer look on the deformation energies shows that one comes into a regime of very soft nuclei with pronounced shape isomerism. The mean-field state represents the one configuration at the absolute minimum of energy. But many other configurations are energetically competitive in soft nuclei. Thus one needs to consider a correlated ground state built from an appropriate coherent mixture of configurations. In practice, we superpose the states along the quadrupole deformation path using the generator-coordinate method [6]. The effect of such correlations is shown in Fig. 2. They wipe out the kinks and produce a smooth trend throughout. There is little correlation effect at the lower end of the chain such that the originally given good agreement with data is maintained. Moreover, correlations bring the predictions from the the various forces closer together again. The then remaining difference is a clear signal of different bulk properties deep within the models, yet to be worked out in detail.

To conclude, mean-field models provide a pertinent description for the Q_α values along the recently measured decay chains of superheavy elements. Correlations effects beyond mean field need to be taken into account for the heavier isotopes.

References

- [1] S. Hofmann *et al.*, GSI preprint 2000-52.
- [2] Yu. Oganessian *et al.*, Phys. Rev. C **62**, 41604 (2000).
- [3] P.-G. Reinhard *et al.*, Comm. Nucl. Part. Sci. (2001).
- [4] K. Rutz *et al.*, Phys. Rev. C **56**, 238 (1997).
- [5] M. Bender *et al.*, Phys. Rev. C **60**, 034304 (1999).
- [6] P.-G. Reinhard, *et al.*, RIKEN Review **26**, 23 (2000)

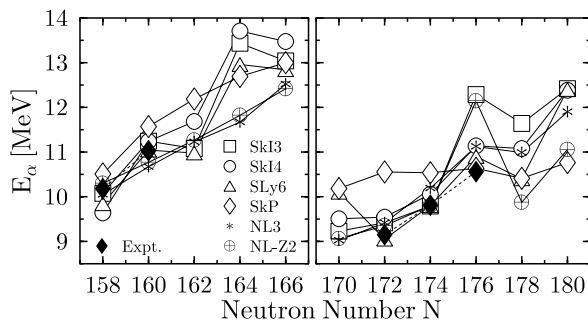


Figure 1: Ground-state-to-ground-state α energies for the α -decay chains containing $^{270}_{160}\text{110}$ (left panel) and $^{282}_{176}\text{116}$ (right panel) from mean-field calculations with the forces as indicated. Filled diamonds denote the experimental values.

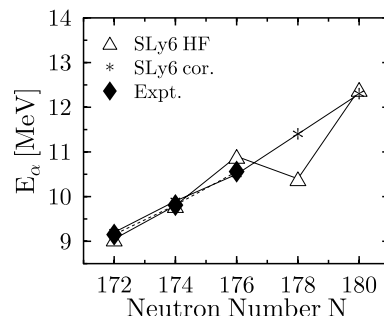


Figure 2: Ground-state-to-ground-state α energies for the decay chain containing $^{282}_{176}\text{116}$ computed with the force SLy6. Compared are calculations with and without taking ground-state correlations into account.

Shell stabilization in superheavy elements^{B+G}

M. Bender,¹ P.-G. Reinhard²

¹ Gesellschaft für Schwerionenforschung, Planckstr. 1, D-64291 Darmstadt

² Institut für Theoretische Physik, Universität Erlangen, Staudtstr. 7, D-91058 Erlangen

Superheavy elements (SHE) are by definition those very heavy nuclei which have a negligible liquid-drop fission barrier. Quantum mechanical shell effects create one or several minima in the potential energy surface which stabilize the nucleus against fission. This additional binding from shell effects is quantified by the shell correction energy which is thus a first hint on the fission stability.

The shell correction energy can be computed by comparing the actual discrete distribution of single-particle energies with a smoothened level density. The weakly-bound SHE require a careful treatment of the continuum which we perform according to the recipe of [1]. Fig. 1 shows the shell correction energies from fully self-consistent calculations with the Skyrme interactions SkI3 and SLy6 and the relativistic mean-field interactions NL3 and NL-Z2. Remind that the shell correction is always sharply peaked at shell closures for nuclei up to Pb. This changes when going to SHE. There emerges a broad island of shell stabilization which spreads around the shell closures predicted by the various forces. Similar pattern are found in macroscopic-microscopic models. As a consequence, the significant differences seen in the prediction of magic numbers when looking at the δ_{2q} [2] are much mellowed by the generally softer pattern of the shell energy which looks similar for all models investigated in [3]. The reason for this behaviour is an accumulation of states with low angular momentum at the Fermi surface for these SHE. On one hand, this causes the fast changes of the various shell closures by small shifts of individual levels [4]. On the other hand, this turns the shell effect of individual levels into the shell effect of a bunch of levels more independent on the subtle details of actual shell closures.

Spherical shell corrections are, of course, a first indicator only for the stability of SHE. What finally counts is the fission barrier. And fission can go unusual paths in SHE.

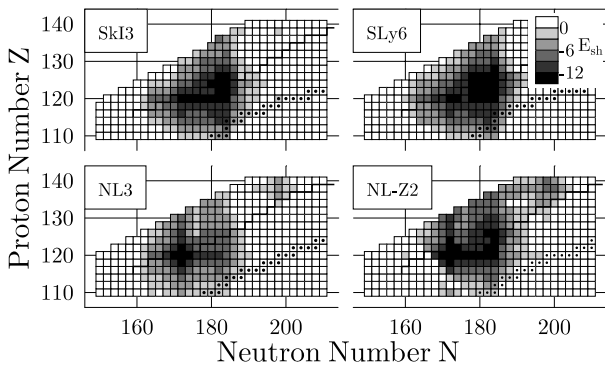


Figure 1: Total shell correction for spherical configurations of superheavy nuclei extracted from self-consistent calculations with the effective interactions as indicated. The (calculated) two-proton drip line and the valley of stability are emphasized. Data taken from [3].

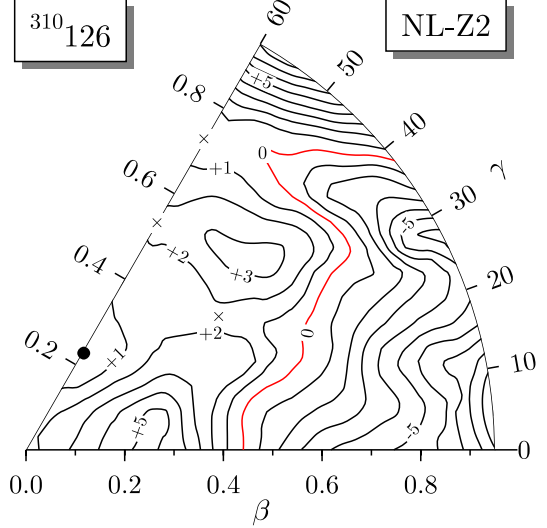


Figure 2: Potential energy surface of $^{310}_{184}126$ in the β - γ plane calculated with the relativistic mean-field interaction NL-Z2. The filled circle denotes the oblate minimum, while crosses denote the various saddle points. Deformation energies in MeV are with respect to the oblate ground state.

Fig. 2 shows as an example the potential energy landscape of $^{310}_{184}126$ in the full triaxial plane. In spite of the huge shell correction of more than -12 MeV at spherical shape the actual ground state of $^{310}_{184}126$ is oblate when calculated with NL-Z2. Triaxial configurations reduce the axial prolate barrier of more than 5 MeV to 1.8 MeV. The result has to be taken with precaution because these detailed fission pattern seem to depend sensitively on the actual nucleus and force used. $^{292}_{172}120$ has spherical shape and a triaxial barrier of nearly 6 MeV when calculated with the same force. Skyrme interactions give a similar potential landscape in $^{310}_{184}126$ but with a spherical ground state and substantially higher barriers around 9 MeV, see [5]. This systematic difference in fission barrier heights when comparing Skyrme interactions and relativistic mean field has already been seen in [6] and still needs to be understood. Fig. 2 demonstrates, however, that one has to be aware of surprises in this region of nuclei and that there is still a bulk of work ahead to uncover all these features.

References

- [1] A. T. Kruppa *et al.*, Phys. Rev. C **61**, 034313 (2000).
- [2] K. Rutz *et al.*, Phys. Rev. C **56**, 238 (1997).
- [3] M. Bender, W. Nazarewicz, P.-G. Reinhard, in preparation.
- [4] M. Bender *et al.*, Phys. Rev. C **60**, 034304 (1999).
- [5] S. Ówiok *et al.*, Nucl. Phys. **A611**, 211 (1996).
- [6] M. Bender *et al.*, Phys. Rev. C **58**, 2126 (1998).

Proton shell closures in proton-rich heavy nuclei

T. Cornelius¹, M. Bender², T. Bürvenich¹, L. Kudling¹, A. Sulaksono¹,
P.-G. Reinhard³, J. A. Maruhn¹, W. Greiner¹

¹ Institut für Theoretische Physik, Universität Frankfurt, Robert-Mayer-Str. 8–10, D–60325 Frankfurt am Main

² Gesellschaft für Schwerionenforschung, Planckstr. 1, D–64291 Darmstadt

³ Institut für Theoretische Physik, Universität Erlangen, Staudtstr. 7, D–91058 Erlangen

Magic numbers are a key feature of any finite Fermion system as they provide crucial clues on the underlying mean field. The study of shell closures is thus very interesting in exotic nuclei. One wants to know how the shell closures develop when moving towards the driplines. It is now well-established for neutron-rich $N=20$ and $N=28$ isotones that the neutron shells fade away. This gives rise to a transient regime of pronounced low-lying collective states and finally to stable ground-state deformation [1]. There are hints from the systematics of 2^+ and 4^+ excitation energies in Cd and Pd isotopes that also the $N=50$ and $N=82$ shells are weakened when going towards neutron-rich nuclei [2]. All these examples concern a weakening of neutron shells. The situation seems to be different for protons. For light nuclei there is no indication that the proton shell closures fade away towards the proton drip line. But the analysis of recent mass measurements [3] shows a substantial weakening of the two-proton shell gap

$$\delta_{2p}(Z, N) = E(Z-2, N) - 2E(Z, N) + E(Z+2, N)$$

for very proton-rich Pb isotopes. It is speculated whether this is related to a weakening of the $Z=82$ shell [4]. This contribution looks at this problem from a theoretical perspective.

As tool we take self-consistent mean-field models which are nowadays well developed and provide a pertinent picture of the nuclear properties throughout the whole mass table. We consider two different models, the Skyrme-

Hartree-Fock approach (SHF) and the relativistic mean-field model (RMF). We take one typical parametrisation for each model, SkI3 for the SHF and NL3 for the RMF, see e.g. [5]. SHF as well as RMF produce single-proton spectra in Pb with a well developed magic gap at $Z=82$ for all isotopes up to the dripline. This is confirmed by the systematics of the shell-correction energies extracted from self-consistent calculations [6]. The δ_{2p} are presented in Fig. 1. The upper panel shows δ_{2p} for spherical calculations in Pb as well as in its $Z\pm 2$ neighbours Po and Hg. The theoretical results give an almost constantly large δ_{2p} along the whole isotopic chain, in compliance with the large spectral gap and shell-correction energy. But the results for δ_{2p} are clearly at variance with the data. This changes dramatically when allowing for ground-state deformation, see the lower panel. While the ground states of Pb isotopes stay spherical, the ground states of proton-rich Hg and Po isotopes become deformed. They thus gain energy which significantly reduces the extremely sensitive double difference δ_{2p} . The findings are consistent with the currently available data which confirm deformation softness in these heavy proton-rich isotopes, see e.g. [7] and references therein. Important for our purpose is: (i) $^{180-190}\text{Hg}$ have oblate deformed ground states, (ii) data on excitation spectra and charge radii for Pb isotopes are consistent with spherical ground states, and (iii) proton-rich Po isotopes show an increased collectivity.

In summary the observed weakening of δ_{2p} around $Z=82$ is caused by the increased collectivity of the Hg and Po isotopes, and not by a quenching of the $Z=82$ shell. Large values of δ_{2p} are a sufficient, but not a necessary indicator for a shell closure. This example shows that a thorough analysis of magic shells requires a simultaneous consideration of various signals, e.g. the δ_{2p} together with energy and strength of low-lying 2^+ and 4^+ states, possibly complemented by α -decay hindrance factors [8]. True proton-shell quenching, however, is expected for the next magic proton number in the realm of superheavy elements [9].

References

- [1] S. Pèru *et al.*, Eur. Phys. J. **A9**, 35 (2000).
- [2] T. Kautzsch *et al.*, Eur. Phys. J. **A9**, 201 (2000).
- [3] T. Radon *et al.*, Nucl. Phys. **A677**, 75 (2000).
- [4] Yu. N. Novikov *et al.*, submitted to Nucl. Phys. A.
- [5] P.-G. Reinhard *et al.*, Comm. Nuc. Part. Sci. (2001)
- [6] M. Bender *et al.*, in preparation.
- [7] K. Heyde *et al.*, Phys. Rev. **C53**, 1035 (1996).
- [8] J. Wauters *et al.*, Phys. Rev. Lett. **72**, 1329 (1994).
- [9] M. Bender *et al.*, Phys. Rev. C **60**, 034304 (1999).

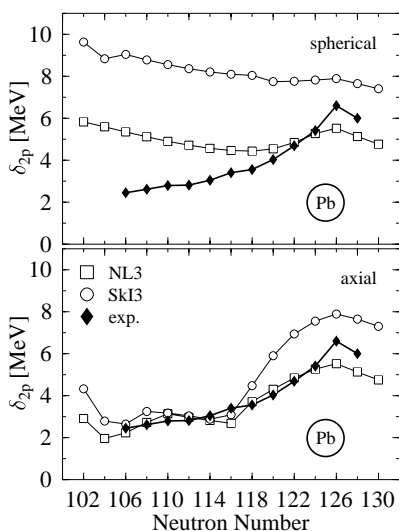


Figure 1: Two-proton shell gap δ_{2p} for Pb isotopes calculated with SHF (force SkI3) and RMF (force NL3) and compared with experimental data. Upper panel: from spherical configurations of all nuclei. Lower panel: allowing for ground-state deformations.

Microscopic Description of Charge and Matter Distributions of Long-Tailed and Halo Nuclei

M. Tomaselli^{a,b}, T. Kühl^{b,c}, P. Egelhof^{b,c}, C. Kozhuharov^b, D. Marx^b, A. Dax^b, S.R. Neumaier^b, W. Nörtershäuser^{b,d}, M. Mütterer^a, H. Wang^{b,e}, H.-J. Kluge^b, and S. Fritzsche^f

^a Darmstadt University, ^b GSI Darmstadt, ^c Mainz University, ^d Tübingen University,

^e Tokyo University, ^f Kassel University

Elastic proton-scattering experiments in inverse kinematics recently performed at GSI [1] have reopened important, partially unresolved questions concerning the physics of the halo nucleus ^{11}Li . In order to obtain a deeper insight into the halo structure of light exotic nuclei and to understand the difference between the matter and the charge distributions, microscopic calculations for the ground states of the $^{6,7,9,11}\text{Li}$ and $^{7,9}\text{Be}$ isotopes have been performed within the Dynamic-Correlation Model (DCM) [2].

The DCM describes the ground states of nuclei in terms of interacting clusters: valence particles and intrinsic vacuum states. The amplitudes of the mixed-mode wave-functions are derived in the framework of non-perturbative solutions of the Equation of Motion. Theoretically, the model spaces for the ground states of the $^{6,7,9,11}\text{Li}$ and the $^{7,9}\text{Be}$ isotopes are constructed by allowing valence particles to be scattered to higher configuration states ($2\hbar\omega$) and to interact with the core intrinsic states formed by exciting particles from the s, p -shell. The single-particle states used as input in the DCM have been approximated by harmonic oscillators with a state-dependent range introduced to reproduce the single-particle radii as calculated in a Wood-Saxon potential well. The single-particle energies are also obtained in this procedure. The two-body matrix elements are the same as used in Ref. [2].

The matter and charge distributions calculated with this microscopic approach can be used to predict experimentally accessible quantities. In this report we present and discuss the matter distributions for the lithium isotopes $^{7,9,11}\text{Li}$. Root-mean-square matter and charge radii obtained for the above mentioned beryllium isotopes are also given.

The DCM matter distributions for the lithium isotopes are presented in Fig. 1. The oscillations in the theoretical matter distribution result from the interferences of the

valence and the intrinsic states. For ^{11}Li two matter distributions are shown. The dotted line has been obtained by taking the three neutrons in the p -shell into account, while the solid line considers the effect of the neutrons moving in the p, s , and d shells and interacting with the vacuum states. It is obvious that the s and d neutrons as well as the core excitations have a profound influence on the halo structure [4]. While there are experimental values for the matter radii of all accessible lithium and beryllium isotopes [5], the charge radii are only known for the stable isotopes [5, 6]. Experimental and theoretical values are in good agreement. However, for a better understanding of the neutron halos influence on the core nucleus, it is desirable to determine the charge radii of the radioactive lithium isotopes experimentally, particularly for ^{11}Li . For this purpose an experiment is being prepared at GSI and ISOLDE, CERN [7] to determine this value by means of an optical isotope-shift measurement. The agreement of the calculated (rms) charge and matter radii for the lithium isotopes with experimental data [5] is good in all cases with the exception of the matter radius of ^{11}Li , which is considerably larger than the experimental value. For ^7Be and ^9Be the calculated radii (Tab.1) are close to the values of Ref. [5]. It should be mentioned that the experimental values for the matter distribution are model-dependent and that new proton-scattering data from GSI [3] indicate a larger matter radius than the one given previously in Ref. [5]. The matter distribution of ^{11}Li (solid line) and the calculated matter radius of 3.64 fm agree with the phenomenological distribution and with the radius of 3.65 fm given in Ref. [3].

Table 1: Rms-mass and -charge radii for beryllium isotopes

	$R_{\text{matter}}^{\text{calc.}}$	$R_{\text{charge}}^{\text{calc.}}$	$R_{\text{matter}}^{\text{exp.}}$ [5]	$R_{\text{charge}}^{\text{exp.}}$ [5]
^7Be	2.38 fm	2.39 fm	2.31(2) fm	? fm
^9Be	2.46 fm	2.62 fm	2.38(1) fm	2.47(1) fm

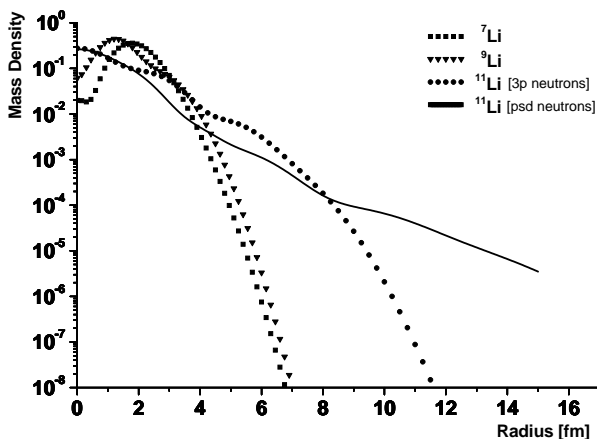


Fig. 1: Calculated mass distribution for $^{7,9,11}\text{Li}$. The halo structure of ^{11}Li is mainly associated to sd neutrons and to core excitations.

References

- [1] S.R. Neumaier et al., submitted to Nucl. Phys. A (2001); G.D. Alkhazov et al., Phys. Rev. Lett. 78, 2313 (1997)
- [2] M. Tomaselli et al., APAC 1999, Hyperfine Interactions 127, 95 (2000); Phys. Rev. C62 (2000), 67305
- [3] A.V. Dobrowolsky et al., GSI Report (1999) and Verhdlg. DPG 35, 5 (2000)
- [4] M. Tomaselli, C. Kozhuharov, and T. Kühl, 2001 in preparation
- [5] I. Tanihata et al., Phys. Lett. B 206, 592 (1988)
- [6] C.W. de Jaeger et al., At. Data, Nucl. Data Tables 14, 479 (1974)
- [7] A. Dax et al., CERN/INTC 2000-006 INTC/P118

Ground-State Structure based on Realistic NN-Potentials

H. Feldmeier, P. Krafft, T. Neff and R. Roth (GSI)

A long standing goal of theoretical nuclear physics is the description of nuclear structure starting from a realistic nucleon-nucleon potential. All realistic NN-interactions show however two characteristics that inhibit a treatment of the many-body problem in a mean-field model. Firstly, the local part of the interaction shows a strong short-range repulsion (the so called *core*) and, secondly, there is a strong tensor part. Both properties give rise to special correlations in the many-body state, which cannot be described by Slater determinants or a superposition of shell model states from a few major shells.

In the framework of the Unitary Correlation Operator Method (UCOM) [1] we describe both types of correlations explicitly by unitary transformations of shell model type many-body states. Thus we obtain states that contain the relevant correlations induced by the interaction between the nucleons.

To describe the short-range correlations caused by the repulsive core of the interaction the unitary correlation operator generates a radial distance-dependent shift in the relative coordinate of each pair of particles. By that the particles are shifted out of the repulsive region of the interaction. Alternatively the correlation operator can be used to transform the Hamilton operator with the bare interaction.

For the correlations induced by the tensor part of the interaction a similar procedure is applied. The new aspect is that tensor interactions correlate coordinate and spin space in a complex way. The unitary transformation, which describes these correlations, acts on the angular part of the relative coordinates in dependence on the spin orientation of the two particles.

As a preliminary step towards a full ab initio calculation on the basis of the central and tensor correlated Bonn-A potential [2] we use a parameterized correction to account for tensor correlations. The core-induced central correlations are fully included by a spin- and isospin-dependent correlation operator [1]. In order to account for tensor correlations we add to the

Bonn-A potential a correction in the $S = 1, T = 0$ channel. According to the structure expected for the tensor correlated interaction the correction consists of an additional attractive central potential and a repulsive momentum-dependent part. Three parameters (strength of local correction, and strength and range of momentum part) are adjusted to reproduce the experimental binding energies and charge radii of ^4He , ^{16}O , and ^{40}Ca .

Based on this correlated Bonn-A potential the many-body problem is treated in the framework of Fermionic Molecular Dynamics (FMD) [3]. The uncorrelated many-body state is described by a Slater determinant of gaussian one-body states, which contain the mean position, mean momentum, complex width and spin orientation as variational parameters. The ground-state wave function is determined by energy minimization with the correlated interaction.

The Figure shows the ground state one-body density distributions of ^{16}O , ^{20}Ne , and ^{24}Mg obtained with this method. For ^{16}O we find a spherical shell-model like distribution with a characteristic depletion of the central density. ^{20}Ne shows a prolate axially symmetric density distribution with α -like structures at the ends and a toroidal distribution in the central plane. Finally ^{24}Mg exhibits a complicated triaxial deformation with some remnants of α -clustering.

These calculations demonstrate the flexibility of the FMD basis as well as the possibility to perform nuclear structure calculations based on realistic NN-interactions in a nearly ab initio way. Our next step will be the inclusion of tensor correlations in a stringent way by calculating the appropriate unitary correlation operator explicitly.

[1] H. Feldmeier, T. Neff, R. Roth, J. Schnack; Nucl Phys. A632 (1998) 61.

[2] R. Machleidt; Adv. Nucl. Phys. 19 (1989) 189.

[3] H. Feldmeier, J. Schnack; Rev. Mod. Phys. 72 (2000) 655.

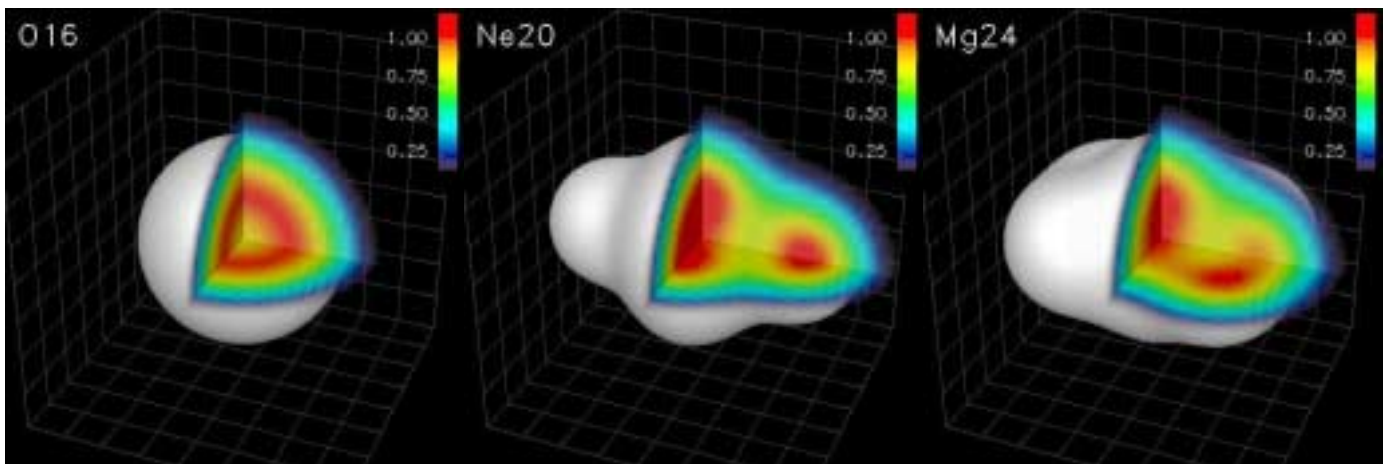


Figure 1: One-body density distributions (3-dimensional) of ^{16}O , ^{20}Ne , and ^{24}Mg . The white body shows the iso-density surface corresponding to half nuclear matter density ($\rho_0 = 0.17\text{fm}^{-3}$). The embedded planar cuts show the interior density distribution with color coding according to the color bar (in units of ρ_0). The mesh size of the background grid is $1\text{fm} \times 1\text{fm}$. Visit the FMD-Gallery at <http://www.gsi.de/~fmd/>.

Stability and instability of a hot and dilute nuclear droplet: adiabatic isoscalar modes

W. Nörenberg, G. Papp* and P. Rozmej†

The diabatic approach to dissipative large-amplitude collective motion [1] is reformulated in a local energy-density approximation. We consider a general displacement field, which is defined by an expansion of the displacement potential in terms of multipoles, and include Coulomb interactions. This expansion allows the analytical evaluation of collective mass and stiffness tensors within a consistent harmonic approximation. The set of eigenvalue equations couple modes with different number of nodes in the radial function of the displacement field. The orthogonal eigenmodes of the droplet are determined as function of the relaxation time τ for the decay of deformations of the local Fermi sphere, *i.e.* continuously from the adiabatic to the diabatic limit. Furthermore we consider also pure surface modes and compare the instability properties for soft and stiff equations of state.

In a first application the adiabatic ($\tau = 0$) isoscalar modes are studied and results for the eigenvalues of compressional (bulk) and pure surface modes are presented as function of density and temperature inside the droplet, as well as for different mass numbers and for soft and stiff equations of state [2]. We have studied these adiabatic isoscalar modes in detail, because they are related to thermodynamics and to many studies performed in the past.

The results on adiabatic isoscalar bulk instabilities are summarized as follows.

- As compared to infinite nuclear matter the spinodal region for compressional (bulk) instabilities shrinks to smaller densities and temperatures with $T_{crit} = 6$ MeV (8 MeV) for a soft (stiff) EOS. The observed fragmentation temperatures of about 5 MeV are consistent with spinodal decomposition after expansion. Typical values for the growth rates are $\gamma \approx 5$ MeV (10 MeV for a stiff EOS) corresponding to growth times $\hbar/\gamma \approx 40$ fm/c (20 fm/c).
- Effects from Coulomb interactions on the bulk instabilities are negligible.
- With decreasing density and temperature the modes with the lowest multiplicities and no radial node become unstable first.
- At densities below $0.3\rho_0$ (with $\rho_0 = 0.16$ fm $^{-3}$) the instability growth rates for different multiplicities ($l = 2, 3, 4, 5$) and number of nodes ($n = 0, 1, 2, 3$) are practically equal. This property can yield a power-law behavior $A^{-\sigma}$ with $\sigma \approx 2.0$ of the fragment-mass distribution in agreement with experimental observations and is not related to the critical point.

*Permanent address: HAS Research Group for Theoretical Physics, Eötvös University, Budapest, Pázmány P. s. 1/A, H-1117 Budapest, Hungary

†Permanent address: Institute of Mathematics, Technical University of Zielona Góra, ul. Podgórna 50, PL-65246 Zielona Góra, Poland

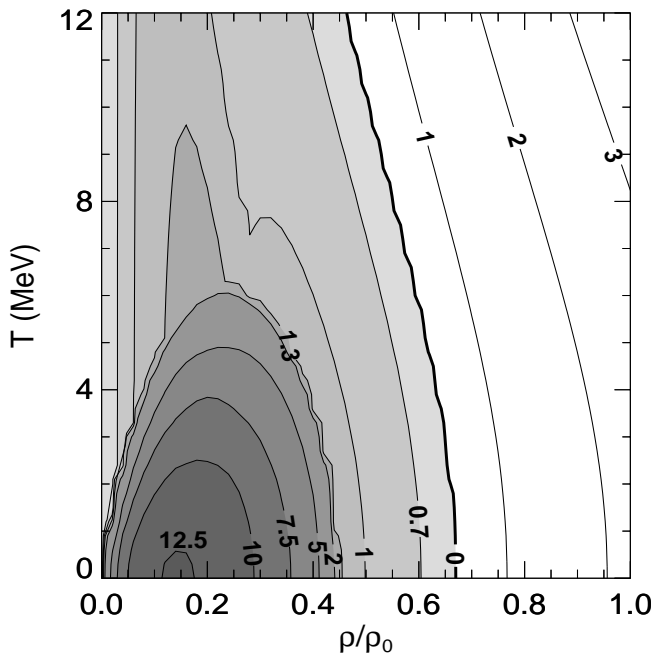


Figure 1: Combined bulk (below $T_{crit} = 6$ MeV) and surface instabilities for a gold-like droplet and a soft EOS. Shown are the largest growth rates (shaded areas) and the lowest vibrational energies (surface modes).

For finite nuclear droplets surface modes are important in addition to the compressional features. Indeed, pure surface modes show some interesting features.

- The instability region of pure surface modes extends to larger densities up to about the spinodal line of infinite nuclear matter and to large temperatures.
- In general the growth times are smaller by half an order of magnitude as compared to the typical values for bulk instabilities.
- In the stable region surface modes are slow, such that deformations initiated in the excitation process will persist during expansion and clustering.
- The surface instability is dominated by quadrupole deformation.

References

- [1] W. Nörenberg, *New Vistas in Nuclear Dynamics*, ed. P.J. Brussaard and J.H. Koch (Plenum Press, New York 1986) p. 91; W. Nörenberg, *Heavy Ion Reaction Theory*, ed. by W.Q. Shen, J.Y. Liu and L.X. Ge (World Scientific, Singapore 1989) p. 1.
- [2] P. Rozmej, W. Nörenberg and G. Papp, *Eur.Phys.J. A* **9**, 327 (2000)

Statistical evolution of fragment isospin in nuclear multifragmentation.

A.S. Botvina, *GSI Darmstadt and INR Moscow.*

The knowledge of the isotope composition of fragments produced in nuclear multifragmentation can help in resolving important problems: Do the fragments keep the memory of the initial dynamical stage or are they produced statistically? How does the isospin influence the disintegration of finite nuclei and what is the difference to the case of nuclear matter? What is the isospin dependence of the nuclear equation of state? Generally, this study addresses an intriguing interdisciplinary problem of the phase transition in a finite-size two-component system (i.e. in a nucleus consisting of neutrons and protons), that is instructive for all fields dealing with finite systems. The problem was investigated within the statistical multifragmentation model (SMM) [1], which is successfully used for explanation of experimental data. A new Markov chain method of partition generation was incorporated in the model [2], that allows for considering the multifragmentation process on a solid microcanonical basis. The reported results reflect statistical properties of the fragment production and can be used for identification of the phenomenon.

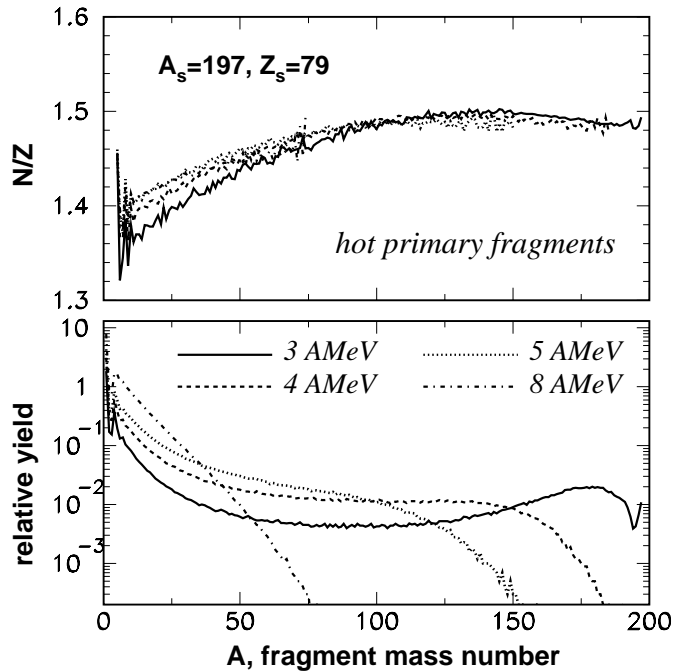


Figure 1: The neutron-to-proton ratio N/Z (top) and relative yield (bottom) of hot primary fragments produced after break-up of Au nuclei at different excitation energies: 3 (solid lines), 4 (dashed lines), 5 (dotted lines) and 8 (dot-dashed lines) MeV per nucleon.

The mass distributions and neutron-to-proton ratios (N/Z) of hot primary fragments produced after multifragmentation of a Au source (mass number $A_s=197$, charge $Z_s=79$) are shown in Fig. 1. One can see a general statistical trend: the N/Z ratio of the fragments increases with

their mass numbers. This is a consequence of the interplay between the Coulomb and symmetry energy contributions to the binding energy of fragments [1]. This trend persists up to $A \leq A_s/2$, while at larger A the finite-size effects due to the mass and charge conservation prevail. In Fig. 1 one can also see the evolution of the N/Z ratio in the excitation energy range $E_s^*=3-8$ MeV/nucleon, where the fragment mass distribution evolves from the U-shape, at the multifragmentation threshold $E_s^* \sim 3$ MeV/nucleon, to an exponential fall at the highest energy. This energy range is usually associated with a liquid-gas type phase transition in finite nuclei: During this evolution the temperature reaches a "plateau" and is nearly constant [1, 3]. As the energy increases the N/Z ratio of primary intermediate mass fragments (IMF, charges $Z=3-20$) increases, too. The reason is that the heaviest neutron-rich fragments are destroyed at increasing excitation energy, and some of their neutrons are bound in the IMFs, since the number of free neutrons is still small at this stage. Simultaneously, the N/Z ratio of the heaviest fragments decreases slightly. At very high excitation energy ($E_s^* > 8$ MeV/nucleon) the N/Z ratio of IMFs does not rise anymore but drops because no heavier fragments are left and the number of free neutrons increases rapidly, together with the temperature. This isospin evolution shows how the isospin fractionation phenomenon predicted for nuclear matter [4] actually shows up in finite nuclear systems. Such a mechanism is consistent with recent experimental data [5]. New experiments for studying mass and isospin effects in multifragmentation are planned at GSI [6].

Interesting phenomena are also predicted for peripheral nucleus-nucleus collisions [2]: 1) The neutron content of IMF increases if a considerable angular momentum is transferred to the source, because of an interplay of the rotational and Coulomb energy. 2) There is a break of the symmetry of the phase space population, including the space isospin distribution, because of the external Coulomb field of the partner nucleus. The space asymmetry leads to predominant population of the midrapidity kinematic region by neutron-rich IMFs, that should be considered as purely statistical alternative to a dynamical explanation of the midrapidity emission [7]. Such processes are examples of a new kind of statistical emission influenced by an inhomogeneous long-range field.

References

- [1] J.P.Bondorf et al., *Phys. Rep.* **257**, 133 (1995).
- [2] A.S.Botvina and I.N.Mishustin. GSI preprint 2000-50, Darmstadt, 2000; nucl-th/0011072, 2000.
- [3] J. Pochodzalla et al., *Phys.Rev.Lett.* **75**, 1040 (1995).
- [4] H.Müller and B.D.Serot, *Phys.Rev.* **C52**, 2072 (1995).
- [5] P.M.Milazzo et al., *Phys.Rev.* **C62**, 041602(R) (2000).
- [6] K.Kezzar et al., Proposal-S254, GSI, 2000.
- [7] J.Lukasik et al., Contrib. to this Scientific Report.

Thermal Boson Expansion

Z. Aouissat and J. Wambach

Institut für Kernphysik, Technische Universität Darmstadt.

Based on recent progress in the application of thermo field dynamics (TFD) [1] to thermal many-body systems, several authors [2, 3, 4] have considered a consistent thermal boson expansion (TBE). In this regard two points of view have been taken [2]. The first (path I) consists of a bosonization of the original degrees of freedom of the system, substituting for these ideal boson images. The thermalization is then achieved by doubling those newly introduced bosons as according to TDF prescription. The second possibility (path II) proceeds on the other hand via a thermalization of the system by doubling the original degrees of freedom and a subsequent bosonization of the entire new system. The two paths do not lead to the same results. Moreover, when applied to the Lipkin model, a closer look shows that the choice of path I implies that the thermal density of states are of bosonic type although the original system is purely fermionic.

To circumvent this problem one may choose path II where the thermal density of states is of fermionic type, since the thermalization is performed on the original fermions. However, inconsistencies related to the quasi-particle energies defining the thermal density of states, emerge. The latter are usually taken as solutions of a Hartree-Fock-Bogoliubov (HFB) approximation which, in most cases, leads to a dynamical mass generation. For massless modes, such as Goldstone modes, this gives the wrong solution. On the other hand, a mean-field description that is compliant with the symmetry requirements, is the Hartree-Bogoliubov (HB) approximation which can be obtained after a bosonization à la Holstein-Primakoff (HP). Therefore, when considering the symmetry constraints, it is rather path I that is favored. Amendments are, however, needed in order to reconcile it with the requirements of the statistics as explained earlier.

It was shown in [5] that a Boson expansion approach that treats on equal footing pair- as well as single-particle mapping offers a simple solution to the problems outlined above. For that matter the extended form of the bosonic HP mapping has been proposed in [6] which accommodates single-boson and boson-pair mappings:

$$\begin{aligned} (\vec{a}\vec{a})_I &= \mathcal{G}_N(n, m)A, & (\vec{a}^+\vec{a})_I &= 2n + m, \\ (a_i)_I &= \mathcal{G}_N(n, m)\Gamma_N(m)\alpha_i + 2\alpha_i^+ A\Gamma_N(m), \\ (\vec{a}^+\vec{a}^+)_I &= (\vec{a}\vec{a})_I^+, & (a_i^+)_I &= (a_i)_I^+, \end{aligned} \quad (1)$$

where N is an integer, $n = A^+A$, $m = \sum_i \alpha_i^+ \alpha_i$, and Γ_N is given by

$$\mathcal{G}_N(n, m) = \sqrt{2N + 4(n + m)}, \quad (2)$$

$$\Gamma_N(m) = \left[\frac{m + N - 2}{2(2m + N)(2m + N - 2)} \right]^{\frac{1}{2}}. \quad (3)$$

Thus, instead of the original bosons a_i , one has an ideal boson α_i which, as was shown in ref. [6], can accommodate the symmetry requirements. This is at the expense

of introducing a power series in an auxiliary boson A . The thermalization of the system is then undertaken in a consistent way by using the TFD formalism. The time-translation operator, $\mathcal{H} = H - \tilde{H}$, of the system is obtained as usual by considering the tilde conjugate of all operators such as A and α_i among others. However, the independent thermal quasiparticle representation is obtained by rotating only the ideal bosons α_i, α_i^+ and their tilde conjugate (t.c.), via a unitary thermal Bogoliubov transformation

$$\alpha_i^+ = u(T)\gamma_i^+ + v(T)\tilde{\gamma}_i, \quad (4)$$

into the thermal quasiboson operators γ_i, γ_i^+ , and their t.c. We insist here on the fact that the bosons A, \tilde{A} need not be transformed since they are only auxiliary modes. This point of view is different from those adopted in all earlier works [2, 3, 4].

For fermionic systems, the situation is rather similar to the bosonic case. The extended form for the fermionic HP mapping proposed by Marshalek [7] is given by

$$\begin{aligned} (J_z)_I &= \frac{1}{2}n_f + B^+B, \\ (J_+)_I &= B^+ \sqrt{N - (B^+B + n_f)}; & (J_-)_I &= (J_+)_I^+ \\ (c_{2p})_I &= N^{-1} \left(\sqrt{N - (B^+B)} a_{2p} + B a_{1p} \right) \\ (c_{1p})_I &= N^{-1} \left(\sqrt{N - (B^+B)} a_{1p} - B a_{2p} \right) \\ n_f &= \sum_{p=1}^N (a_{2p}^+ a_{2p} - a_{1p}^+ a_{1p}). \end{aligned} \quad (5)$$

where B^+ and a_{ip}^+ are ideal boson and fermion operators, respectively. It allows a consistent mapping of pairs and single-fermion states. The thermalization is again obtained following the amended path I. Thus one introduces as previously the thermal Bogoliubov transformation which rotates only the ideal fermions and their tilde transform, such that

$$a_{ip}^+ = x_i \beta_{ip}^+ + y_i \tilde{\beta}_{ip}, \quad (6)$$

while the auxiliary bosons B are left unaltered. Obviously our procedure cures the problems of path I that were encountered in ref. [2] regarding the fermion statistics [5].

References

- [1] Y. Takahasi, H. Umezawa, Coll. Pheno., 2 (1975) 55.
- [2] T. Hatsuda, Nucl. Phys. A492 (1989) 187.
- [3] N. R. Walet, A. Klein, Nucl. Phys. A510 (1990) 261.
- [4] O. Civitarese et al., Phys. Rev. C60 (1999) 34302.
- [5] Z. Aouissat, A. Storozhenko, A. Vdovin, J. Wambach, Submitted to Phys. Rev. C.
- [6] Z. Aouissat, Phys. Rev. C62 (2000) 012201(R)
- [7] E.R. Marshalek, Nucl. Phys. A224 (1974) 221.

Chiral Phase Transition in the scaled $O(4)$ -Model

O. Bohr, B.-J. Schaefer, J. Wambach

Institut für Kernphysik, Technische Universität Darmstadt.

Due to the non-Abelian character of QCD gluons self-interact and form bound states, so-called glueballs. Such glueballs have been seen in recent lattice simulations and are actively searched for in experiment. Glueballs can be used to construct effective models of QCD which respect the symmetries and anomaly structure of the theory.

At the classical level and in the limit of vanishing quark masses QCD for n flavors exhibits a global chiral $U(n)_L \times U(n)_R$ symmetry and is in addition invariant under scale transformations. Due to anomalies not all of the associated currents are conserved and the symmetry is broken down to $SU(n)_L \times SU(n)_R$ which, in the case of two flavors, is isomorphic to $O(4)$. This symmetry is spontaneously broken to $SU(n)_{L+R}$. The divergence of the anomalous scale current is given by the trace of the energy-momentum tensor which, in the limit of massless quarks, is given by

$$\langle \theta_\mu^\mu \rangle = \langle \frac{\beta(g)}{2g} G_{\mu\nu}^a(x) G^{a\mu\nu}(x) \rangle, \quad (1)$$

where $G_{\mu\nu}^a(x)$ denotes the gluonic field-strength tensor and $\beta(g)$ is the usual QCD beta function. An effective realization of the scale anomaly can be achieved by adding to the classical Lagrangian a scalar color singlet dilaton field χ with an interaction potential of the form

$$V(\chi) = h \left(\frac{\chi}{\chi_0} \right)^4 \left(\ln \frac{\chi}{\chi_0} - \frac{1}{4} \right), \quad (2)$$

where h is a constant that is related to the vacuum energy density ε_{vac} via $h = -4\varepsilon_{vac}$, when there are no quarks. The potential has a minimum at $\chi = \chi_0$.

In a previous work [?] we have tested a novel renormalization group approach to investigate chiral symmetry restoration at finite temperature and could analyze the critical behavior at the chiral phase transition of the $O(N)$ -model. In this work we investigate the influence of the additional dilaton field on the chiral phase transition and the critical behavior. Therefore we couple a massive scalar dilaton field, which breaks the scale invariance, to the $O(4)$ -model. Here we follow here the work in [?] and consider the following Lagrangian

$$\begin{aligned} \mathcal{L} = & \frac{1}{2} \partial_\mu \sigma \partial^\mu \sigma + \frac{1}{2} \partial_\mu \vec{\pi} \partial^\mu \vec{\pi} + \frac{1}{2} \partial_\mu \chi \partial^\mu \chi \\ & - \frac{\lambda}{4} \left(\sigma^2 + \vec{\pi}^2 - \frac{\chi^2}{\zeta^2} \right)^2 - V(\chi), \end{aligned} \quad (3)$$

where σ , $\vec{\pi}$ denote the sigma- and the pion fields respectively.

Lattice calculations hint that the lightest glueball has a mass of 1.3 - 1.6 GeV. We use this mass as a constraint to fix the parameters of the model at $T = 0$. We then perform a finite-temperature calculation, where we calculate the vacuum expectation value (VEV) of the meson fields and the critical exponents of the chiral phase transition.

From a comparison with the $O(4)$ -model calculation without the dilaton field we can then estimate the influence of the dilaton field on the chiral phase transition.

The temperature dependence of the scalar mesonic VEV $\langle \phi \rangle$ (cf. Fig. 1) is very similar to the temperature dependence in the pure $O(4)$ -model calculation without the dilaton field. Around T_c we again obtain a scaling behavior of the VEV $\langle \phi \rangle$ and of the mesonic coupling constant λ with critical exponents $\beta = 0.39$ and $\nu = 0.79$.

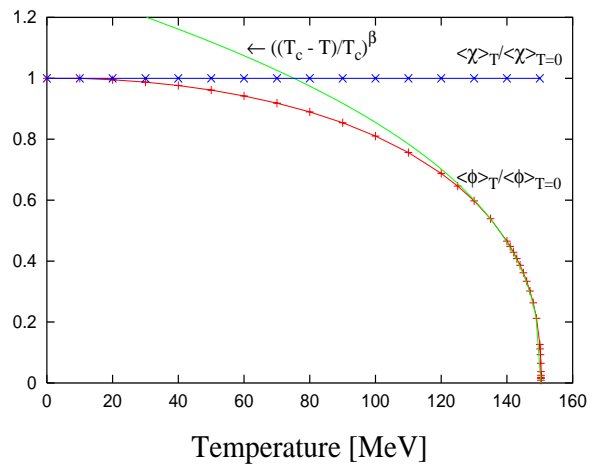


Figure 1: The temperature evolution of the vacuum expectation values of the dilaton field $\langle \chi \rangle$ and the scalar meson field $\langle \phi \rangle$ in the chiral limit.

These values of the exponents coincide within the estimated numerical error bars with the pure $O(4)$ -model values.

On the other hand the glueballs themselves change very little in the temperature region up to the chiral phase transition. The change of the mass as well as of the VEV of the dilaton field (cf. Fig. 1) is less than 0.1% in this region. Calculations within the framework of a pure dilaton model show that the glueballs begin to be modified considerably at temperatures around 250 MeV.

In summary we can conclude that the glueballs, due to their high mass of ≈ 1.5 GeV, have very little influence on the temperature evolution in the mesonic sector where we still find a second order chiral phase transition with $O(4)$ critical exponents.

References

- [1] O. Bohr, B.-J. Schaefer and J. Wambach, eprint: hep-ph/0007098
- [2] H. Gomm, J. Schechter, Phys. Lett **B158** (1985) 449; E. K. Heide, S. Rudaz, P. J. Ellis, Phys. Lett. **B293** (1992) 259.

Chiral Fluctuations in Nuclei

Z. Aouissat, C. Isselhorst and J. Wambach

Institut für Kernphysik, Technische Universität Darmstadt.

The near-threshold enhancement in the $\pi^+\pi^-$ invariant mass distribution in nuclei, observed by CHAOS collaboration [1] and for $\pi^0\pi^0$ pairs by the Crystal Ball collaboration [2], offers the interesting possibility of directly observing a signal for partial restoration of chiral symmetry in a dense medium. There seems to be theoretical consensus on a strong in-medium reshaping of the s-wave isoscalar pion-pair correlations as a direct consequence of increased fluctuations of the chiral order parameter. This translates into a significant downward shift of the strength in the $\pi\pi$ T -matrix in the scalar-isoscalar channel as seen in Fig. 1.

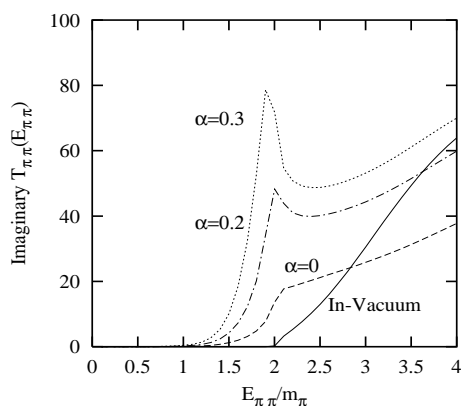


Figure 1: The imaginary part of the in-medium $\pi\pi$ T -matrix at normal nuclear density. The parameter α represents the medium effects on the mean field sigma-mass. See ref. [3] for details.

The reaction theory for the $A(\pi, 2\pi)$ knockout process has been thoroughly studied in the past [4], but only recently has the in-medium $\pi\pi$ final-state interaction (FSI) been seriously considered [5]. Taking into account the elementary $\pi\pi$ production process on the nucleon, the experimental acceptance, the Pauli constrained phase-space, and the nuclear absorption of the incoming and outgoing pions, the total cross-section for the $A(\pi, 2\pi)$ process in local density approximation reads

$$\begin{aligned} \sigma &= \frac{\pi}{q} \int d^2b dz A_{in}(\rho(\vec{r})) A_{out}^+(\rho(\vec{r}_1)) A_{out}^-(\rho(\vec{r}_2)) \\ &\int \frac{d^3k}{(2\pi)^3} \frac{d^3q_1}{(2\pi)^3} \frac{d^3q_2}{(2\pi)^3} n(\vec{k}) [1 - n(\vec{q} + \vec{q} - \vec{q}_1 - \vec{q}_2)] \\ &\delta(q_0 + \varepsilon_{\vec{k}} - \omega_{\vec{q}_1} - \omega_{\vec{q}_2} - \varepsilon_{\vec{k} + \vec{q} - \vec{q}_1 - \vec{q}_2}) \frac{1}{2\omega_{\vec{q}_1}} \frac{1}{2\omega_{\vec{q}_2}} \\ &|T(\pi N \rightarrow \pi\pi N)|^2 \left| \frac{T_{\pi\pi}}{V_{\pi\pi}} \right|_{FSI}^2 \times \text{Acceptance}. \end{aligned} \quad (1)$$

To remove both experimental and theoretical uncertainties in the reaction dynamics, the CHAOS collaboration has considered the composite ratio, $C_{\pi\pi}^A = \frac{\sigma^A(M_{\pi\pi})}{\sigma_T^A} / \frac{\sigma^N(M_{\pi\pi})}{\sigma_T^N}$, where $\sigma^A(M_{\pi\pi})$ ($\sigma^N(M_{\pi\pi})$) denotes the invariant mass distribution in the nucleus (nucleon), while σ_T^A (σ_T^N) is the corresponding total cross section for the $A(\pi, 2\pi)$ process

[6]. Comparing this ratio for both $\pi^+\pi^-$ and $\pi^+\pi^+$ final states, one can argue that the observed near-threshold enhancement must be an $I = 0$ effect. The theoretical pre-

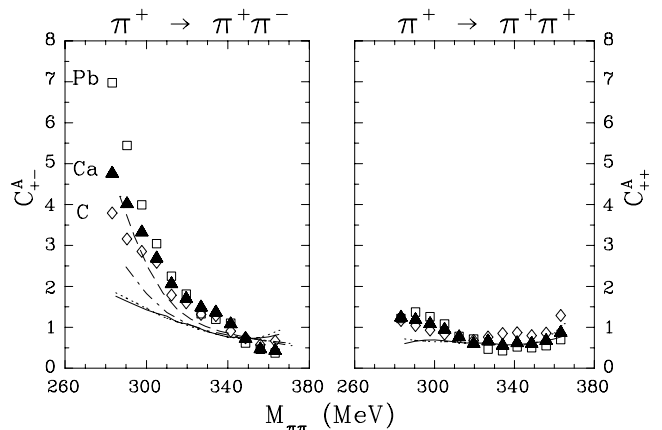


Figure 2: The ratio $C_{\pi\pi}^A$ for various nuclear targets [6].

dictions shown on Fig. 2 assume the effect of the FSI as appearing in Fig. 1. The various curves reflect the current state-of-the-art calculations by different groups (see [7] for details). The dashed curve uses the model in [3].

However, improvements in the reaction calculations are needed. The kinematical analysis of the 3-body final state, for instance, reveals that the average momentum of the pion-pair is about 200 MeV/c. Therefore the back-to-back kinematics assumption used in all previous calculations needs to be revised [8].

On the experimental side, a very exciting possibility which circumvents the strong absorption in the initial state is the photoproduction $A(\gamma, 2\pi^0)$. Such experiments have been conducted at MAMI in Mainz and are currently analyzed [9]. A theoretical description is also in progress [8].

References

- [1] F. Bonutti et al., Phys. Rev. Lett. 77 (1996) 603.
- [2] A. B. Starostin et al., submitted to Phys. Rev. Lett.
- [3] Z. Aouissat, G. Chanfray, P. Schuck, J. Wambach, Phys. Rev. C 61, (2000) 12202
- [4] M. J. Vicente Vacas, E. Oset, nucl-th/9907008
- [5] P. Schuck, Z. Aouissat, F. Bonutti, G. Chanfray, E. Fragiaco, N. Grion, J. Wambach, Proceedings of the XXXVI, international Winter Meeting on Nuclear Physics, Ed. I. Iori, Bormio (Italy), January 1998.
- [6] F. Bonutti et al., Nucl. Phys. A677 (2000) 213.
- [7] J. Wambach, Z. Aouissat, P. Schuck, to appear in Nucl. Phys. A.
- [8] Z. Aouissat, C. Isselhorst, J. Wambach, in progress.
- [9] V. Metag, to appear in Nucl. Phys. A.

Nonperturbative renormalization flow and infrared physics

J. Meyer, K. Schwenzer, T. Spitzenberg and H.J. Pirner,

Institut für Theoretische Physik der Universität Heidelberg

Renormalization group flow equations have proved to be a good tool to analyze the dynamics of strong interaction in the nonperturbative region. They have been successfully applied to effective mesonic models in a thermal environment and revealed detailed insight into the chiral phase transition [1]. The basic aim of the renormalization group treatment is to systematically integrate out quantum and/or thermal fluctuations with momenta above a certain cutoff scale k and include them into the couplings of an effective action.

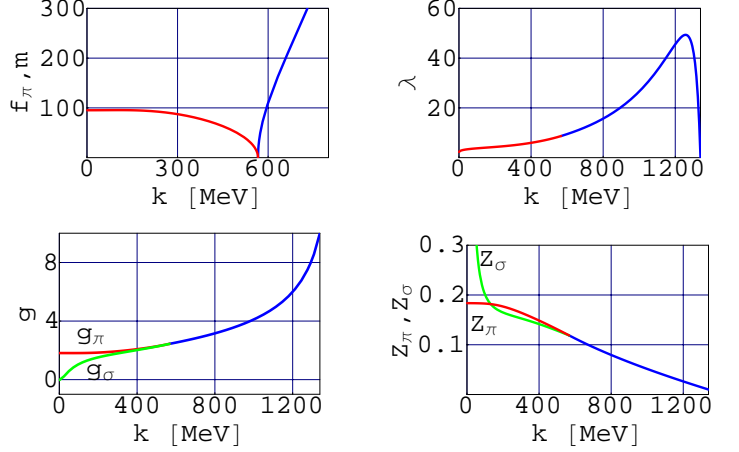
We are interested in the low energy theory of strong interaction resulting from the integration of high momentum modes. Assuming a dominant one gluon exchange or a instanton vacuum, gluonic degrees of freedom can be absorbed into an instantaneous four fermion interaction described by the NJL-model. Our analysis shows that the standard solution of the NJL-model and the flow of the linear σ -model, which we are using, coincide in the large N_C -limit, where the dynamics is dominated by fermion loops. In the full solution though, the additional dynamics of the mesonic degrees of freedom becomes important and yields an improved low energy behaviour compared to the NJL-model. The linear σ -model describes a massless two flavour quark field q interacting with chiral fields $\Phi = (\sigma, \vec{\pi})$ and is believed to give a valid description of chiral dynamics at scales $\leq 1\text{GeV}$. It has the action

$$S_{UV} = \int d^4x \left[\bar{q} (i\cancel{\partial} - g(\sigma + i\vec{\tau}\vec{\pi}\gamma_5)) q + \frac{1}{2} (\partial\Phi)^2 - U(\Phi^2) \right],$$

with a general $O(4)$ symmetric potential $U(\Phi^2)$. From this, we compute the effective action in a one loop approximation using Schwinger proper time regularization [2]. The resulting expression is truncated to second order derivative in order to include the relevant terms for the flow. This inclusion of higher order terms, results in a splitting in the dynamics of the massive σ -mode and the massless Goldstone-bosons. By a renormalization group improvement the one loop expressions are turned into nonperturbative flow equations. The resulting flow for the most important parameters is plotted below. An interesting feature is, that like the four boson coupling λ also the Yukawa coupling g_σ vanishes in the infrared. Therefore, aside from providing a broken vacuum, the σ decouples from the dynamics and leaves the pions as the only dynamic particles. We obtain the resulting infrared effective action

$$\Gamma_{IR} = \int d^4x \left[\bar{q} \left(i\cancel{\partial} - m_q - ig_\pi \vec{\tau}\vec{\pi}\gamma_5 + \frac{g_\pi}{f_\pi} \pi^2 \right) q - \frac{1}{2} (\partial\vec{\pi})^2 + \text{derivative couplings} \right].$$

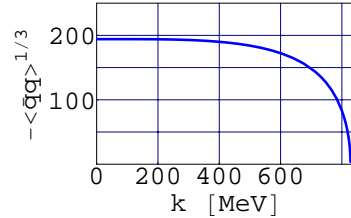
Our approximation obeys the chiral Ward identities and ensures that the $\pi\pi$ -scattering amplitude vanishes at tree level due to a $\bar{q}q\pi^2$ -contact term that cancels the 1π -contributions in the IR.



Once the flow equations for the linear σ -model are written down, the chiral order parameter $\langle \bar{q}q \rangle$ can be calculated from the partition function. Using the same cutoff function as for the flow equations one obtains in the local potential approximation

$$\partial_k \langle \bar{q}q \rangle = - \frac{N_c g k^5 \phi_k}{2\pi^2 (k^2 + g^2 \phi_k^2)^2}.$$

Starting in the symmetric regime where the order parameter is zero, we find a value of $\langle \bar{q}q \rangle = -(194\text{MeV})^3$, as shown below.



It is now tempting to derive a flow equation for the spectral density $\rho(\lambda)$ of the Dirac operator. This may be done by establishing a relation between $\langle \bar{q}q \rangle(\lambda)$ and $\rho(\lambda)$ similar to the Banks-Casher relation. It would be interesting to compare the results with recent data available from lattice QCD.

Another promising idea is to connect our cutoff parameter to a physical momentum scale and continue our Euklidian flows to the full complex plane. By this, it would be possible to compute spectral functions of mesonic resonances and make a direct connection to low energy hadron phenomenology.

References

- [1] J. Berges, N. Tetradis and C. Wetterich, to appear in Phys. Rep., hep-ph/0005122
- [2] B.-J. Schaefer and H.-J. Pirner, Nucl. Phys. **A660** (1999) 439, nucl-th/9903003

e^+e^- -pair production in π^-p reactions

Matthias Lutz, Bengt Friman (GSI) and Madeleine Soyeur (CE Saclay)

The cross section for the reaction $\pi^-p \rightarrow e^+e^-$ is computed, using vector-meson dominance and the amplitudes for the processes $\pi^-p \rightarrow \rho^0 n$ and $\pi^-p \rightarrow \omega n$, obtained in a coupled channel analysis of meson-nucleon scattering at energies near the threshold for vector-meson production [1]. These amplitudes are sensitive to the coupling of the vector mesons to baryon resonances below the vector meson production threshold. Data that directly reflect these amplitudes would provide very useful constraints on the dynamics of vector mesons propagation in nuclear matter and e^+e^- pair production in heavy-ion collisions. The $\pi^-p \rightarrow e^+e^-n$ reaction offers the possibility to experimentally test the pion induced vector meson production amplitudes below threshold. The interference of the two light vector mesons in the e^+e^- channel is sensitive to the magnitudes and the relative phase of the ρ^0 and ω production amplitudes (see Fig. 1). An experimental test of the $N^*N\rho^0$ and $N^*N\omega$ vertices through the $\pi^-p \rightarrow e^+e^-n$ reaction below the vector meson production threshold would be a most valuable constraint on the in-medium propagation of ρ^0 - and ω -mesons.

We shall restrict our discussion to e^+e^- pairs of invariant masses ranging from 0.5 to 0.8 GeV. The exclusive measurement of the e^+e^-n outgoing channel ensures that the e^+e^- pairs come from vector meson decays (pseudoscalar mesons decay into an e^+e^- pair and an additional photon). We note however that only s- and d-wave pion-nucleon resonances are at present included in the model of Ref. [1]. To be complete, the description of the $\pi^-p \rightarrow e^+e^-n$ reaction in the energy range discussed in this work ($1.2 < \sqrt{s} < 1.8$ GeV) should include also the effect of other partial waves.

The magnitude of the $\rho^0 - \omega$ interference in the $\pi^-p \rightarrow e^+e^-n$ is illustrated in Fig. 2, where we show the cross section for this reaction as function of the total center of mass energy. We have selected e^+e^- pairs of invariant mass $m=0.55$ GeV. This figure elucidates the role of baryon resonances with masses in the range of 1.5 to 1.6 GeV in generating strong interference effects.

Above the vector meson threshold, the $\rho^0 - \omega$ interference in the $\pi^-p \rightarrow e^+e^-n$ cross section is particularly interesting for e^+e^- pair invariant masses close to the ω mass. This effect is manifested in the invariant mass spectrum shown in Fig. 3 ($\sqrt{s}=1.8$ GeV). The model of Ref. [1] for the $\mathcal{M}_{\pi^-p \rightarrow \rho^0 n}$ and $\mathcal{M}_{\pi^-p \rightarrow \omega n}$ amplitudes predicts a constructive interference at this energy. This feature appears to be a very sensitive test of the model.

References

- [1] M. Lutz, G. Wolf and B. Friman, Nucl. Phys. **A 661** (1999) 526c and Proc. of Hirscheegg 2000.
- [2] M. Lutz, B. Friman and M. Soyeur, in preparation.

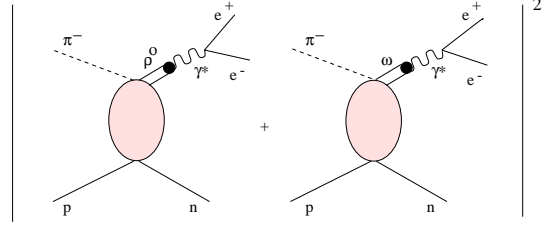


Figure 1: Squared amplitude for the $\pi^-p \rightarrow e^+e^-n$ reaction with intermediate ρ^0 - and ω -mesons.

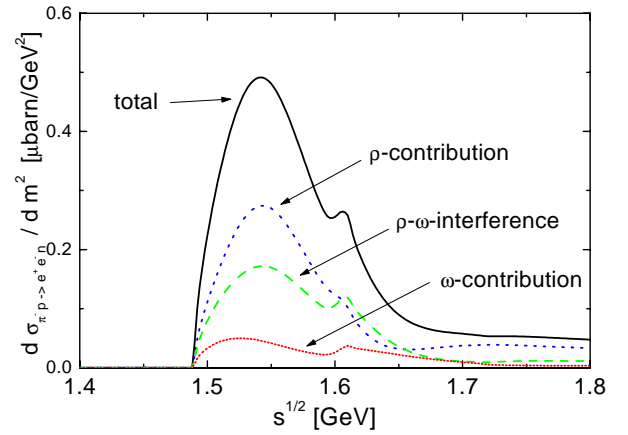


Figure 2: Differential cross section $d\sigma/dm^2$ for the $\pi^-p \rightarrow e^+e^-n$ reaction as function of \sqrt{s} for a fixed e^+e^- pair invariant mass $m=0.55$ GeV.

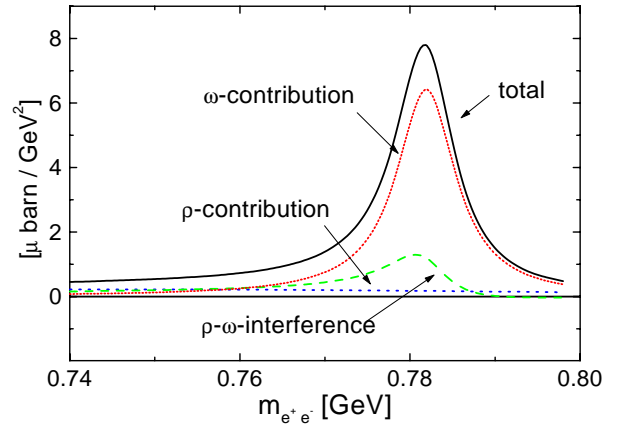


Figure 3: Differential cross section $d\sigma/dm^2$ as function of the e^+e^- pair invariant mass for a fixed total center of mass energy $\sqrt{s}=1.8$ GeV.

e^+e^- production in pp , pd and pA reactions at SIS energies

E.L. Bratkovskaya, W. Cassing, and U. Mosel
University of Giessen

The modification of hadron properties in the nuclear matter is of fundamental interest. The dilepton data from heavy-ion experiments at SPS energies have provided first experimental evidence for a change of the vector meson properties, however, the heavy-ion data can be interpreted within different scenarios of in-medium modifications, i.e. by the dropping mass scenario or the collisional broadening approach. Since in heavy-ion experiments the nuclear matter is probed at different densities and temperatures within the complex dynamical evolution, it will be very useful to have independent experimental information from photon-nucleus, pion-nucleus or proton-nucleus reactions, where the properties of vector mesons are probed at normal nuclear density or below. This question becomes very actual with respect to the HADES experiments coming up at GSI soon [1].

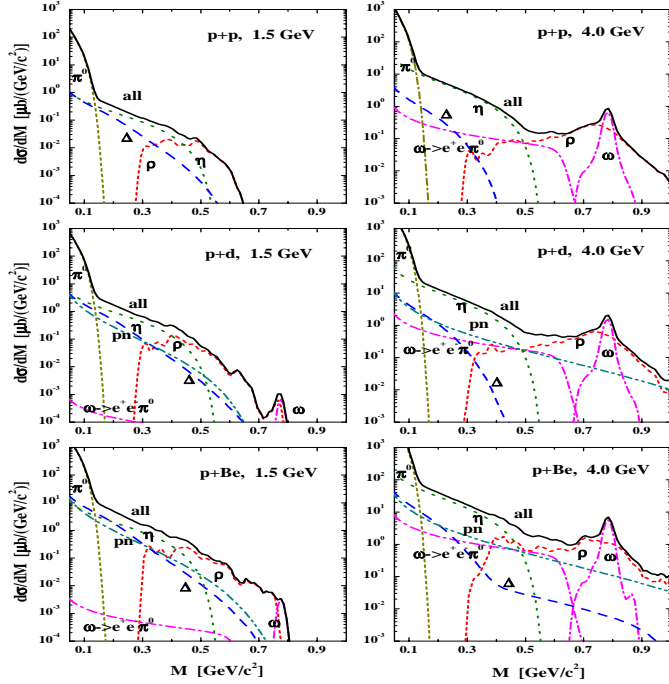


Figure 1: The dilepton invariant mass spectra $d\sigma/dM$ for pp (upper part), pd (middle part) and pBe collisions (lower part) at 1.5 GeV (left panel) and 4.0 GeV (right panel) including a 10 MeV mass resolution [2].

Dilepton production in from pp , pd and pBe collisions from 1 – 5 GeV has been studied in Ref. [2] within the framework of the combined resonance-string approach [3]. here, it has been found that the DLS data for pp and pd collisions can be reasonably well described whereas for pBe systems (especially at 4.9 GeV) our calculations give slightly higher dilepton yield. We have demonstrated, furthermore, the importance to measure dileptons from pp and pd (or even pBe) collisions simultaneously since such data provide constraints on the isospin dependence of pp and pn interactions, which is important for an understand-

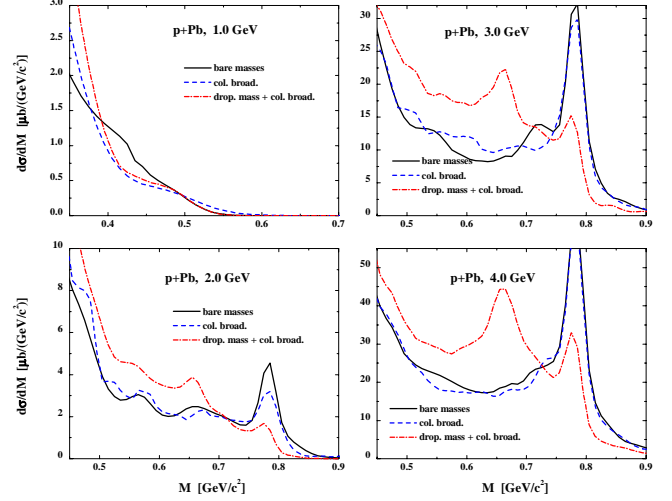


Figure 2: The comparison of different in-medium modification scenarios, i.e. collisional broadening (dashed lines) and collisional broadening + dropping vector meson masses (dash-dotted lines), with respect to the bare mass case (solid lines) for $p + Pb$ from 1–4 GeV [4].

ing of heavy-ion data.

In Fig. 1 we show our detailed predictions for the differential dilepton spectra from pp , pd and pBe collisions at 1.5 and 4.0 GeV energy with a 10 MeV mass resolution that can be controlled experimentally by the HADES Collaboration in near future.

A comparison of the different in-medium modification scenarios is shown in Fig. 2, i.e. collisional broadening (dashed lines) and collisional broadening + dropping vector meson masses (dash-dotted lines), with respect to the bare mass case (solid lines) on a linear scale for $p + Pb$ collisions from 1–4 GeV. The collisional broadening + 'dropping mass' scenario leads to an enhancement of the dilepton yield in the range $0.5 \leq M \leq 0.75$ GeV and to a reduction of the ω -peak, which is more pronounced for heavy systems (up to a factor 2 for $p + Pb$ at 3–4 GeV), since most of the ρ 's and ω 's now decay in the medium approximately at density ρ_0 . This leads to a pronounced peak around $M \approx 0.65$ GeV, which can be attributed to the in-medium ω decay since the ρ spectral strength is distributed over a wide low mass regime. Especially when comparing dilepton spectra from C and Pb targets, it should be experimentally possible to distinguish an in-medium mass shift of the ω meson by taking the ratio of both spectra.

References

- [1] The HADES Collaboration, Proposal, GSI 1994.
- [2] E.L. Bratkovskaya et al., Nucl. Phys. A 686 (2001) 476.
- [3] M. Effenberger et al., Phys. Rev. C 60 (1999) 044614.
- [4] E.L. Bratkovskaya, nucl-th/0101067.

Renormalisation of Self-consistent Resummation Schemes^G

H. van Hees, J. Knoll (GSI)

For the description of physical systems with strong interactions generally perturbative methods are insufficient. Rather on the basis of effective field theories non-perturbative methods such as partial resummation schemes have to be applied. There are a couple central questions connected with such methods which concern symmetries and conservation laws as well as thermodynamic consistency and detailed balance. While the question of conserving approximations was addressed by Baym's Φ -functional method [1, 2, 3], in field theoretical descriptions a further complication arises, namely that of renormalization. Loop integrals generally diverge and renormalization concepts were developed in perturbation theory. In the context of resummation schemes the question arises under which conditions they are still renormalizable with temperature and density independent counter terms. In the past only a few specific examples were investigated.

Our purpose was to analyze self consistent partial Dyson resummation schemes defined by a set of basic generating self energy diagrams with dressed propagators. In terms of perturbative diagrams this leads to an infinite iterative insertion of all basic diagrams. The sum of all these perturbative diagrams defines the self consistent self energy which determines the dressed propagator, cf. (1). All diagram subpieces with the topology of a single loop which are connected to the rest of the diagram at most via two vertices, are divergent and have to be renormalized. These structures, however, appear in a nested way such that first the most inner ones have to be renormalized through counter-terms given by the reduced diagrams where the divergent sub-pieces are contracted to a point. The so obtained reduced diagrams themselves are to be subjected to the same procedure. This iterative process is formalized as the BPHZ-renormalization scheme. For the self consistent scheme under consideration the key issue is to find a compact iteration scheme that generates all the required counter terms at once.

For an initial study we choose a simple scalar field theory model, the ϕ^4 -model. For the Hartree approximation given by the tadpole self-energy diagram the subtraction scheme can be formulated as a gap equation. As a new part we included a genuine two-point contribution, namely the

sunset diagram. The latter gives rise to an imaginary part in the self-energy, i.e., a finite width for the particles in the medium. In terms of perturbative diagrams the self consistent scheme then leads to all kinds of "super-daisy", "super-sunset" diagrams and all possible mixtures of them, cf. (1).

It could be shown that also this approximation can be renormalized in a BPHZ-type procedure (for details see [4]). The considerations show that one first has to solve the problem in the vacuum where subtracted dispersion relations can be used to renormalize the self-energy. In the same way one obtains the renormalized vertex functions which are needed to replace the corresponding divergent vacuum sub-diagrams in the finite temperature case. This means that for the renormalization of the finite temperature case one needs only *local temperature independent vacuum counter-terms* in perfect analogy to the well known theorem for perturbative finite-temperature quantum field theory.

We argue that the Φ -functional properties of the self energies indeed enforces the consistency of the counter-terms and symmetry factors for the explicit as well as the hidden nested and overlapping divergences since the divergent sub-diagrams are given by higher derivatives of the Φ -functional with respect to the dressed Green's function.

This substitution of divergent sub-diagrams together with direct subtractions of counter-terms on the level of the integrands provides a scheme where one has to deal only with convergent integrals without any explicit beforehand regularization which opened the possibility to calculate the self-energy and thermodynamic quantities such as the entropy in full self-consistency.

The results are important, e.g., for the description of hadrons in dense matter, e.g. [5] or for an effective description of gauge fields such as QCD in cases where the damping width of the particles is of considerable importance. Supplementary to the renormalization question functional methods have been developed on the basis of the Φ -functional concept, which permit to investigate and cure possible violations of symmetries and conservation laws at the level of higher order correlation functions [4]. This is of particular importance for gauge theories[5].

$$\Sigma = \underbrace{\text{tadpole} + \text{bubble}}_{\text{basic diagrams}} + \dots + \underbrace{\text{super-daisy} + \text{super-sunset}}_{\text{generated perturbative diagrams}} \quad (1)$$

The equation shows the self-energy Σ as a sum of two groups of diagrams. The first group, labeled 'basic diagrams', consists of a tadpole diagram (a circle with a single external line) and a bubble diagram (a circle with two external lines). The second group, labeled 'generated perturbative diagrams', consists of a super-daisy diagram (a bubble with multiple tadpoles attached) and a super-sunset diagram (a sunset diagram with additional internal lines). Ellipses indicate that there are more diagrams in each group.

References

- [1] G. Baym, Phys. Rev. **127** 1391 (1962).
- [2] Y. B. Ivanov, J. Knoll, D. N. Voskresensky, Nucl. Phys. **A657** 413 (1999), hep-ph/9807351.
- [3] Y. B. Ivanov, J. Knoll, D. N. Voskresensky, Nucl. Phys. **A672** 313 (2000), nucl-th/9905028.
- [4] H. van Hees, Renormierung selbstkonsistenter Näherungen in der Quantenfeldtheorie bei endlichen Temperaturen, Ph.D. thesis, TU Darmstadt (2000), <http://elib.tu-darmstadt.de/diss/000082/>.
- [5] H. van Hees, J. Knoll, Nucl. Phys. **A683** 369 (2001), hep-ph/0007070.

Vector mesons within a conserving self-consistent approximation^G

H. van Hees, J. Knoll (GSI)

The experimental results on di-lepton production in heavy ion collisions by the CERES and DLS collaborations has shown an enhancement of the di-lepton production rate in the invariant pair mass region between 300-600 MeV compared to the rate to be expected from proton-proton collisions. Since dileptons are direct signals from the decay of vector mesons within the hot reaction zone this enhancement points towards in-medium modifications of vector-mesons in dense hadronic matter.

From the theoretical point of view a consistent description of such phenomena within effective quantum field theoretical models needs a treatment of particles which considers the finite spectral width. This concerns not only the widths of resonances but also the width due to collisions of the particles within the hot and dense medium. For such questions a perturbative approach is generally insufficient and a self-consistent treatment is at place.

There is a class of self-consistent approximations derived from a generating functional which leads to a closed set of conserving equations of motion for the mean fields and the Dyson resummed dressed propagators [1]. They possess exact conservation laws for the expectation values for conserved Noether-currents (including those from space-time symmetry, i.e., energy, momentum and angular momentum).

A detailed symmetry analysis nevertheless shows that on the level of higher order correlation functions such as propagators the Ward-Takahashi identities (WTI) of the underlying symmetries are not fulfilled [2]. In the case of vector or gauge fields this has serious consequences: The WTI are necessary to ensure the physicality of states. A violation of this symmetry causes the excitation of unphysical degrees of freedom and violates unitarity and causality

within the dressed propagators and currents are no longer conserved at the correlator level.

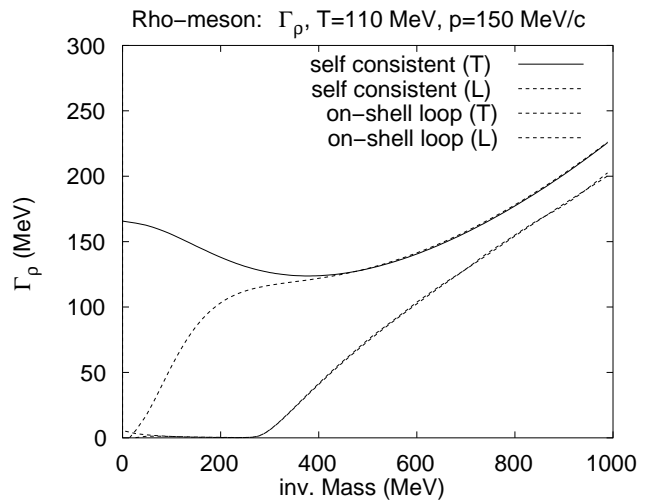
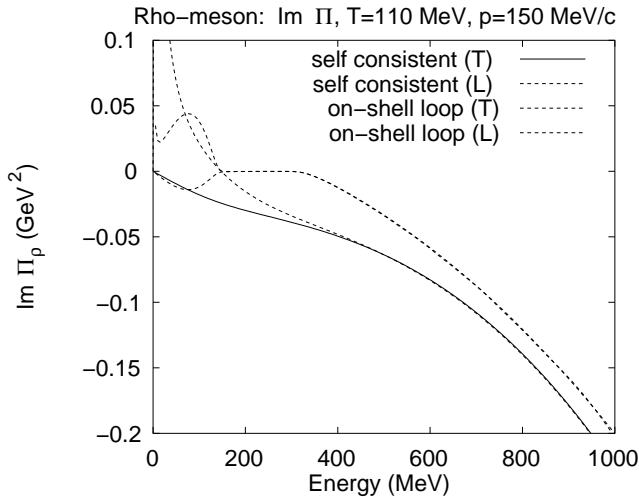
On the other hand corrections which restore current conservation on the correlator level have been studied within a diffusion equation approximation of the according kinetic equation (Fokker-Planck-equation) [3]. The study shows that the space components of the polarization tensor suffer only small corrections, if the scattering of a particle is isotropic on the average. The self consistent time component, however has a completely wrong behavior as it also exponentially decay in time within this approximation, while it should stay constant in time due to charge conservation.

In order to cure this defect we have invented a particular projection method. It discards the wrong time components of the polarization tensor and solely uses the space components. This way a 4-dimensionally transverse polarization tensor for the vector field can be constructed. The two independent components of the thermal polarization tensor, the longitudinal and transverse components, $\Pi_T(q)$ and $\Pi_L(q)$, can be obtained from

$$2\Pi_T + g_{ik}\Pi^{ik} = -\frac{q_i q_k}{\vec{q}^2}\Pi^{ik} = -\frac{(q^0)^2}{q^2}\Pi_L.$$

Here the indices (i, k) run over the spatial components from 1 to 3. We have numerically solved the coupled self-consistent equations of motion for this projected self-energies. For details see [2, 4].

The results show a significant enhancement of the spectral width in the low energy mass region and all thresholds, present in the perturbative quantities, are gone due to collision broadening of the self-consistently treated pions.



The transverse components of the imaginary part of the self-consistent ρ -meson self-energy (left) and the corresponding spectral width (right).

References

- [1] G. Baym, Phys. Rev. **127** 1391 (1962).
- [2] H. van Hees, Renormierung selbstkonsistenter Näherungen in der Quantenfeldtheorie bei endlichen Temperaturen, Ph.D. thesis, TU Darmstadt (2000), <http://elib.tu-darmstadt.de/diss/000082/>.
- [3] J. Knoll, D. Voskresensky, Annals of Physics **249** 532 (1996).
- [4] H. van Hees, J. Knoll, Nucl. Phys. **A683** 369 (2001), <http://de.arXiv.org/abs/hep-ph/0007070>.

Exact Conservation Laws in the Gradient Expanded Kadanoff–Baym Equations^G

Jörn Knoll, Yuri B. Ivanov, and Dmitri N. Voskresensky
GSI Darmstadt

One of the challenging problems in quantum many-body physics is the appropriate inclusion of resonances or particles with broad damping width into a self-consistent non-equilibrium dynamics. Such kind of description can be constructed on the basis of the so called Kadanoff–Baym equations (KBE) derived within the non-equilibrium Green function technique [1]. While the KBE are exact, in actual calculations one has to rely on further approximations. They provide (a) a truncated self-consistent scheme and (b) through the gradient approximation they lead to transport type of equations of motion. Interested in the dynamics of particles with broad mass width one has to avoid the quasi-particle approximation, and solely rests on the first-order gradient approximation of the KBE. This concept was first addressed by Kadanoff and Baym [1] and recently reconsidered in the context of hadronic matter and heavy ion collisions [2–7]. As for any such approximation, however, symmetries and conservation laws as well as detailed balance and thermodynamic consistency may no longer a priori be guaranteed.

In ref. [8] we re-investigated a generalization of the Φ derivable method of Baym [9] to the real-time Green function technique which provides truncated self-consistent approximations which are conserving and thermodynamically consistent at the level of KBE. In particular a conserved energy-momentum tensor could be derived for local field couplings. The subsequent gradient approximation leads to two coupled equations: a quantum transport equation, which governs the four-phase distribution functions $f(\vec{x}, t, p)$, and a retarded equation, which determines the time evolution of the spectral function $A(\vec{x}, t, p)$. For this approximate set of equations the conservation laws generally are expected to become only *approximate*. Such approximate nature of conservation laws may be well acceptable theoretically as its accuracy precisely corresponds to that of the approximation. Nevertheless, both from a principle perspective and also from a practical point of view this situation is less satisfactory.

In this work [10] we investigated the quantum kinetic equations in the form originally derived by Kadanoff and Baym. The key point is to do a systematic first-order gradient expansion of all gradient terms even those internally present in the self-energies. Through a careful investigation of all gradient terms we could in fact prove that the quantum kinetic equations possess the generic feature of exact conservation laws at the expectation value level.

The conserved currents and the energy-momentum tensor take the original Noether form [8] ($X = (\vec{x}, t)$)

$$J^\mu(X) = \int \frac{d^4p}{(2\pi)^4} p^\mu f(X, p) A(X, p), \quad (1)$$

$$\Theta_{\text{loc}}^{\mu\nu}(X) = \int \frac{d^4p}{(2\pi)^4} v^\mu p^\nu f(X, p) A(X, p) + g^{\mu\nu} (\mathcal{E}_{\text{loc}}^{\text{int}}(X) - \mathcal{E}_{\text{loc}}^{\text{pot}}(X)) \quad (2)$$

now however in the so called local form, i.e. void of any gradient corrections. For the energy–momentum tensor the first term accounts for the single particle part which by itself overcounts the interaction energy. This is compensated by gradient terms which assemble to the difference between interaction energy density and single-particle potential energy density, $\mathcal{E}_{\text{loc}}^{\text{int}}(X) - \mathcal{E}_{\text{loc}}^{\text{pot}}(X)$, both obtained from the same Φ -functional in the local approximation as the self-energies driving the gradient expanded KBE.

In order to preserve the exact conserving property, a few conditions have to be met. First, the original KBE should be based on a Φ -derivable approximation scheme that guarantees that the KBE themselves are conserving [8, 9]. Second, all possible memory effects due to internal vertices within the self-energy diagrams are also consistently expanded to first-order gradients. Finally it is important that after the gradient expansion no further approximations are applied that violate the balance between different first-order gradient terms.

The presence of exact conservations puts the Kadanoff–Baym formulation of quantum transport on the level of generic phenomenological equations. They offer a phenomenological approach to the dynamical description of particles with broad damping widths, such as resonances, with built-in consistency and exact conservation laws. For practical simulations of complex dynamical systems this approach may even be applied in cases, where the smallness of the gradients can not always be guaranteed.

References

- [1] L.P. Kadanoff and G. Baym, *Quantum Statistical Mechanics*, Benjamin, 1962.
- [2] Yu.B. Ivanov, J. Knoll, and D.N. Voskresensky, *Nucl. Phys. A* **672** (2000) 313.
- [3] M. Effenberger, U. Mosel, *Phys. Rev. C* **60** (1999), 51901.
- [4] W. Cassing and S. Juchem, *Nucl. Phys. A* **665** (2000), 377; **672** (2000), 417.
- [5] S. Leupold, *Nucl. Phys. A* **672** (2000), 475.
- [6] Yu. B. Ivanov, J. Knoll, H. van Hees and D. N. Voskresensky, e-Print Archive: nucl-th/0005075; *Yad. Fiz.* **64** (2001).
- [7] H. van Hees, and J. Knoll, *Nucl. Phys. A* **683** (2001), 369.
- [8] Yu.B. Ivanov, J. Knoll, and D.N. Voskresensky, *Nucl. Phys. A* **657** (1999) 413.
- [9] G. Baym, *Phys. Rev.* **127** (1962) 1391.
- [10] J. Knoll, Yu.B. Ivanov, and D.N. Voskresensky, nucl-th/0102044, submitted to *Ann. Phys. (NY)*

Production of vector mesons in pion nucleus reactions^{B,G}

W.Schön, R.Schneider, W.Weise
Physik-Department TU-München

Model independent constraints from QCD sum rules connect the vector meson mass with the gap Δ between the $n\pi$ continuum and the $\langle q\bar{q} \rangle$ vacuum state. At normal nuclear density, Δ is expected to be reduced by about 15% as a consequence of the restauration of chiral symmetry [1, 2]. In this work, the spectral functions of the vector mesons calculated in infinite matter are combined with a Monte Carlo simulation of π^- induced production and propagation of vector mesons inside nuclei.

The self-energy of the vector mesons in matter Π_v is based on the low density approximation which connects the vacuum self-energy Π_0 with the meson nucleon scattering matrix T_{vN} : $\Pi_v(\omega, \vec{q}, \rho) = \Pi_0(\omega, \vec{q}) - \rho T_{vN}(\omega, \vec{q})$. The potential (and therefore the mass shift) depends to leading order linearly on the baryon density ρ : $2\omega U = \Pi_v(\omega, \vec{q}, \rho) - \Pi_0 = \rho T_{vN}(\omega, \vec{q})$. The resulting spectral functions for infinite matter at $\rho = \rho_0$ show a different behavior for the ω - and the ρ meson. While the pole mass of the ρ meson is shifted only slightly, its width is heavily influenced by $\rho N \rightarrow \pi N$, $\rho N \rightarrow \pi \Delta \rightarrow \pi \pi N$ and $\rho N \rightarrow \omega N \rightarrow \pi \pi \pi N$ scattering. Effectively the ρ -meson is dissolved in the nuclear medium. The ω -meson pole mass is shifted by about -80 MeV/c² and the width is broadened from 8 to 40 MeV/c². However at $\rho = \rho_0$ the ω -meson still keeps its quasi-particle character. The MC-simulation is based on measured cross sections for $\pi^- + p \rightarrow \rho, \omega, \phi + n$ reactions. The absorption channels are calculated via detailed balance. The baryon density distribution of the Pb nucleus is based on measured charge distributions. The fermi motion of the nucleons is taken into account. With an elementary ω -meson cross section of 2.5 mb ($p_{\pi^-} = 1.3$ GeV/c) one could expect $Z_{Pb} * 2.5 \approx 200$ mb for a Pb nucleus. However the effective cross section results in only 33 mb. Because of the strong interaction of π^- with nuclear matter, only the hemisphere of the nucleus facing the beam takes part in the reaction (shadowing, Fig. 1). The mesons are produced with vacuum pole mass. In case of decay the mass of the meson is sampled according to the local baryon density at this "freezeout" point based on the spectral functions for infinite matter. The sampling is done in accordance with energy conservation. The spectral functions in the finite system (Fig. 2) are obtained by integration over the probability distribution of the meson decays. The majority of the ω -mesons decay outside the Pb nucleus and produce a narrow structure. The contributions from the inner part of the nucleus (full shift of the ω -meson mass) and the surface (reduced shift) increase the broadening of ω -mesons from 40 to about 80 MeV/c². This additional broadening is a consequence of the finite size of the system. The reaction $\pi^- Pb$ seems to be a promising experiment to probe the in-medium spectral distribution of vector mesons. The predicted dilepton spectra could be measured with the HADES spectrometer [3]. In Fig. 2 the HADES resolution is taken into account.

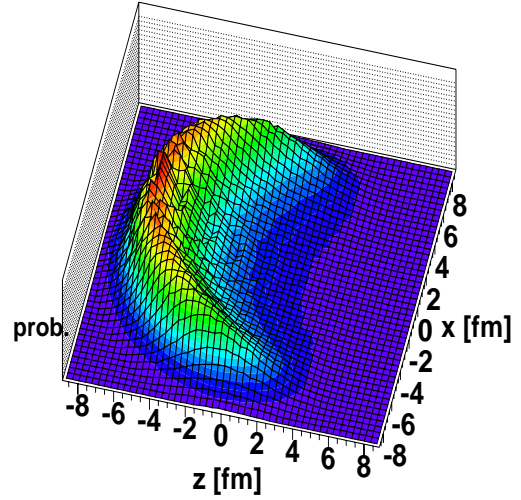


Figure 1: Spatial probability distribution of meson creation for $\pi^- Pb$ at $p_{\pi}=1.3$ [GeV/c].

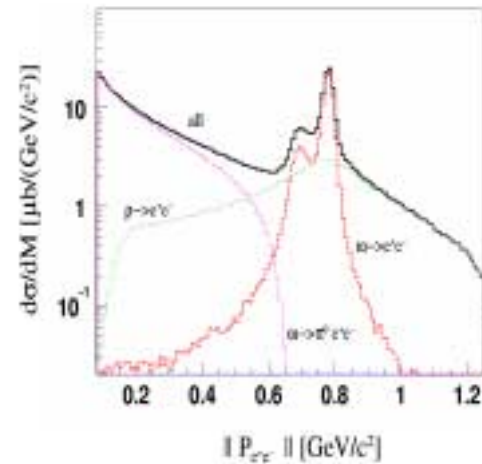


Figure 2: ρ - and ω -meson contributions to the dilepton spectra for $\pi^- Pb$ at $p_{\pi}=1.3$ [GeV/c].

Below the η mass strong contributions from η Dalitz and other channels are expected. In the mass region of the (shifted) ω peak both πN Bremsstrahlung [4] and combinatorial background from π Dalitz decay [5] contribute still below the ρ -meson contribution.

References

- [1] F.Klingl and W.Weise EPJ A4 (1999) 225
- [2] E.Marco and W.Weise Phys. Lett. B482 (2000) 87
- [3] J.Fries et.al. Nucl. Phys A654,(1999) 268
- [4] W.Cassing et.al. Phys. Rep. 308, 65 (1999)
- [5] W.Schön et.al. Act. Phys. Pol B27 Number 11 (1996)

Modifications in resonance life times and cross sections in a test-particle description of off-shell processes in transport theory

A.B. Larionov*, S. Leupold, U. Mosel
University of Giessen

For the understanding of heavy-ion collisions semi-classical transport theory has become an indispensable tool. While former works have focused their attention more or less on the quasi-particle regime the extension of the formalism to off-shell phenomena has become a topic of growing interest in the last few years since it has been realized that the collision rates present in high energetic nucleus-nucleus collisions typically are so large that an on-shell approximation seems to be inappropriate. In addition, the resonances excited during the reaction may have large decay widths. Therefore, a representation of these states by stable particles may not be a proper approximation. The usual approach to solve a transport equation is the representation of the phase-space density by test-particles. If not only asymptotically stable states but also resonances are simulated by test-particles, one has to attribute to those ‘resonance test-particles’ finite life times and arbitrary invariant masses (chosen according to their spectral distribution), i.e. the generalized test-particle representation is given by $\sum_i \delta^{(3)}(\vec{x} - \vec{x}_i(t)) \delta(p_0^2 - E_i^2(t)) \delta^{(3)}(\vec{p} - \vec{p}_i(t))$. Note that here in contrast to the quasi-particle approximation the test-particles are allowed to have arbitrary energies. The question which (in general energy- or mass-dependent) life time has to be attributed to the resonance test-particles is under present discussion. The commonly used recipe is to take the inverse of the decay width Γ of the resonance, evaluated for the respective invariant mass. Near threshold the width becomes small due to the available phase-space. Hence the life time — if identified with the inverse width — becomes large. In [1] it was suggested to rather calculate the life time from the time delay that the particles suffer which form the resonance. This time delay is given by the energy derivative of the scattering phase shift of these particles: $\tau = \partial\delta/\partial p_0$. This quantity vanishes near threshold. Hence the two expressions for the life time show a completely different behavior as functions of the invariant mass of the resonance as shown in Fig. 1 for the $\Delta(1232)$ resonance. Recently a novel approach to solve these questions has been presented [2, 3]. It has been shown there that the life time of an off-shell test-particle is indeed given by $\tau = \partial\delta/\partial p_0$. In addition, the cross section for any collision which involves an off-shell test-particle in the incoming channel is subject to an in-medium modification: the cross section has to be divided by $r = 2\sqrt{s}\Gamma\mathcal{A}(1-K)$ where Γ is the total width of the particle, \mathcal{A} its spectral function and $1-K$ a renormalization factor (cf. [2, 3] for details).

To test the ideas above, we applied the BUU model in version [4] with the resonance production/absorption quenching [5]. The most sensitive observable for the Δ -resonance life time modifications turns out to be the invariant mass spectrum of the correlated proton-pion pairs.

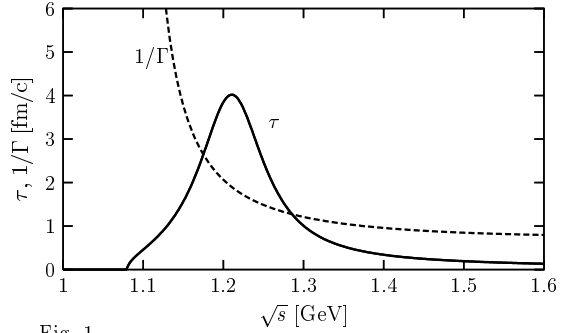


Fig. 1

Fig. 2 shows the invariant mass (p, π^+) spectra for a central Au+Au collision at 1.06 AGeV calculated without life time modifications (solid line), with modified Δ -resonance life time only (dashed line) and with both modified Δ -resonance life and $N\Delta \rightarrow NN$ cross section (dotted line). The life time modification leads to a sharper peaked spectrum at $M \simeq 1.2$ GeV due to longer life time of the Δ -resonances near the pole mass (Fig. 1). An additional modification of the $N\Delta \rightarrow NN$ cross section produces an even more sharp spectrum, since the absorption of the Δ -resonances near the pole mass gets reduced. Thus we conclude that the resonance life time modifications somewhat increase the deviation of the BUU calculation with the data [6] on the spectrum of the (p, π^+) pairs. Further studies will show if this effect could be counterbalanced by the off-shellness of the produced pions (work in progress).

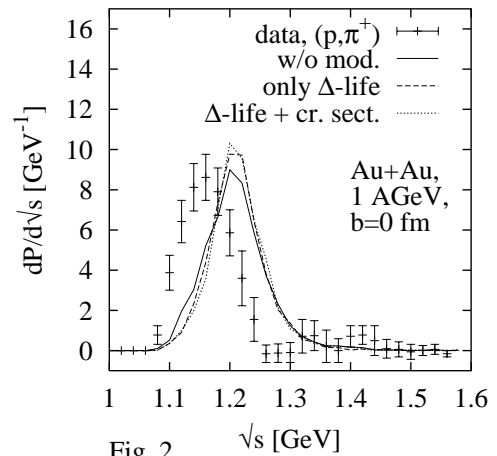


Fig. 2

References

- [1] P. Danielewicz, S. Pratt, Phys. Rev. **C53**, 249 (1996).
- [2] S. Leupold, Nucl. Phys. **A672**, 475 (2000).
- [3] S. Leupold, nucl-th/0008036, subm. to Nucl. Phys. A.
- [4] M. Effenberger, E.L. Bratkovskaya, U. Mosel, Phys. Rev. **C60**, 044614 (1999).
- [5] A.B. Larionov, W. Cassing, S. Leupold, U. Mosel, contr. to this Annual Report.
- [6] M. Eskef et al., Eur. Phys. J. **A3**, 335 (1998).

*On leave of absence from RRC "I.V. Kurchatov Institute", 123182 Moscow, Russia

Strange Particle Production and Equilibration at SIS energies within a Semiclassical Off-shell Transport Approach

W. Cassing, S. Juchem
University of Giessen

Recently we have formulated a novel transport approach that incorporates the propagation of particles off the mass-shell [1]. It goes beyond the conventional transport description within the on-shell quasiparticle limit to propagate particles with a finite lifetime by means of a dynamical spectral function. This spectral function is directly determined by the spacetime and momentum-dependent imaginary part of the particle self-energy. By this procedure it is guaranteed, that the actual spectral function is consistently adjusted to the scatterings and decays of the particle in the nuclear medium as well as in vacuum.

Within this off-shell transport approach we have studied strange meson production in the SIS energy regime. When treating baryons as well as antikaons off-shell we obtain an increase by a factor of about two for the production of K^- mesons in comparison to the on-shell calculation for $Ni + Ni$ at 1.8 A GeV (Fig. 1). This enhancement arises since antikaons couple strongly to nucleons such that they achieve a considerable collision width in the nuclear medium which leads to an effective lowering of their production threshold. So the antikaons might be produced at subthreshold energies and enhance the final K^- -yield when becoming asymptotically on-shell. The inclusion of the off-shell propagation therefore gives a (partial) explanation for the high K^- abundancy that has been measured by the FRS, KaoS and FOPI Collaborations [2,3]. The data are still underestimated by the off-shell calculations that have been performed without any potentials for the strange mesons. Thus antikaon potentials will still be necessary to get a full description of the experimental results. We have also investigated the production of K^+ mesons in

to nucleons [1b].

Furthermore, we have studied equilibration phenomena in the off-shell transport approach. For this aim we have confined the system to a box in coordinate space with periodic boundary conditions (using a density of $\rho = \rho_0$). We find that the off-shell generalization has practically no influence on the equilibration time of the nuclear system for various bombarding energies up to 1 A GeV [1c].

In order to study the equilibrium properties we compare the results of our transport (box) calculations with a simple statistical model for an ideal hadron gas. All hadron species that are propagated in the transport calculation (N, Δ, π) are also taken into account in the statistical model within the grand canonical ensemble. In Fig. 2 we

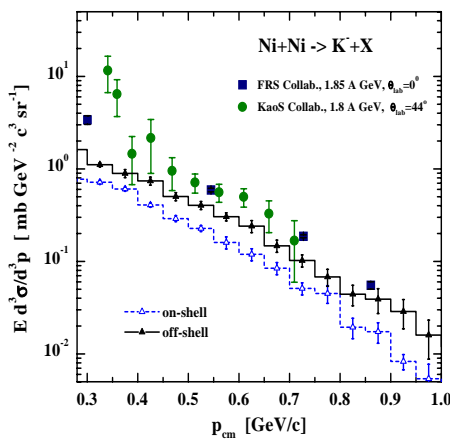


Figure 1: The inclusive spectra of K^- for $Ni + Ni$ at 1.8 A GeV within the off-shell transport approach (solid histogram, full triangles) and in the on-shell limit (dashed histogram, open triangles). The data are from [2] for $\theta_{lab} = 0^\circ$ (squares) and from [3] for $\theta_{lab} = 44^\circ$ (circles).

the same reaction, however, find only a small enhancement within the off-shell treatment relative to the on-shell limit which should be attributed to the weak coupling of kaons

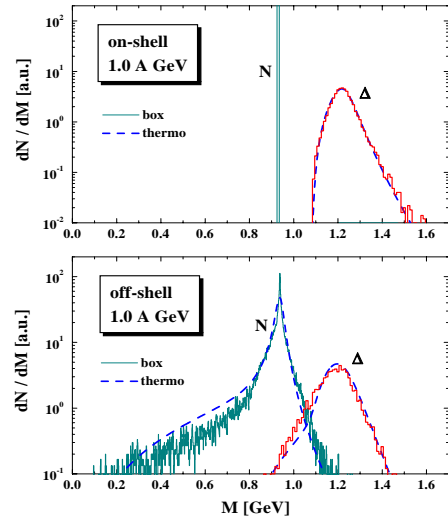


Figure 2: Differential distribution in mass for nucleons and Δ resonances for a bombarding energy 1 A GeV at $\rho = \rho_0$.

show the differential distributions in mass for nucleons and Δ resonances in the long time limit of the transport (box) calculations in comparison to the statistical model (dashed lines) for a bombarding energy of 1 A GeV. We find that the transport theoretical treatment yields nearly the same distributions in mass as the thermodynamical model, when for the latter the same spectral functions as in the transport calculation are employed. A temperature of 97 MeV (deduced from a transverse mass analysis of the particle spectra) has been used here. This result indicates that the actual realization of the off-shell dynamics guarantees the correct stationary solution in the long time limit.

References

- [1] W. Cassing, S. Juchem, Nucl. Phys. A 665 (2000) 385; Nucl. Phys. A 672 (2000) 417; Nucl. Phys. A 677 (2000) 445.
- [2] A. Schröter et al., Z. Phys. A 350 (1994) 101.
- [3] P. Senger et al., Acta Phys. Pol. B27 (1996) 2993.

Probing the nuclear equation of state by K^+ production in heavy ion collisions

C. Fuchs, Amand Faessler, E. Zabrodin, Yu-Ming Zheng
Institut für Theoretische Physik, Universität Tübingen

From the very beginning kaons have been considered as one of the best probes to study dense and hot nuclear matter formed in relativistic heavy ion collisions. In particular at incident energies below the corresponding production thresholds in free space K^+ mesons are created in the early and high density phase of such reactions and – due to strangeness conservation – are not reabsorbed by the nuclear environment. Furthermore, there exist strong evidences that kaons change their properties inside the nuclear medium as predicted by effective chiral models. The aim of the present work is to study if decisive information on the nuclear EOS can be extracted from subthreshold kaon production by new high precision data [1]. The KaoS Collaboration has performed systematic measurements of the K^+ production far below threshold in heavy ($Au + Au$) and light ($C + C$) systems [2]. Looking at the ratios built from heavy and light systems possible uncertainties which might still exist in the theoretical calculations should cancel out to a large extent which allows to draw reliable conclusions. Furthermore, far below threshold the kaon production is a highly collective process and a particular sensitivity to the compression of the participant matter is expected. The present investigations are based on the Quantum Molecular Dynamics (QMD) transport model. For the nuclear EOS we adopt soft and hard Skyrme forces corresponding to a compression modulus of $K=200$ MeV and 380 MeV, respectively, and with a momentum dependence adjusted to the empirical optical nucleon-nucleus potential.

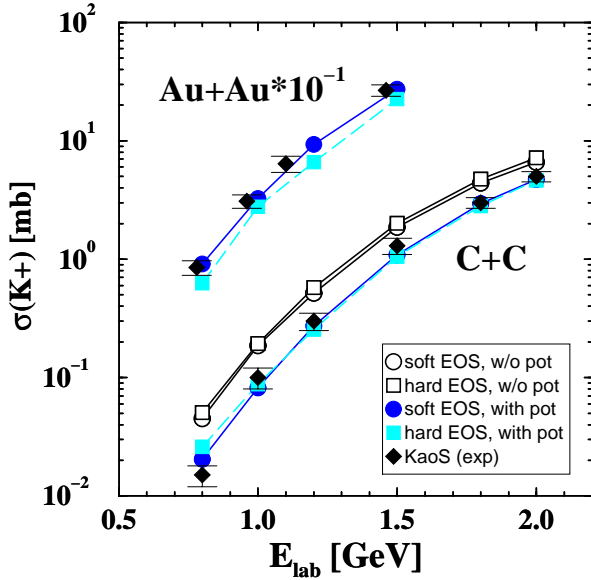


Figure 1: Excitation function of the K^+ cross section in $C+C$ and $Au+Au$ reactions. The calculations are performed with in-medium kaon potential and using a hard/soft nuclear EOS. For $C+C$ also results without in-medium kaon potential are shown.

In Fig. 1 the K^+ excitation function for $Au+Au$ and $C+C$ reactions starting from 0.8 A-GeV which is far below threshold ($E_{thr} = 1.58$ GeV) are shown. The calculations are performed for a soft/hard EOS including the in-medium kaon potential. For both systems the agreement with the KaoS data [3, 2] is very good when a soft EOS is used. In the large system

there is a visible EOS effect which is absent in the light system. To estimate the influence of the in-medium kaon potential for $C+C$ also calculations without potential are shown. Already in the light system the K^+ yield is reduced by about 50% by the influence of the potential which is essential to reproduce the yields [3]. The comparison to the new KaoS data [2] is made

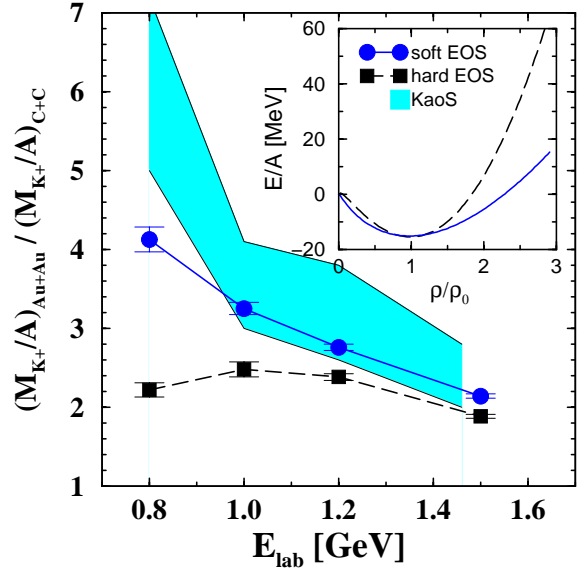


Figure 2: Excitation function of the ratio R of K^+ multiplicities obtained in inclusive $Au+Au$ over $C+C$ reactions. The calculations are performed with in-medium kaon potential and using a hard/soft nuclear EOS and compared to the experimental range of R (shaded area) given by the data from the KaoS Collaboration [2].

in Fig. 2. Here only calculations including the kaon potential are shown since it is already clear from Fig. 1 that without the potential one is not able to reproduce the experimental yields. The calculations are performed under minimal bias conditions with $b_{max} = 11$ fm for $Au+Au$ and $b_{max} = 5$ fm for $C+C$ and normalised to the experimental reaction cross sections [3, 2]. Both calculations show an increase of R with decreasing incident energy down to 1.0 A-GeV. However, this increase is much less pronounced using the stiff EOS. In the latter case R even drops for 0.8 A-GeV whereas the soft EOS leads to an unrelieved increase of R . Using the light system as reference frame there is a visible sensitivity on the EOS. Results for the K^+ excitation function in $Au+Au$ over $C+C$ reactions as measured by the KaoS Collaboration, strongly support the scenario with a soft EOS. The ratio itself is rather independent on the existence of the in-medium potential, but the potential is necessary to reproduce the total yields.

References

- [1] C. Fuchs, A. Faessler, E. Zabrodin, Y.-M. Zheng, Phys. Rev. Lett. (2001) in press.
- [2] C. Sturm *et al.*, Phys. Rev. Lett. **86**, 39 (2001).
- [3] F. Laue *et al.*, Phys. Rev. Lett. **82**, 1640 (1998).

Kaon Production via High Mass Resonances in UrQMD^{B,G}

H. Weber, S.A. Bass[†], S. Soff[§], H. Stöcker and W. Greiner

Institut für Theoretische Physik, Universität Frankfurt am Main, Germany

The investigation of strange matter in heavy ion collisions is of great interest, as the s and \bar{s} -quarks are not present in the initial projectile and target matter. Therefore the measurement of strange particles might yield deep insight into the reaction dynamics during the high density phase.

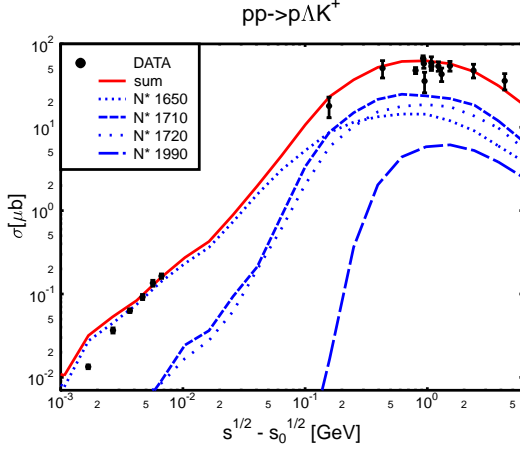


Figure 1: $pp \rightarrow p\Lambda K^+$ cross section in UrQMD compared to data.

For our investigation, we use the Ultrarelativistic Quantum Molecular Dynamics model (UrQMD) [1]. UrQMD provides a good description of NN and A+A collisions over a wide range of energies from a few hundred MeV/A up to hundreds of GeV/A. The production threshold for the lightest strange particle (K^+) via the process $NN \rightarrow N\Lambda K^+$ is 1.58 GeV. Particularly for SIS energies, the correct description of the production cross section near the threshold is very important. In contrast to most other models, UrQMD treats the elementary K^+ production via two-step processes

$$pp \rightarrow pB^* \rightarrow p\Lambda K^+, \quad pp \rightarrow pB^* \rightarrow p\Sigma K$$

B^* are the high mass resonances N_{1650}^* , N_{1710}^* , N_{1720}^* , N_{1990}^* and Δ_{1920}^* . For the decay into the hyperon-kaon channel we use the experimental branching ratios, where available.

Figure 1 shows the cross section for the reaction $pp \rightarrow p\Lambda K^+$ as a function of energy above threshold. The dotted lines are contributions of the five resonances to the total cross section (solid line). With this approach we are able to describe the experimental data (dots) reasonably well, even a few MeV above the threshold (COSY data [2])

The $pp \rightarrow p\Sigma^0 K^+$ and the $pp \rightarrow p\Sigma^+ K^0$ channel can be described as well with this approach. Figure 2 shows these channels in UrQMD compared to data.

For higher collision energies, kaon production via string fragmentation becomes important. Figure 3 shows an excitation function of the K^+ to K^- ratio for central Pb+Pb

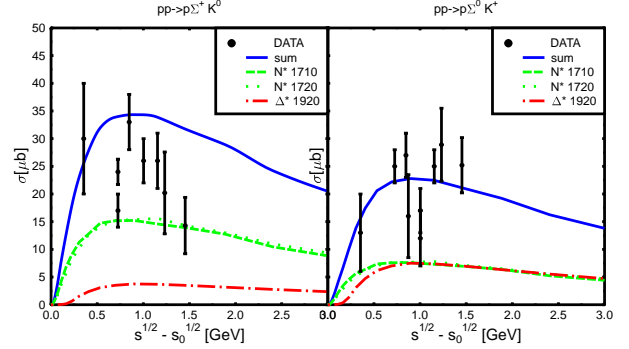


Figure 2: $pp \rightarrow p\Sigma^+ K^0$ and $pp \rightarrow p\Sigma^0 K^+$ cross section in UrQMD compared to data.

events calculated with the UrQMD model. The dots are experimental data from E802, E866/E917 [3] and NA49 [4, 5]. The model shows a good overall agreement with the experiments, except for the preliminary 40 GeV measurement from NA49 [5] which is slightly underestimated. Interestingly this good agreement for the K^+ to K^- ratio with the data can be obtained without invoking any medium dependent effects, such as in-medium masses.

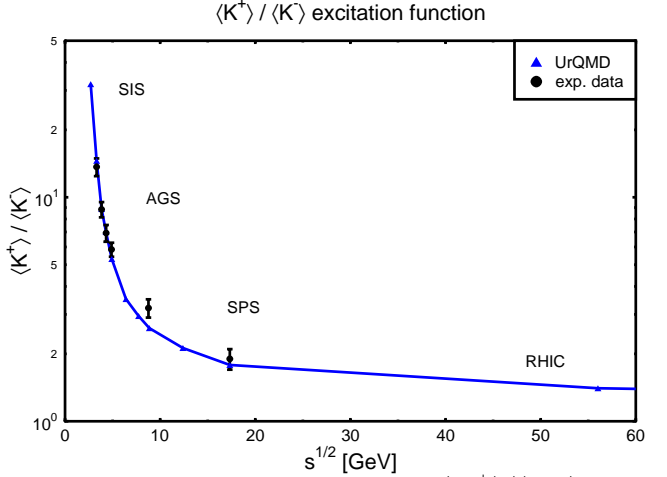


Figure 3: Excitation function of the $\langle K^+ \rangle / \langle K^- \rangle$ ratio in central Pb+Pb or Au+Au collisions compared to data from E802, E866, E917 and NA49

References

- [1] S. A. Bass *et al.*, Prog. Part. Nucl. Phys. **41**, 225 (1998)
- [2] J. T. Balewski *et al.*, Phys. Lett. B **420**, 211 (1998)
- [3] L. Ahle *et al.* [E866 Collaboration], Phys. Lett. B **490**, 53 (2000) [nucl-ex/0008010].
- [4] J. Bachler *et al.* [NA49 Collaboration], Nucl. Phys. A **661**, 45 (1999).
- [5] C. Blume *for the NA49 collaboration*, QM2001, to appear in the proceedings.

[†] Duke University and RIKEN BNL Research Institute, USA

[§] LBL Berkeley, USA (Lynen-Fellow of the Humboldt-Foundation)

Collective flow in heavy ion collisions from SIS to SPS energies

E. Zabrodin, C. Fuchs, L. Bravina, and Amand Faessler, University of Tübingen

Collective effects, such as the transverse flow of particles produced in ultrarelativistic heavy ion collisions, are very important for the study of the nuclear equation of state (EOS) and for the search of a predicted transition to the quark-gluon plasma (QGP). At present the transverse flow is believed to be one of the most clear signals to detect the creation of the QGP in heavy-ion experiments. This explains the great interest of both experimentalists and theoreticians in the collective flow phenomenon [1].

The distribution of the particles in the azimuthal plane can be presented as [2]

$$\frac{dN}{d\phi} = a_0 \left[1 + 2 \sum_{n=1}^{\infty} v_n \cos(n\phi) \right], \quad (1)$$

where ϕ is the azimuthal angle between the momentum of the particle and the reaction plane. The first two coefficients, v_1 and v_2 , colloquially known as directed and elliptic flow, are the amplitudes of the first and second harmonics in the Fourier expansion of the azimuthal distribution, respectively. The directed and elliptic flow of hadrons in heavy-ion collisions is very sensitive to the EOS of the nuclear medium. The formation of small domains of a QGP phase might happen already at the SPS energies or even below. Accompanied by the hadronization this enforces a softening of the EOS due to the dropping pressure. Thus, the disappearance of the directed flow in midrapidity range can be considered as an indication of a new state of matter. This conclusion is supported by hydrodynamic simulations with and without the QGP phase.

Microscopic models, which do not imply the QGP formation, describe the dynamics of nuclear collisions at energies up to $\sqrt{s} \approx 2A$ GeV in terms of reactions between hadrons and their excited states, resonances. At higher energies additional degrees of freedom, strings, should be taken into account to describe correctly the processes of multiparticle production. We employ the quantum molecular dynamics (QMD) model [3] at the SIS energies, while at the AGS and SPS energies the quark-gluon string model (QGSM) [4] is applied. For the simulations at 1A GeV, 11.6A GeV, and 160A GeV, we choose light (S+S) and heavy (Au+Au and Pb+Pb) symmetric systems [5].

The deviations of the nucleon directed flow from the straight line behavior start to develop already at AGS energies (Fig. 1) due to the shadowing effect, which plays a decisive role in the competition between normal flow and antinflow in (semi)peripheral heavy-ion collisions. Hadrons, emitted with small rapidities at the onset of the collision in the antinflow area can propagate freely, while their counterparts will be absorbed by the flying massive spectators. The signal becomes stronger with the rise of the impact parameter and with the rise of the incident energy. In the latter case the spectators are more Lorentz-contracted and more hadrons can be emitted unscreened with small rapidities in the direction of antinflow. This effect should appear

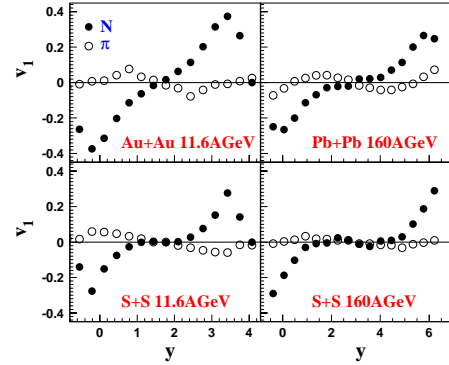


Figure 1: $v_1^{N, \pi}(y)$ in min. bias events at AGS and SPS.

in semicentral collisions with $b \leq 3$ fm at RHIC energies, and can mimic the softening of the EOS of hot and dense nuclear matter. However, the disappearance of directed flow due to shadowing is more distinct for light systems, such as S+S or Ca+Ca, while in the QGP case the effect should be more pronounced in heavy systems. Thus, one can distinguish between the two phenomena by the comparison of the directed flow of nucleons in the midrapidity range in light and heavy-ion collisions.

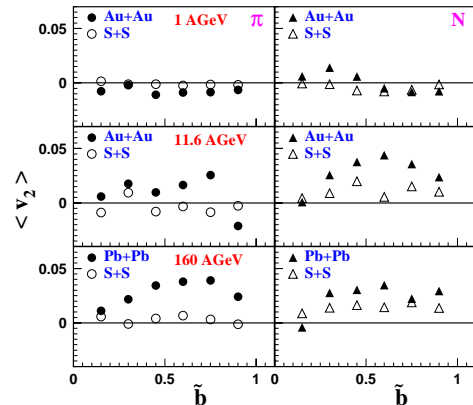


Figure 2: The mean elliptic flow of N 's and π 's in light and heavy system colliding at SIS, AGS, and SPS energies.

The elliptic flow of nucleons and pions is found to change its orientation from out-of-plane at 1A GeV to in-plane at 11.6A GeV (Fig. 2). The effect can be explained by stronger Lorentz-contraction of colliding nuclei. Also, at higher colliding energies the contracted spectators leave the reaction zone faster, thus giving space for the growth of elliptic flow in the reaction plane [5].

References

- [1] Proc. of the QM'2001 conf.: Nucl. Phys. A (in press).
- [2] S. Voloshin, Y. Zhang: Z. Phys. C 70 (1996) 665
- [3] J. Aichelin: Phys. Rep. 202 (1991) 233;
C. Fuchs et al: J. Phys. G 22 (1996) 131
- [4] N.S. Amelin et al: Phys. Rev. C 47 (1993) 2299
- [5] L. Bravina, E. Zabrodin, C. Fuchs, Amand Faessler: Phys. Lett. B 470 (1999) 27; Phys. Rev. C 61 (2000) 064902; Phys. Rev. C 62 (2001) (in press).

Microscopic Interactions and Flow in Heavy Ion Collisions^B

T. Gaitanos¹, C. Fuchs², H. H. Wolter¹, Amand Faessler²

¹Sektion Physik, Universität München, ²Inst. für Theor. Physik, Universität Tübingen

Relativistic heavy ion collisions have been extensively investigated to determine the equation-of-state (eos) of nuclear matter using phenomenological effective fields of the non-relativistic Skyrme or the relativistic Walecka type. It is found generally that a soft eos with momentum dependence can describe much of the data in the SIS energy range. It is, however, of fundamental interest to test also microscopic fields derived from NN- interactions by many-body theory. We have previously used self energies from relativistic Brueckner calculations (DB) and have shown that these satisfactorily explain the data for flow observables [1], however, only if non-equilibrium effects are considered, i.e. taking into account that the momentum distribution is not equilibrated during a large part of an energetic heavy ion collision, which changes the effective fields. The non-equilibrium effects effectively soften the eos.

However, different approximations have been used in DB calculations, which may lead to similar saturation properties and results for finite nuclei but to different behaviours for higher density and momentum. It may thus be possible to distinguish different DB models in heavy ion collisions. Here we have tested two particular DB models: one from the Groningen group (DBHM)[2], and a more recent one from the Tübingen group (DBT) [3]. The latter takes care to eliminate spurious contributions from negative energy states, and leads to a softer eos at higher densities and to less repulsion at higher momenta.

We have performed a detailed study of flow observables in $Au + Au$ collisions [4], which have been investigated extensively by the FOPI collaboration [5]. We discuss differential flow observables: stopping or longitudinal flow and transverse in-plane and out-of-plane flow. We have used the common description in terms of the Fourier coefficients of the azimuthal distributions: v_1 (flow) and v_2 (elliptic flow), as functions of the normalized rapidity $Y^{(0)}$ and the total transverse momentum $p_t^{(0)}$. As an example in fig.1 we show for forward rapidities and different fragments the flow as a function of the transverse momentum. It is seen that the two DB models yield different results and that the DBT model reproduces preliminary FOPI data [5] better, which was not so clearly seen in global observables, like the directed flow (not shown here [4]). Similar in fig.2 we show an excitation function of the elliptic flow compared to data from different sources. We see that the DBT model reproduced the data considerably better, in particular the recent FOPI data between 400 MeV and 1 GeV. Similar results are found for other flow observables: above 400 MeV the softer and less repulsive DBT model seems to be preferred, below in some cases the DBHM model has advantages.

Thus we generally find that microscopic fields succeed also to reproduce more exclusive flow variables, thus leading to a rather unified picture of nuclear fields for nuclear matter, finite nuclei and heavy ion collisions. In the more

detailed comparisons it was shown that different DB approximations can indeed be distinguished by looking at differential flow observables.

References

- [1] T. Gaitanos, C. Fuchs, H.H. Wolter, Nucl. Phys. **A650** (1999) 97.
- [2] B. ter Haar, R. Malfliet, Phys. Rep. **149** (1987) 207.
- [3] C. Fuchs, T. Waindzoeh, A. Faessler, D.S. Kosov, Phys. Rev. **C58** (1998) 2022; T. Gross-Boelting, C. Fuchs, A. Faessler, Nucl. Phys. **A648** (1999) 105.
- [4] T. Gaitanos, C. Fuchs, H.H. Wolter, A. Faessler, EPJ submitted, nucl-th/0102010.
- [5] A. Andronic, FOPI collaboration, Nucl. Phys. **A661** (1999) 333c, and references cited there.

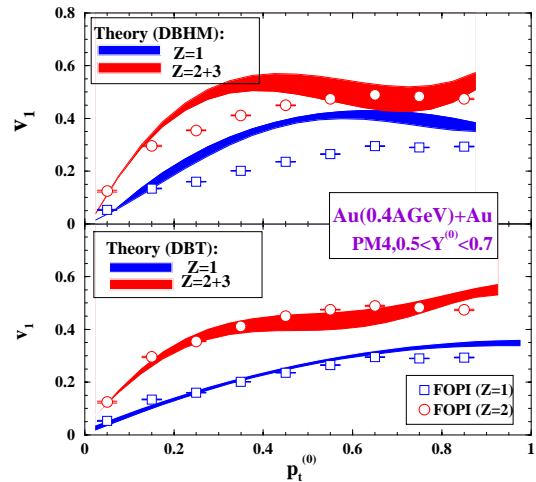


Figure 1: In-plane flow for semi-central $Au+Au$ collisions at 400 AGeV for protons and light fragments [5] in comparisons to calculations using different DB fields. Statistical errors of the calculation are indicated by bands.

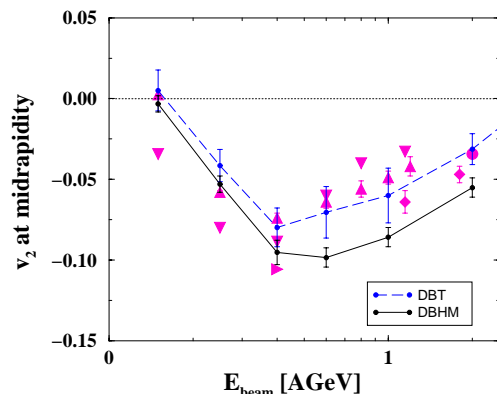


Figure 2: Energy dependence of the elliptic flow v_2 at midrapidity. The data denoted by upright triangles are taken from the FOPI collaboration [5], the others from other sources [4].

Directed Flow of Baryons in Heavy-Ion Collisions^G

Yu.B. Ivanov, E.G. Nikonov, W. Nörenberg, A.A. Shandenko and V.D. Toneev
GSI Darmstadt

The collective motion of nuclear matter observed in heavy-ion interactions is essentially caused by the pressure gradients arising during the time evolution in the collision, and hence opens a promising way for obtaining information on the equation of state (EoS) and, in particular, on a possible phase transition. We analyze the collective motion of nucleons from high-energy heavy-ion collisions within a relativistic two-fluid model for different equations of state [1].

Our consideration is essentially based on the recently proposed Mixed-Phase (MP) model [2]. The underlying assumption of the MP model is that unbound quarks and gluons *may coexist* with hadrons forming a *homogeneous* quark/gluon-hadron phase. Since the mean distance between hadrons and quarks/gluons in this mixed phase may be of the same order as that between hadrons, the interaction between all these constituents (unbound quarks/gluons and hadrons) plays an important role and defines the order of the phase transition. For the case of quarks of two light flavors at zero baryon density ($n_B = 0$), the MP model is consistent with lattice QCD data providing a continuous phase transition of the cross-over type with a deconfinement temperature $T_{dec} = 153$ MeV. In a two-phase approach based on the bag model a first-order deconfinement phase transition occurs with a sharp jump in energy density ε at T_{dec} close to the value obtained from lattice QCD. A particular feature of the MP model is that, for $n_B = 0$ the *softest point* of the EoS, defined as a minimum of the function $p(\varepsilon)/\varepsilon$, is not very pronounced and located at comparatively low values of the energy density: $\varepsilon_{SP} \approx 0.45$ GeV/fm³, which roughly agrees with the lattice QCD value. In contrast, the bag-model EoS exhibits a very pronounced softest point at large energy densities $\varepsilon_{SP} \approx 1.5$ GeV/fm³.

We have studied experimental consequences of these differences in EoS within the hydrodynamic approach. We use the 3D relativistic two-fluid model with a finite stopping power [3]. These two fluids, initially associated with target and projectile nucleons, are described by a set of hydrodynamic equations with the coupling term, which characterizes friction between the counter-streaming fluids. The friction term originates from both elastic and inelastic NN collisions and gives rise to a direct emission of mesons in addition to the thermal mesons in the fluids [3].

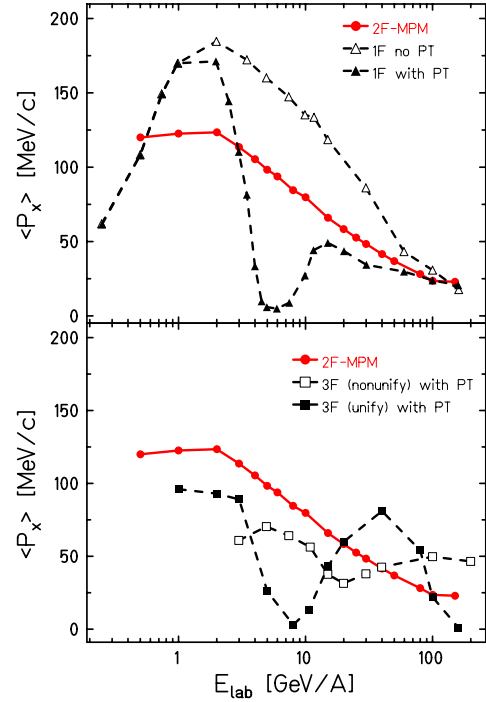
The average directed flow is defined by

$$\langle P_x \rangle = \frac{\int dp_x dp_y dy p_x \left(E \frac{d^3 N}{dp^3} \right)}{\int dp_x dp_y dy \left(E \frac{d^3 N}{dp^3} \right)},$$

where the integration in the c.m. system runs over the rapidity region $[0, y_{cm}]$. The calculated excitation functions for $\langle P_x \rangle$ of baryons within different models are shown in the figure for $Au+Au$ collisions at the impact parameter $b = 3$ fm. As shown in the upper panel, conventional one-fluid (1F) hydrodynamics for pure hadronic matter [4] results in a very large directed flow due to the inherent instantaneous stopping of the colliding matter. This instantaneous stopping is unrealistic at high beam energies. If the deconfinement phase transition (PT), based on the bag-model EoS [4], is included, the excitation function of $\langle P_x \rangle$ exhibits a deep minimum near $E_{lab} \approx 6$ A-GeV, which is a manifestation of the strong softest-point effect in the bag-model EoS.

The result of two-fluid (2F) hydrodynamics with the MP EoS noticeably differs from the one-fluid calculations. After a maxi-

mum around 1 A-GeV, the average directed flow decreases slowly and smoothly. This difference is caused by the fact that the softest point of the MP EoS is washed out for $n_B \gtrsim 0.4$ and also by dynamical reasons, i.e. the finite stopping power and direct



pion emission change the evolution pattern. The latter point is confirmed by comparison to three-fluid calculations with the bag EoS [5] plotted in the lower panel of the figure. As seen, the minimum of the directed flow excitation function, predicted by the one-fluid hydrodynamics with the bag EoS, survives in the three-fluid (nonunified) regime, but its value decreases and its position shifts to higher energies. If one applies the *unification procedure* of [5], which favors fusion of two fluids into a single one, and thus making stopping larger, three-fluid hydrodynamics gives results, which are very similar to those of the one-fluid model, and predicts in addition a bump at $E_{lab} \approx 40$ A-GeV.

Recent experimental results confirm that the excitation function of the directed baryonic flow is a smooth function in the 2-8 A-GeV energy range [6], which is in agreement with our MP EoS.

- [1] Yu.B. Ivanov, E.G. Nikonov, W. Nörenberg, A.A. Shandenko and V.D. Toneev, GSI Preprint 2000-39; nucl-th/0011004.
- [2] E.G. Nikonov, A.A. Shandenko, and V.D. Toneev, Heavy Ion Phys. **8** (1998) 89; nucl-th/9802018. V.D. Toneev, E.G. Nikonov, and A.A. Shandenko, Preprint GSI 98-30, Darmstadt, 1998.
- [3] I.N. Mishustin, V.N. Russkikh, and L.M. Satarov, Nucl. Phys. **A494** (1989) 595; Yad. Fiz. **54** (1991) 429.
- [4] D.H. Rischke, Y. Pürsün *et al.*, Heavy Ion Phys. **1** (1996) 309; D.H. Rischke, Nucl. Phys. **A610** (1996) 88c.
- [5] J. Brachmann *et al.*, Phys. Rev. C **61** (2000) 024909.
- [6] E895 Collaboration, H. Liu *et al.*, Phys. Rev. Lett. **84** (2000) 5488.

Maximum Strangeness Content in Heavy Ion Collisions Around 30 A·GeV^{B,G}

J. Cleymans, University of Cape Town, South Africa
H. Oeschler, Technische Universität Darmstadt
K. Redlich, University of Wrocław, Poland and GSI, Darmstadt

Strangeness production in heavy ion collisions at relativistic energies provides one of the key information about the reaction mechanism and could indicate the onset of new phenomena.

The attempts to describe the measured particle ratios including strange hadrons at AGS and SPS and recently also at RHIC using a strangeness fugacity are very successful [1, 2, 3, 4, 5]. However, the usual grand-canonical treatment of strangeness conservation is not sufficient, if the number of strange particles is small [6]. This requires local strangeness conservation which is done in the statistical model using the canonical formulation of strangeness conservation [7].

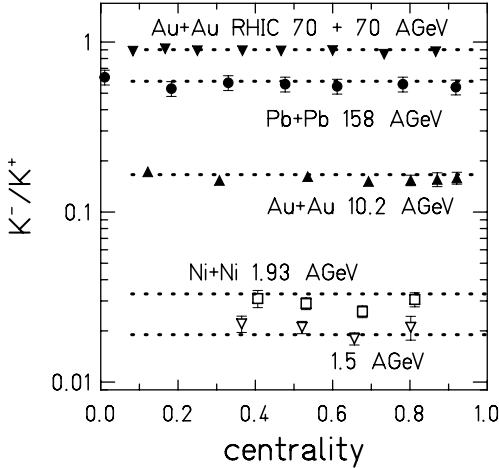


Figure 1: K^+/K^- ratio is independent of the number of participating nucleons at incident energies from 1.5 A·GeV up to RHIC energies. The dashed lines show the values of the statistical model.

The canonical approach describes the measured particle ratios at SIS energies and is able to explain the different excitation functions of K^+ and K^- in heavy ion collisions which – when plotted as a function of $\sqrt{s} - \sqrt{s}_{threshold}$ – cross around 1 A·GeV [8]. The canonical description also explains that $M(K^+)/A_{part}$ rises linearly with A_{part} as observed in Au+Au collisions at 1 A·GeV [7, 9] which is in contrast to the behavior of $M(\pi)/A_{part}$ which is independent of A_{part} . This difference is due to the volume term in the canonical description [7]

$$n_{K^+} \sim \exp\left(-\frac{E_{K^+}}{T}\right) \left[g_{\Lambda} V \int \frac{d^3p}{(2\pi)^3} \exp\left(-\frac{(E_{\Lambda} - \mu_B)}{T}\right) \right]$$

which takes care of the fact that strange particles are produced associately with another strange particle (e.g. a K^+ together with a Λ). The volume term V , however, drops out when studying the ratio of K^-/K^+ as for the produc-

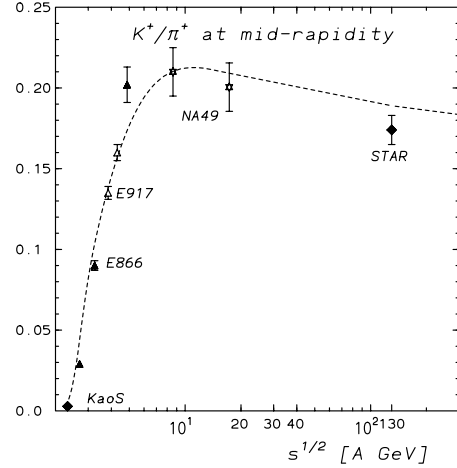


Figure 2: K^+/π^+ ratio obtained around midrapidity as a function of \sqrt{s} from the various experiments. The dashed line shows the calculation with the statistical model.

tion of K^- an analogous formula holds

$$n_{K^-} \sim \exp\left(-\frac{E_{K^-}}{T}\right) \left[g_{K^+} V \int \frac{d^3p}{(2\pi)^3} \exp\left(-\frac{E_{K^+}}{T}\right) \right].$$

Indeed, the measured ratios do not vary with the number of participating nucleons in Ni+Ni collisions [10]. This feature is found at all incident energies from 1.5 A·GeV up to RHIC energies as shown in fig. 1 [11, 12, 13]. The above result is especially interesting since between 1.5 and 2.5 A·GeV K^+ production is above while K^- production is below the corresponding NN thresholds.

The enhancement of multi-strange baryons from p+A to A+A collisions might be explainable by a transition from canonical to grand-canonical description as demonstrated in [14].

Recently, the evolution of the K^+/π^+ ratio as a function of \sqrt{s} has attracted great interest as a maximum seemed to appear around 40 A·GeV. Figure 2 shows this ratio obtained at midrapidity from SIS energies up to RHIC [12, 13, 15]. Indeed, a maximum around the data point obtained at 40 A·GeV is seen. In general, statistical-model calculations should be compared with 4π integrated results. Then the maximum is even more pronounced. The extrapolation to 4π is, however, in some cases not well established.

The fact that the statistical model based on the general freeze-out curve [16] (dashed line in Fig. 2 exhibits a maximum, too, might appear surprising. Intuitively, one expects that the fraction of strange particles increases with increasing incident energy. So, the question arises whether the maximum is caused by the distribution of strange quarks among the hadrons at freeze out or whether

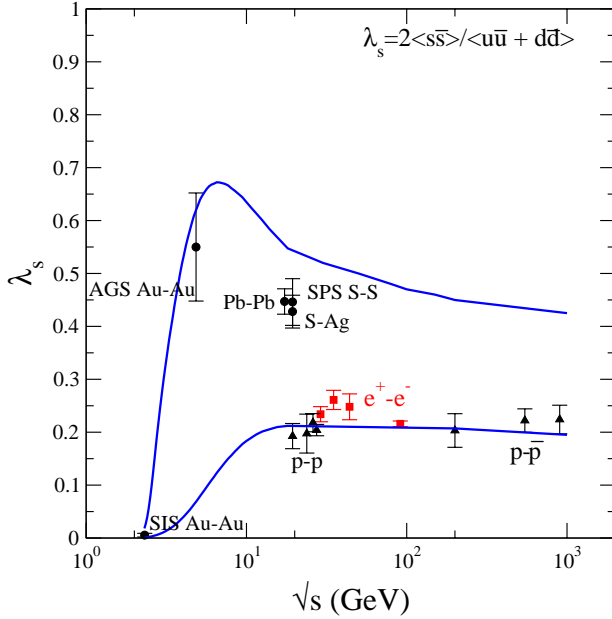


Figure 3: The Wroblewski ratio λ_s as a function of \sqrt{s} . The points refer to measured values (not measured particles species with generally rather small cross sections are added according to the statistical model). The solid lines shows the statistical model results for PbPb and pp collisions.

less strange quarks are produced in total above a certain incident energy.

To clarify this point, we study next the Wroblewski ratio [17], which is a measure of the strangeness content produced in the collisions. It is defined as

$$\lambda_s = \frac{2N(s\bar{s})}{N(u\bar{u}) + N(d\bar{d})}$$

where $N(q\bar{q})$ is the number of produced quark-antiquark pairs of the given species. The Wroblewski ratio varies from 0 at low incident energies, where no strange particle are produced to a upper limit of 1 for infinite temperature where the difference in masses can be neglected.

Figure 3 shows the values of λ_s extracted from the experimental data. The solid lines in Fig. 3 are the results of the statistical model based on the general freeze-out curve [16]. The results for pp, p \bar{p} , e⁺e⁻ are also included. The lower values of λ_s in elementary compared to AA collisions are due to canonical suppression [18]. From Fig. 3 we conclude that around 30 A-GeV the strangeness content in heavy ion collisions reaches a maximum and decreases slightly towards higher incident energies. This is evidenced in Fig. 4 which shows contour lines of constant λ_s in the $T - \mu_B$ plane. As expected λ_s rises with increasing T . With decreasing μ_B , μ_s decreases and hence λ_s . Following the general freeze-out curve, shown as full line in Fig. 4, λ_s rises quickly at SIS and AGS energies, reaches then a maximum around 30 A-GeV.

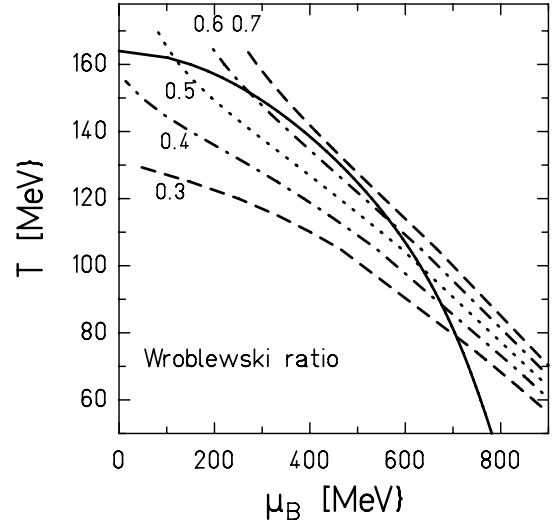


Figure 4: Lines of constant strangeness content λ_s in the $T - \mu_B$ plane together with the general freeze-out curve (full line) [16].

References

[1] J. Cleymans and H. Satz, Z. Phys. **C57** (1993) 135.

- [2] P. Braun-Munzinger, J. Stachel, J.P. Wessels and N. Xu, Phys. Lett. **B344** (1995) 43.
- [3] J. Sollfrank, J. Phys. G: Nucl. Part. Phys. **23** (1997) 1903.
- [4] P. Braun-Munzinger, I. Heppe, J. Stachel, Phys. Lett. **B465** (1999) 15.
- [5] V.D. Toneev et al., submitted to J. Phys. G: Nucl. Part. Phys.
- [6] R. Hagedorn and K. Redlich, Z. Phys. **A27** (1985) 541.
- [7] J. Cleymans, H. Oeschler and K. Redlich, Phys. Rev. **C59** (1999) 1663.
- [8] J. Cleymans, H. Oeschler and K. Redlich, Phys. Lett. **B485** (2000) 27.
- [9] M. Mang, Dissertation, University of Frankfurt, (KaoS Collaboration), 1997.
- [10] M. Menzel, Dissertation, U. Marburg, (KaoS Collaboration), 2000.
- [11] L. Ahle et al., (E802 Collaboration), Phys. Rev. **C60** (1999) 044904.
- [12] C. Blume, (NA49 Collaboration), Conference on "Quark Matter 2001", Stony Brook, Jan. 2001....
- [13] J. Harris, (STAR Collaboration), idem.
- [14] S. Hamieh, K. Redlich, A. Tounsi, Phys.Lett. **B486** (2000) 61.
- [15] L. Ahle et al., (E866/E917 Collaboration), Phys. Lett. **B476** (2000) 1.
- [16] J. Cleymans and K. Redlich, Phys. Rev. Lett. **81** (1998) 5284; Phys. Rev. **C60** (1999) 054908.
- [17] A. Wroblewski, Acta Physica Polonica **B16** (1985) 379.
- [18] F. Becattini et al., hep-ph/0002267.

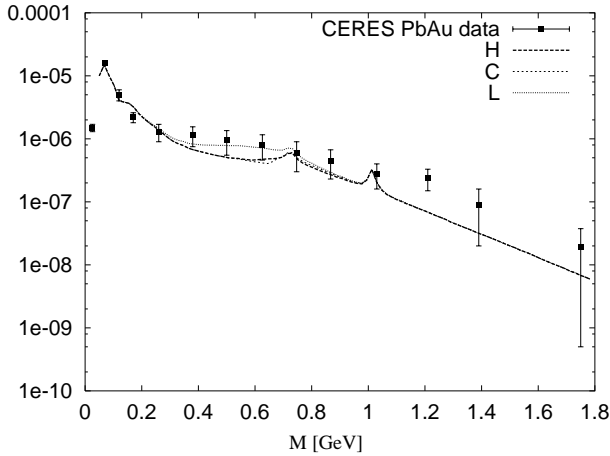
A model for dilepton production from an expanding fireball

R.A. Schneider, T. Renk and W. Weise, TU München

The search for the quark-gluon plasma (QGP) at CERN and RHIC requires a detailed understanding of the properties of hot QCD. It has become clear over the last years that a perturbative approach to thermal QCD is insufficient to calculate properties of the QGP because of the occurrence of infrared divergences and gauge dependencies of physical quantities. Even the Hard Thermal Loop resummation is likely to be applicable only for very large temperatures far outside the scope of present and future experiments. Clearly, nonperturbative input, e.g. from lattice simulations of QCD is needed to improve the situation.

Lattice results indicate that the equation of state (EOS) of a QGP can be fit with a relatively simple quasiparticle model, where quarks and gluons acquire thermal masses. For these quasiparticle masses, the ansatz $m_{th} \sim g(T)T$ is used, where the coupling $g(T)$ is fit to the lattice data. One finds effective quark masses of ~ 300 MeV.

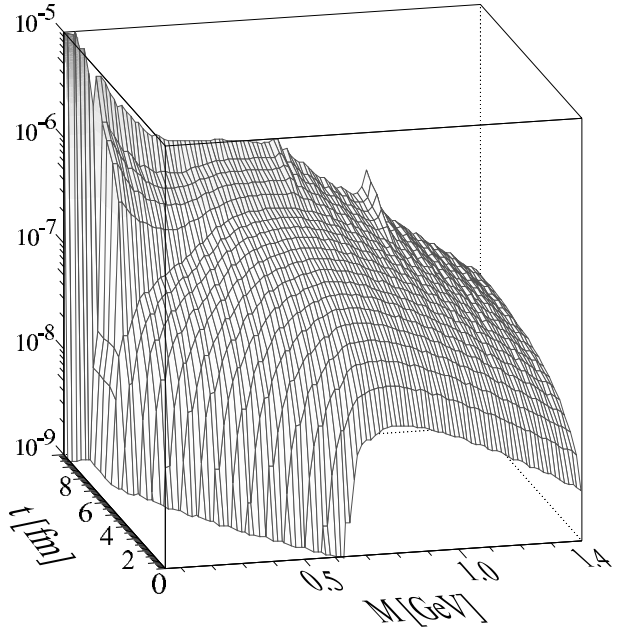
Figure 1: Different quasiparticle scenarios [2] in comparison to the CERES Pb-Au data



We employ this model for the calculation of the dilepton production in a fireball produced by a heavy ion collision and compare to data taken by the CERES collaboration at the SPS. The relevant degrees of freedom in the model above the phase transition temperature T_C are now quarks and antiquarks as thermal quasiparticles which couple to the photon with the standard quark charge, whereas all QCD corrections are already incorporated in the quasiparticle masses. Several scenarios are discussed for the quasiparticle masses close to T_C . In some models, these thermal masses appear to become heavy near T_C . On the other hand, chiral restoration at T_C would imply that the quark masses drop close to the transition. We therefore investigate three cases as to their influence on the spectra of the produced dileptons: a 'heavy' mass scenario (H), a 'light' one (L) which simulates the dropping of effective quark masses near T_C and a 'constant' one (C) in which the quasiparticle mass is kept at ~ 300 MeV at all tem-

peratures.

Figure 2: Time evolution of the dilepton production yield under CERES conditions in the 'light' quasiparticle scenario, as function of the e^+e^- invariant mass M .



We use a model specified in [1] for the expansion of the fireball. For the hadronic phase below T_C , we use an improved Vector Meson Dominance model with ρ , ϕ and ω as the dominant degrees of freedom, combined with pionic excitations carrying the same quantum numbers. We assume factorization of finite baryon density effects and thermal effects and calculate the spectral function using perturbative methods.

The result describes the CERES data nicely (Fig. 1). The simple model for the fireball allows detailed insight into the expansion including its time evolution, this is shown for the 'light' scenario in Fig. 2. The low-mass region between 0.3 - 0.7 GeV is quite insensitive to the detailed parametrization of the thermal quark masses.

In conclusion, we have shown that a quasiparticle model of the QGP phase and, at $T < T_C$, a hadronic theory with finite density and temperature effects lead to a successful description of the CERES data, whereas a purely hadronic description fails in the low invariant mass region as well as in the high mass region.

References

- [1] R.A. Schneider, and W. Weise, Eur. Phys. J. **A9** (2000) 357
- [2] R.A. Schneider, T. Renk and W. Weise; in preparation

Work supported in part by BMBF and GSI.

The color dipole approach to the Drell-Yan process

B.Z. Kopeliovich¹, J. Raufeisen², A.V. Tarasov^{1,3}
¹MPI K Heidelberg, ²LANL, ³University of Heidelberg

The high center of mass energies at RHIC and LHC will allow one to study the Drell-Yan(DY) process in a kinematical region, where the dilepton mass M is much smaller than the center of mass energy \sqrt{s} . This region is the DY analog to small Bjorken- x_{Bj} DIS. In addition, coherence effects due to multiple scattering in proton-nucleus (pA) collisions can also be studied.

We developed an approach [1, 2], in which the DY cross section is expressed in terms of the same color dipole cross section as DIS. Our approach is formulated in the rest frame of the target, where DY dilepton production looks like bremsstrahlung of massive photons, rather than parton annihilation, fig. 1. The projectile quark is decomposed into a series of Fock states,

$$|q\rangle = \sqrt{Z_2}|q_{bare}\rangle + \Psi_{\gamma^*q}|\gamma^*q\rangle + \dots \quad (1)$$

The cross section for production of a virtual photon in quark-proton scattering reads then [1, 3]

$$\frac{d\sigma(qp \rightarrow \gamma^* X)}{d\ln \alpha} = \int d^2\rho |\Psi_{\gamma^*q}(\alpha, \rho)|^2 \sigma_{q\bar{q}}(\alpha\rho). \quad (2)$$

Here, $\sigma_{q\bar{q}}$ is the cross section for scattering a $q\bar{q}$ -dipole off a proton which depends on the $q\bar{q}$ separation $\alpha\rho$. The photon-quark transverse separation is denoted by ρ and α is the fraction of the light-cone momentum of the initial quark taken away by the photon.

This approach is especially suitable to describe nuclear effects, since it allows one to apply Glauber multiple scattering theory. At very high energy, the transverse separation between γ^* and q in the $|\gamma^*q\rangle$ state is frozen during propagation through the nucleus, due to Lorentz time dilatation. Therefore, partonic configurations with fixed separations in impact parameter space are eigenstates of the interaction and one can generalize (2) to nuclear targets by replacing $\sigma_{q\bar{q}}(\alpha\rho)$ with

$$\sigma_{q\bar{q}}^A(\alpha\rho) = 2 \int d^2b \left\{ 1 - \exp\left(-\frac{\sigma_{q\bar{q}}(\alpha\rho)}{2} T(b)\right) \right\}. \quad (3)$$

Here $T(b)$ is the nuclear thickness at impact parameter b .

The frozen approximation (3) is however not well justified at presently achievable fixed target energies, where the size of the $|\gamma^*q\rangle$ -state may fluctuate on length scales of the order of the nuclear radius. In pA scattering, this leads to transitions between states which are eigenstates in proton-proton (pp) scattering. We go beyond the frozen approximation by summing over all possible trajectories of the quark in the $|\gamma^*q\rangle$ -state. This summation can be formulated in terms of the Green function for a two dimensional Schrödinger equation with an imaginary potential proportional to $\sigma_{q\bar{q}}(\alpha\rho)$ [3, 4]. In the limit of very high energy of the projectile quark, one recovers the frozen approximation (3). The formulae are however too complicated to be displayed here.

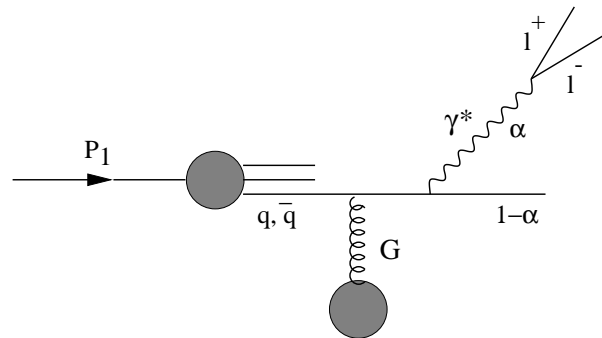


Figure 1: In the target rest frame, DY dilepton production looks like bremsstrahlung. A quark or an antiquark inside the projectile hadron scatters off the target color field and radiates a massive photon, which subsequently decays into the lepton pair. The photon can also be radiated before the quark hits the target.

Before calculating nuclear effects, we checked that the dipole approach is in agreement with DY data from pp collisions. We are able to reproduce E772 data well, without K factor [5]. The transverse momentum distribution of DY pairs in pp collisions is also calculated. The result does not diverge at zero transverse momentum due to the saturation of the dipole cross section at large separations. Note that first order pQCD leads to a divergent result.

The shadowing for DY in pA collisions at large Feynman- x_F measured at FNAL is then also well reproduced [4]. Nuclear effects on the transverse momentum distribution of the pairs are studied, too. While shadowing is predicted for dileptons with low transverse momenta, an enhancement at intermediate transverse momentum $q_\perp \sim 2$ GeV is expected. Nuclear effects vanish at very large q_\perp . For pA collisions at RHIC energies, considerable shadowing of DY dileptons is predicted for the whole x_F -range.

References

- [1] B.Z. Kopeliovich, proc. of the workshop Hirschegg '95: Dynamical Properties of Hadrons in Nuclear Matter, Hirschegg January 16-21, 1995, ed. by H. Feldmeyer und W. Nörenberg, Darmstadt, 1995, p. 102 (hep-ph/9609385).
- [2] S. J. Brodsky, A. Hebecker, and E. Quack, Phys. Rev. **D55** (1997) 2584.
- [3] B.Z. Kopeliovich, A. Schäfer and A.V. Tarasov, Phys. Rev. **C59** (1999) 1609, extended version in hep-ph/9808378.
- [4] J. Raufeisen, Ph.D. thesis, hep-ph/0009358.
- [5] B.Z. Kopeliovich, J. Raufeisen and A.V. Tarasov, hep-ph/0012035, submitted to Phys. Lett. B.

Particle ratios in Pb+Pb at SPS in a chiral $SU(3) \times SU(3)$ model^{B,G}

D. Zschesche^a, C. Beckmann^a, K. Balazs^a, S. Schramm^a, J. Schaffner-Bielich^b

H. Stöcker^a, W. Greiner^a

^a *Institut für Theoretische Physik J.W. Goethe Universität, D-60054 Frankfurt am Main*

^b *Riken BNL Research Center, Brookhaven National Lab, Upton, New York 11973*

Ideal gas model calculations have been used for a long time to calculate particle production in relativistic heavy ion collisions, (see e.g. [1, 2] and references therein). Fitting the particle ratios as obtained from those noninteracting gas calculations to the experimental measured ratios at SIS, AGS and SPS for different energies and different colliding systems yields a curve of chemical freeze-out in the $T - \mu$ plane. Now the question arises, how much the deduced temperatures and chemical potentials depend on the model employed. Especially the influence of changing hadron masses and effective potentials should be investigated, as has been done for example in [3, 4, 5, 6]. This is of special importance for the quest of a signal of the formation of a deconfined phase, i.e. the quark-gluon plasma. As deduced from lattice data [7], the critical temperature for the onset of a deconfined phase coincides with that of a chirally restored phase. Chiral effective models of QCD therefore can be utilized to give important insights on signals from a quark-gluon plasma formed in heavy-ion collisions.

We compare experimental measurements for Pb+Pb collisions at SPS with the results obtained from a chiral $SU(3) \times SU(3)$ model [6, 8]. This effective hadronic model predicts a chiral phase transition at $T \approx 150$ MeV. Furthermore the model predicts changing hadronic masses and effective chemical potentials, due to strong scalar and vector fields in hot and dense hadronic matter, which are constrained by chiral symmetry.

In [2] the noninteracting gas model was fitted to particle ratios measured in Pb+Pb collisions at SPS. The lowest χ^2 is obtained for $T = 168$ MeV and $\mu_q = 88.67$ MeV. Using these values as input for the chiral model leads to dramatic changes due to the changing hadronic masses in hot and dense matter [6] and therefore the freeze-out temperature and chemical potential have to be readjusted to account for the in-medium effects of the hadrons in the chiral model. We call the best fit the parameter set that gives a minimum in the value of χ^2 , with $\chi^2 = \sum_i \frac{(r_i^{exp} - r_i^{model})^2}{\sigma_i^2}$. Here r_i^{exp} is the experimental ratio, r_i^{model} is the ratio calculated in the model and σ_i represents the error in the experimental data points as quoted in [2]. In all calculations μ_s was chosen such that the overall net strangeness f_s is zero. The best values for the parameters are $T = 144$ MeV and $\mu_q \approx 95$ MeV. While the value of the chemical potential does not change much compared to the noninteracting gas calculation, the value of the temperature is lowered by more than 20 MeV. Using the best fit parameters a reasonable description of the particle ratios used in the fit procedure can be obtained (see fig.1, data from [2]).

This shows, that in spite of the strong assumption of

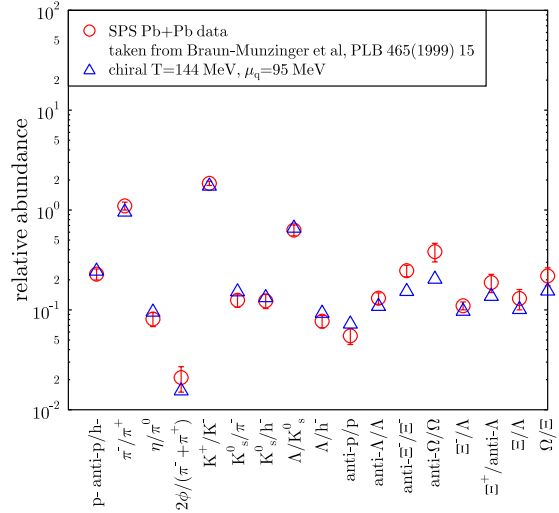


Figure 1: Particle ratios as predicted by the chiral $SU(3) \times SU(3)$ model ($T = 144$ MeV and $\mu_q \approx 95$ MeV, $f_s = 0$) compared to SPS Pb+Pb data (taken from [2]).

thermal and chemical equilibrium the obtained values for T and μ differ significantly depending on the underlying model, i.e. whether and how effective masses and effective chemical potentials are accounted for. Note that we assume implicitly, that the particle ratios are determined by the medium effects and freeze out during the late stage expansion - no flavor changing collisions occur anymore, but the hadrons can take the necessary energy to get onto their mass shell by drawing energy from the fields. Rescattering effects will alter our conclusion but are presumably small when the chemical potentials are frozen.

References

- [1] D. Hahn and H. Stöcker, Nucl. Phys. **A452**, 723 (1986).
- [2] P. Braun-Munzinger, J. Heppe, and J. Stachel, Phys. Lett. B **465**, 15 (1999).
- [3] H. Stöcker, W. Greiner, and W. Scheid, Z. Phys. A **286**, 121 (1978).
- [4] J. Theis *et al.*, Phys. Rev. D **28**, 2286 (1983).
- [5] J. Schaffner, I. N. Mishustin, L. M. Satarov, H. Stöcker, and W. Greiner, Z. Phys. **A341**, 47 (1991).
- [6] D. Zschesche *et al.*, Springer Tracts in Modern Physics **163**, 129 (2000).
- [7] F. Karsch, hep-lat/9903031 (1998).
- [8] P. Papazoglou *et al.*, Phys. Rev. C **59**, 411 (1999).

Effects of coherence in nuclear and hadronic collisions

J.Hüfner^{1,2}, B.Z. Kopeliovich^{2,3}, J. Raufeisen⁴, A.V. Tarasov^{2,3}

¹University of Heidelberg, ²MPI-K Heidelberg, ³University of Regensburg, ⁴LANL

The light-cone QCD approach incorporating the effects of the nonperturbative interaction between produced quarks and gluons suggested in [1] is applied in [2] to calculation of nuclear shadowing for longitudinal and transverse photons. This work was motivated by the results of the HERMES experiment observed unusual shadowing at small Q^2 where perturbative methods cannot be used. Although an exciting effect of strong dependence of the coherence length on the photon polarization was discovered in [2], data of HERMES remain unexplained.

The strong nonperturbative interaction of radiated gluons leads not only to a substantially weaker shadowing in heavy ion collisions, but also for the first time explains the observed smallness of large mass diffraction and allows to explain in a parameter free way the energy dependence of elastic scattering of hadrons [3, 4] in a good agreement with data.

The phenomena related to propagation of fast partons through medium are important for prediction of the initial condition in heavy ion collisions and also for the so called jet quenching probe for the produced matter. Broadening of the transverse momentum of a quark propagating through nuclear medium is calculated in [5]. It is found to be a color filtering effect and expressed in terms of the universal color dipole cross section which is fitted to data for the proton structure function. The calculated broadening of p_T for a quark propagating through a nucleus is somewhat larger than what was measured in Drell-Yan reaction on nuclei.

Energy loss of a quark propagating through nuclear matter can be also measured in Drell-Yan reaction. The main problem is to discriminate between this effect and nuclear shadowing. This is done in [6] employing our experience in parameter free calculation of shadowing. The analysis of data for Drell-Yan reaction from the E772 and E866 experiments at Fermilab resulted in a rather large rate of energy loss $dE/dz \approx -2 \text{ GeV}/fm$. This is the first observation of a nonzero energy loss effect.

It is usually believed that energy loss leads to baryon stopping in heavy ion collisions. A different point of view is presented in [7] where it is shown that the dominant mechanism of stopping is baryon number transfer by gluons. Nearly the same stopping is expected at RHIC as at SPS, as is confirmed by the preliminary data from RHIC.

Charmonium suppression is considered as one of the main probes for creation of a hot deconfined matter in relativistic heavy ion collisions. The conventional base line for search of new physics relates charmonium suppression to simple absorption in cold nuclear matter. First of all, one needs to know the charmonium-nucleon cross section. It is predicted in [8] quite reliably employing the light-cone dipole formalism with the realistic charmonium wave functions and phenomenological dipole cross section fitted to DIS data. This method is tested comparing to data

on charmonium photoproduction. The important effect missed in previous calculations is the relativistic spin rotation which increases the production rate of Ψ' by factor of 2-3. The cross sections are predicted for J/Ψ , Ψ' and χ , and with a proper mixture of these states the effective absorption cross section in cold nuclear matter is found.

In heavy ion collisions all nucleons which the produced charmonium interacts with, have already had a chance to interact with other nucleons and are in color-excited states. It is found in [9] that the colored 3-quark system interacts up to about 60% stronger than colorless one. Although this effect is not sufficiently strong to explain the observed anomalous E_T dependence of J/Ψ absorption, it must be included together with other missed effects in the interpretation of the experimental results. In particular, fluctuations of transverse energy should be taken into account, especially for most central collisions. It is demonstrated in [10] that they strongly correlate with fluctuation of charmonium suppression by interaction with the produced medium.

Coherent effects in elastic proton-nucleus scattering are proved to keep unchanged compared to pp scattering the ratio of spin-flip to non-flip amplitudes. This allows to use coulomb-nuclear interference in polarimetry as a basis for polarimetry. This method suggested in [11, 12] is accepted for polarimetry at RHIC.

References

- [1] B.Z. Kopeliovich, A. Schaefer, A.V. Tarasov, Phys. Rev. D62 (2000) 054022
- [2] B.Z. Kopeliovich, J. Raufeisen, A.V. Tarasov, Phys. Rev. C62 (2000) 035204
- [3] B.Z. Kopeliovich, I.K. Potashnikova, B. Povh, E. Predazzi, Phys. Rev. Lett. 85 (2000) 507
- [4] B.Z. Kopeliovich, I.K. Potashnikova, B. Povh, E. Predazzi, Phys. Rev. D63 (2001) 054001
- [5] M.B. Johnson, B.Z. Kopeliovich, A.V. Tarasov, Phys. Rev. C63 (2001) 035203
- [6] M.B. Johnson, B.Z. Kopeliovich, I.K. Potashnikova and the E772 Collaboration, hep-ex/0010051, submitted to Phys. Rev. Lett.
- [7] G.T. Garvey, B.Z. Kopeliovich, B. Povh, hep-ph/0006325, accepted in Comments Nucl. Part. Phys.
- [8] J. Hüfner, Yu.P. Ivanov, B.Z. Kopeliovich, A.V. Tarasov, Phys. Rev. D62 (2000) 094022
- [9] J. Hüfner, B.Z. Kopeliovich, A. Polleri, hep-ph/0010282, accepted in Eur. Phys. J. A.
- [10] J. Hüfner, B.Z. Kopeliovich, A. Polleri, nucl-th/0012003, submitted to Phys. Lett.
- [11] B.Z. Kopeliovich, T.L. Trueman, hep-ph/0012091, submitted to Phys. Rev. D
- [12] B.Z. Kopeliovich, A.V. Tarasov, Phys. Lett. B497 (2001) 44

Production of hard partons from soft gluonic fields^{B+G}

Dennis D. Dietrich, Gouranga C. Nayak, Walter Greiner, Johann Wolfgang Goethe Universität

We study parton-pair production from a space-time dependent chromofield via vacuum polarization by using the background field method of QCD. The processes we consider are both leading and higher order in gA but first order in the action. We derive general expressions for the corresponding probabilities. Parton production from a space-time dependent chromofield will play a crucial role in the production and equilibration of the quark-gluon plasma in ultra relativistic heavy-ion collisions at RHIC and LHC. In ultra relativistic heavy-ion collisions, when two highly Lorentz contracted nuclei pass through each other a chromofield is formed between them due to the exchange of soft gluons [1]. The chromofield so formed polarizes the QCD vacuum and produces $q\bar{q}$ -pairs and gluons via a Schwinger-like mechanism [2]. As seen in numerical studies [3], the chromofield acquires a strong space-time dependence due to a combination of such effects as expansion, background acceleration, color rotation, collision and parton production. In situations like this, the parton production from a constant chromofield is not justified and one has to find the corresponding expression for a general space-time dependent chromofield.

The e^+e^- pair production from a weak space-time dependent classical field is studied by Schwinger [2]. Because of the same structure of the interaction lagrangian density the production of a $q\bar{q}$ pair is similar to the e^+e^- case except for color factors [5]. (*N.B.*: Only the real parts of the following expressions are to be taken.) Details are given in [6]:

$$\begin{aligned} \frac{dW_{q\bar{q}}}{d^4x d^3k} = & \frac{g^2 m}{(2\pi)^5 k^0} A_\mu^a(x) e^{ik \cdot x} \int d^4x_2 A_\nu^a(x_2) e^{-ik \cdot x_2} \\ & (i[k^\mu(x-x_2)^\nu + (x-x_2)^\mu k^\nu + k \cdot (x-x_2)g^{\mu\nu}] \\ & (\frac{K_0(m\sqrt{-(x-x_2)^2})m\sqrt{-(x-x_2)^2} + 2K_1(m\sqrt{-(x-x_2)^2})}{[\sqrt{-(x-x_2)^2}]^3} \\ & - m^2 g^{\mu\nu} \frac{K_1(m\sqrt{-(x-x_2)^2})}{\sqrt{-(x-x_2)^2}}). \end{aligned}$$

The computation of the probability for the production of gluons is not straight forward and there is no counter part to this in QED. The processes which in leading order of the action contribute to gluon pair production are evaluated following the background field method of QCD [7] which, in a gauge invariant manner incorporates a classical background field and a quantum gluonic field simultaneously. The probability is obtained by spin-summing the phase-space integral over the absolute square of the amplitudes. The Feynman rules for the production of two gluons by coupling to the A -field once or twice can be read from the Lagrangian density and are given in [8, 6]. To obtain the correct physical gluon polarizations in the final state we put the sums over the polarizations of the outgoing gluons equal to the negative of the metric tensor and afterwards deduct the corresponding ghost contributions. The vertices involving two ghosts and one classical field and two ghosts and two classical fields respectively can again be read from the lagrangian density and are also found in [8, 6]. We obtain the probability per unit time and unit volume of the phase space for the pro-

duction of a real gg pair from a space-time dependent classical chromofield A [6]:

$$\begin{aligned} \frac{dW_{gg}}{d^4x d^3k} = & \frac{1}{(2\pi)^5 k^0} \int d^4x' e^{ik \cdot (x-x')} \frac{1}{(x-x')^2} \\ & \{ \frac{3}{4} g^2 A^{a\mu}(x) A^{a\mu'}(x') [3k_\mu k_{\mu'} - 8g_{\mu\mu'} k^\nu i \frac{(x-x')_\nu}{(x-x')^2} + 6 \frac{g_{\mu\mu'}}{(x-x')^2} \\ & + 5(k_\mu i \frac{(x-x')_{\mu'}}{(x-x')^2} + k_{\mu'} i \frac{(x-x')_\mu}{(x-x')^2}) - 12 \frac{(x-x')_\mu (x-x')_{\mu'}}{(x-x')^4}] \\ & - 3ig^3 A^{a\mu}(x') A^{c\lambda}(x') A^{a'\mu'}(x) f^{a'ac} K_\lambda g_{\mu\mu'} \\ & - \frac{1}{16} g^4 A^{a\mu}(x) A^{c\lambda}(x) A^{a'\mu'}(x') A^{c'\lambda'}(x') [24g_{\mu\mu'} g_{\lambda\lambda'} f^{acx} f^{a'c'x} \\ & + g_{\mu\lambda} g_{\mu'\lambda'} (f^{abx} f^{xcd} + f^{adx} f^{xcb}) (f^{a'bx'} f^{x'c'd} + f^{a'dx'} f^{x'c'b})] \}. \end{aligned}$$

As a simple example we choose the field to be

$$A^{a3}(t) = A_{in} e^{-|t|/t_0}, \quad t_0 > 0, \quad a = 1, \dots, 8.$$

The exponential decay of the source terms originates from the decay of the model-field. Their oscillatory behavior is due to the exponential factor, already present in the general formula.

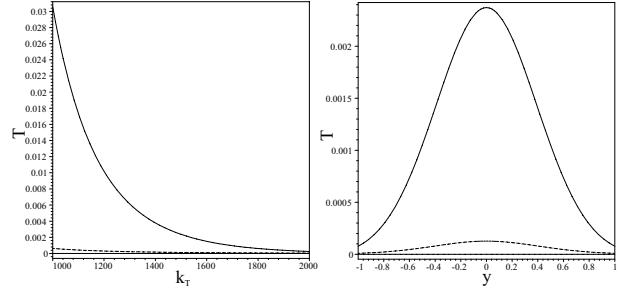


Fig. 1 Dimensionless time-integrated source terms for quarks (dash) and gluons (solid) versus transverse momentum k_T in MeV and rapidity y for the parameters $\alpha_S = 0.15$, $A_{in} = 1.5 GeV$, $t_0 = 0.5 fm$, $k_T = 1.5 GeV$, $y = 0$.

The decay behavior with the transverse momentum k_T in MeV is mostly due to the choice of the field. Only in the second contribution to the gluon source term there is already a factor $1/(k^0)^2$ present in the general formula. As the momentum structure of the general equations is mostly based on the k^0 -component, the origin for the typical rapidity y behavior is mainly linked to the behavior for changing transverse momentum. For this model field, a stronger coupling, a stronger chromofield and/or a slower varying field emphasize dominance of the gluon-pair production over the production of $q\bar{q}$ pairs even more.

References

- [1] F. E. Low, Phys. Rev. **D12** (1975) 163; S. Nussinov, Phys. Rev. Lett. **34** (1975) 1286; K. Kajantie and T. Matsui, Phys. Lett. **B164** (1985) 373; A. Karman, T. Matsui and B. Svetitsky, Phys. Rev. Lett. **56**, 219 (1986); G. Gattoff, A. K. Kerman and T. Matsui, Phys. Rev. **D36** (1987) 114; A. Bialas, W. Czyz, A. Dyrek and W. Florkowski, Nucl. Phys. **B296** (1988) 611; B. Banerjee, R. S. Bhalerao and V. Ravishankar, Phys. Lett. **B224** (1989) 16; M. Asakawa and T. Matsui, Phys. Rev. **D43** (1991) 2871; K. J. Eskola and M. Gyulassy, Phys. Rev. **C47** (1993) 2329; J. M. Eisenberg, Found. Phys. **27** (1997) 1213.
- [2] J. Schwinger, Phys. Rev. **82**, 664 (1951).
- [3] G. C. Nayak and V. Ravishankar, Phys. Rev. **D55** (1997) 6877; Phys. Rev. **C58** (1998) 356; R. S. Bhalerao and G. C. Nayak, Phys. Rev. **C61**, 054907 (2000).
- [4] C. Itzykson and J. Zuber, *Quantum Field Theory* (McGraw-Hill Inc., 1980), R. S. Bhalerao and V. Ravishankar, Phys. Lett. **B409**, 38 (1997).
- [5] G. C. Nayak and W. Greiner, hep-ph/0001009.
- [6] D. D. Dietrich, G. C. Nayak and W. Greiner, hep-ph/0009178; hep-th/0007139.
- [7] B. S. DeWitt, Phys. Rev. **162**, 1195 and 1239 (1967); in *Dynamic theory of groups and fields* (Gordon and Breach, 1965); G. 't Hooft, Nucl. Phys. **B62**, 444 (1973).
- [8] L. F. Abbott, Nucl. Phys. **B185**, 189 (1981).

Nonequilibrium quark dynamics in ultrarelativistic heavy ion collisions^{B,G}

S. Scherer¹, M. Hofmann¹, M. Bleicher², L. Neise¹, H. Stöcker¹, W. Greiner¹

¹ Institut für Theoretische Physik, J. W. Goethe-Universität Frankfurt am Main, Germany,

² Nuclear Science Division, Lawrence Berkeley Laboratory, Berkeley, U.S.A.

Heavy ion collisions at the CERN-SPS are supposed to reach the transition from hadronic matter to the quark-gluon plasma. The analysis of collective observables such as flow allows to speculate that this transition may show up even down to AGS energies. The description of such a collision by microscopic models thus must treat properly the degrees of freedom emerging from soft QCD.

Such a model can be realized by treating quarks as classical particles interacting according to a two-body color potential [1]. The Hamiltonian of this quark molecular dynamics (qMD) reads

$$\mathcal{H} = \sum_{i=1}^N \sqrt{\mathbf{p}_i^2 + m_i^2} - \frac{1}{2} \sum_{i,j} C_{ij}^c \left(\frac{3}{4} \frac{\alpha_s}{|\mathbf{r}_i - \mathbf{r}_j|} + \kappa |\mathbf{r}_i - \mathbf{r}_j| \right)$$

where the well known Cornell-potential is used to describe the quark interaction. Sign and relative strength of the interaction are described by the color factor C_{ij}^c , depending on the color combination of each pair. Confining properties are ensured by the linear increase of $V(r)$ at large distances. The time evolution of such a system yields colorless quark clusters which are mapped to hadrons.

When coupled to a hadronic transport model such as UrQMD[2] to create the initial quark distribution, the qMD can provide us with detailed information about the dynamics of the quark system and the parton-hadron conversion. Correlations between the quarks clustering to build new hadrons can be studied [3].

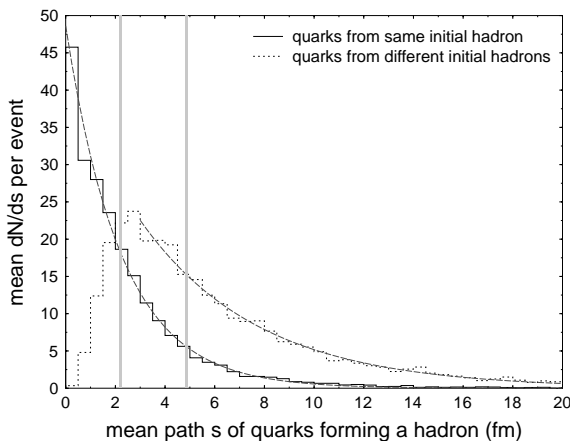


Figure 1: Hadronization in S+Au collisions at 200 GeV/N: Mean diffusion path of quarks forming a hadron from the same initial hadron (solid line) and from different initial hadrons (dashed line) within qMD. Fitting the decay profiles yields diffusion lengths of 2.2 fm and 4.8 fm.

Hadrons of the colliding nuclei are propagated in UrQMD, producing new hadrons in inelastic collisions and preformed hadrons in string excitations. Once complete

overlap of the impinging nuclei is reached, all hadrons with at least one collision or within their formation time are broken up in their (valence) quark content. These quarks are then propagated in qMD, finally hadronizing again.

Figure 1 shows (for S+Au collisions at SPS energies of 200 GeV/N) the distribution for the mean path travelled by quarks forming a hadron (a) from the same initial hadron (solid line) and (b) from different initial hadrons (dotted line).

A measure of the relative mixing within the quark system and thus for thermalization is the relative number of hadrons formed by quarks from the same initial hadron versus hadrons formed by quarks from different initial hadrons. This ratio is $r = 0.574 \pm 0.008$ for the S+Au collision (spectators are not included). Since a value of $r = 1$ indicates complete rearrangement of quarks and thus complete loss of correlations in the quark system, one would expect a much larger value of r , considering the presumed transition to the quark-gluon plasma in Pb+Pb collisions at 160 GeV/N,

First results for the excitation function of this ratio in Pb+Pb collisions, however, shows a different picture (Figure 2): a nearly constant value of about 0.3 is obtained for energies in the range from 20 to 160 GeV/N, nearly independent of the impact parameter. This surprising behavior needs clarification by further investigations.

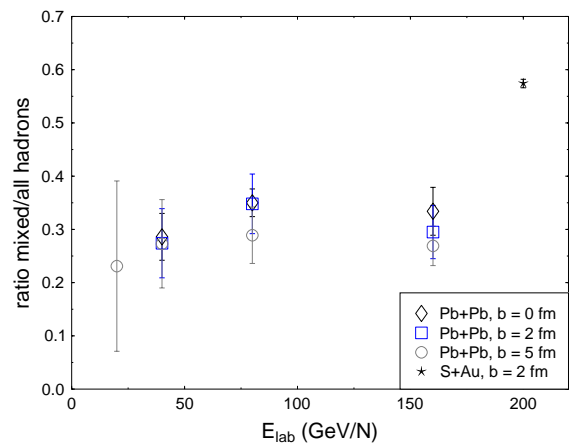


Figure 2: Excitation function of ratio of mixed to total hadrons for Pb+Pb collisions. The value for S+Au collision at 200 GeV/N is also shown.

References

- [1] M. Hofmann et al., Phys. Lett. **B478** (200) 161 (nucl-th/9908030); nucl-th/9908031.
- [2] S. A. Bass et al., Phys. Rev. C **60** (1999) 021902 [nucl-th/9902062].
- [3] S. Scherer et al., N. Journ. Phys. *to be publ.*

Deconfinement, Color Screening and Quarkonium Suppression

S. Digal, M. Nardi, P. Petreczky and H. Satz, Universität Bielefeld

The study of color deconfinement in strongly interacting matter leads to challenging problems of theoretical as well as of more phenomenological nature. How does the transition from hadronic matter to a quark-gluon plasma take place - is it a genuine phase transition or some less 'singular' cross-over, and what are the basic properties of the new deconfined medium? In the chiral limit ($m_q = 0$) and in the limit of pure gauge theory ($m_q = \infty$) we do have critical behavior in the classical sense, with well-defined order parameters and singularities in the partition function and hence in thermodynamic observables. Is there some way to really 'define' the transition in full QCD with light but not massless quarks? On the other hand, the aim of high energy nuclear collisions is to investigate the transition and the predicted new deconfined state of matter in the laboratory. What probes exist for these tasks? Is there an experimentally accessible deconfinement order parameter, and how can the temperature dependence of the hot deconfined medium be tested?

The role of the effective quark mass in QCD is similar to that of an ordering external field H in spin theories [1]. For $H = 0$, spin systems show at $T = T_c$ the familiar order-disorder transition, which disappears for $H \neq 0$. The critical behavior at $T = T_c$ can be described either in terms of singularities of thermal observables, or equivalently, as singular behavior of suitably defined geometric cluster variables. Such singular cluster percolation features persist, however, even for $H \neq 0$. It is thus of particular interest to see if the deconfinement transition can in some way be associated to the onset of percolation of clusters of deconfined medium. The answer to this question requires a systematic study of percolation in QCD. First steps had indicated that in the strong coupling limit Polyakov loop percolation indeed led to the correct deconfinement transition in pure Gauge theory [2]. In recent work it was shown that this conclusion can in fact be extended to $SU(2)$ gauge theory in general [3]. Studies of full QCD with dynamical quarks are under way. They could eventually check if the cross-over line between confined and deconfined matter in the $m_q - T$ plane coincides with the line of singular behavior defined through cluster percolation [1].

The behavior of a deconfined medium can be tested by studying the dissociation of quarkonium states through color screening [4]. A prerequisite for this is an understanding of the heavy quark potential in a hot medium, which can in principle be obtained through finite temperature lattice studies. Such studies, however, require extensive computational efforts which have become possible only recently; hence the past year has led to pioneering work in this field [5, 6]. The results of this work will certainly have an impact on the application of quarkonium dissociation as deconfinement probe in nuclear collisions.

The results of experimental studies of J/ψ production in

nuclear collisions at the CERN-SPS have made this a particularly interesting as well as challenging probe [7]. While peripheral $Pb-Pb$ collisions lead only to the pre-resonance absorption, already seen in pA and light ion interactions, there appears at a certain centrality a rather sudden onset of an additional 'anomalous' suppression, and for very central collisions a second further drop of the production rate occurs (see Fig. 1). Such a pattern is in fact expected from sequential charmonium suppression, leading first to the dissociation of the χ_c state and of its J/ψ decay products, then to the dissociation of the directly produced J/ψ [8]. More detailed recent investigations have led to a behavior which is qualitatively in accord with data [9, 10]; in particular, however, the central second drop appears to be much stronger than predicted by an onset of direct J/ψ suppression. The possible effects of fluctuations must therefore be taken into account in more detail [9, 11]. Such work is under way.

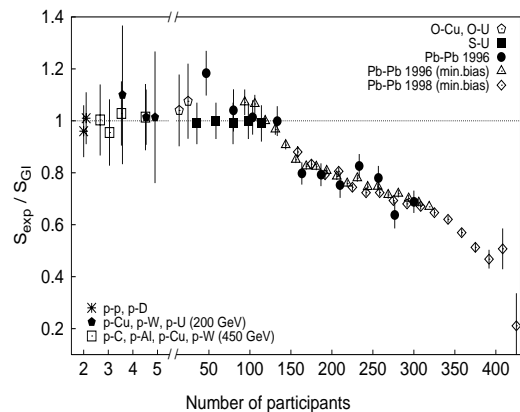


Figure 1: J/ψ production in different interactions

References

- [1] H. Satz, Nucl. Phys. A642 (1998) 130.
- [2] H. Satz and S. Fortunato, Phys. Lett. B475 (2000) 311.
- [3] S. Fortunato, F. Karsch, P. Petreczky, H. Satz, hep-lat/0011084, to appear in Nucl. Phys. B.
- [4] T. Matsui and H. Satz, Phys. Lett. 178 B (1986) 416.
- [5] A. Cucchieri, F. Karsch and P. Petreczky, Phys. Lett. B497 (2001) 80.
- [6] F. Karsch, E. Laermann and A. Peikert, hep-lat/0012023.
- [7] see M. Abreu et al. (NA50), Nucl. Phys. A663 (2000) 721.
- [8] S. Gupta and H. Satz, Phys. Lett. B383 (1992) 439.
- [9] H. Satz, Nucl. Phys. A 661 (1999) 104c.
- [10] M. Nardi and H. Satz, Phys. Lett. B442 (1998) 14.
- [11] J.-P. Blaizot M. Dinh and J.-Y. Ollitrault, Phys. Rev. Lett. 85 (2000) 4012.

Quarkonium at Collider Energies^{B+G}

L. Gerland, H. Stöcker, W. Greiner

J.W.G. Universität, D-60054 Frankfurt a. M., Germany

There are different time scales relevant for the production of quarkonium states:

- 1) the time needed to produce a heavy quark pair in a hard collision,
- 2) the time needed for a $Q\bar{Q}$ pair to form a bound state.

The production time of a $Q\bar{Q}$ pair in its rest frame is given by $\tau_p = \frac{1}{m_Q}$. This is 0.13 fm/c for $c\bar{c}$ and 0.05 fm/c for $b\bar{b}$. The Lorentz factor of the pair at midrapidity in the rest frame of the target is $\gamma \approx 10, 100$ and 3000 for a Quarkonium state at SPS, RHIC and LHC energies. At SPS fixed target energies $\gamma c\tau_p$ is smaller than the average internucleon distance in nuclei $r_{NN} \approx 1.8$ fm. Thus, the production of heavy quark pairs is incoherent. At RHIC the production distance of $c\bar{c}$ pairs is already as large as the diameter of a gold nucleus, and for $b\bar{b}$ pairs $c\tau_p > 1.8$ fm, but this is still small as compared to the nuclear radius. At LHC both production distances exceed the diameter of a lead nucleus by an order of magnitude. The hadronisation time t_H resp. the coherence length l_c of heavy Quarkonium is $l_c = c \cdot t_H = \frac{1}{\Delta E} \approx \frac{\gamma}{\Delta M}$ with:

$$\Delta E = \sqrt{p^2 + (M_{Q\bar{Q}} + \Delta M)^2} - \sqrt{p^2 + M_{Q\bar{Q}}^2} \approx \frac{(M_{Q\bar{Q}} + \Delta M)^2 - M_{Q\bar{Q}}^2}{2p} \approx \frac{M_{Q\bar{Q}} \Delta M}{p} = \frac{\Delta M}{\gamma}.$$

p is the momentum of the Quarkonium in the rest frame of the target, $M_{Q\bar{Q}}$ is the mass of the $Q\bar{Q}$ -pair and $\Delta M = \int \psi^2(k) \frac{k^2}{M_Q} d^3k / \int \psi^2(k) d^3k$, $\psi(k)$ is the wavefunction of the Quarkonium state in momentum space, we use here the wave functions from the refs. [1, 2]. ΔM is the average kinetic energy of the $Q\bar{Q}$ -pair in the bound state and $l_c/\gamma = 0.44(0.34)$ fm for the J/Ψ (Υ).

Thus, for charm and bottom production at RHIC and LHC $l_c > 2 \cdot R_A$ (R_A is the nuclear radius), $l_c < 2 \cdot R_A$ for fixed target SPS energies. The applicability of the approach developed in this paper requires that $l_c > 2 \cdot R_A$ which is fulfilled at RHIC and LHC.

We assume here that $Q\bar{Q}$ pairs are produced in AB collisions predominantly in hard collisions. The basic quantity is the cross section of production of $Q\bar{Q}$ pairs with light cone momenta z_i, k_i , which we parametrize as $\frac{d\sigma(AB \rightarrow Q\bar{Q}+X)}{d^2k_1 d^2k_2 d^2z_1 d^2z_2} = D_{AB}(z_1, z_2) \cdot \exp(-B(AB)(k_1^2 + k_2^2))$. Here k_i $\{i = 1, 2\}$ are the transverse momenta of the Q and the \bar{Q} quark and z_i $\{i = 1, 2\}$ are the fractions of their longitudinal momenta. Such a factorization does not contradict the data in pp collisions [3].

To evaluate the suppression of hidden heavy flavour production resulting from the broadening of the transverse momentum distributions of Q quarks due to final state interaction, we deduce first a relationship between the slopes for the various processes of heavy quark production. In the following we use the relative transverse momentum $k_t = \frac{k_1 - k_2}{2}$ and the total transverse momentum $p_t = k_1 + k_2$ of the pair, writing $\frac{d\sigma(AB \rightarrow Q\bar{Q}+X)}{d^2k_t d^2p_t d^2z_1 d^2z_2} = D_{AB}(z_1, z_2) \exp\left(-B(AB)\left(-\frac{p_t^2}{2} - 2k_t^2\right)\right)$.

To take into account possible nuclear effects on the longitudinal momentum distribution we make the ansatz $D_{AB}(z_1, z_2) = D(AB) \cdot f_{AB}(p_z) \cdot \exp\left(-\frac{k_z^2}{C_{AB}^2}\right)$, where p_z and k_z are the total and relative longitudinal momentum. We further assume that $f_{AB}(p_z) = f_{pp}(p_z)$, which means that we neglect parton energy losses of the pair, this effect will be discussed later on. The normalization condition follows from the QCD factorization the-

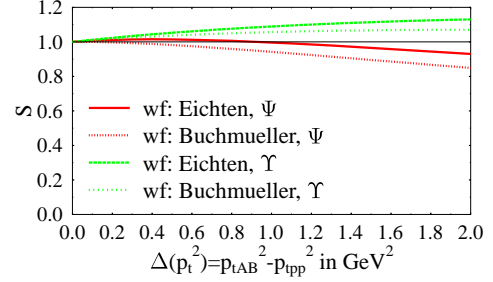


Figure 1: The righthandside of eq.(1) vs. the transverse momentum broadening for the J/Ψ and the Υ is plotted.

orem [4] for the total cross section: $\frac{D(AB)}{B(AB)^2 \cdot C_{AB}} = \frac{AB \cdot D(pp)}{B(pp)^2 \cdot C_{pp}}$. The differential cross sections are proportional to the square of the two body wave functions ϕ .

The production cross section of bound states of heavy quarks is proportional to the overlap integral of the two-body wave function and the wave function of the bound $\psi(k_t)$ state to get $\frac{d^3\sigma(AB \rightarrow Quarkonium+X)}{d^2p_t dp_z} \propto |\langle \psi(k_t, k_z) | \phi_{AB}(k_t, p_t, k_z, p_z) \rangle|^2$. Here we neglected the difference between the current quark mass in the two body wave function and the constituent quark mass in the wave function of the bound state. With this one can evaluate the survival probability:

$S \equiv \frac{\sigma(AB \rightarrow Quarkonium+X)}{AB \cdot \sigma(p+p \rightarrow Quarkonium+X)}$. Our final result is then

$$S = \frac{B(AB)C_{AB}}{B(pp)C_{pp}} \left| \frac{\int d^3k \psi(k) \exp(-B(AB)k_t^2) \exp\left(-\frac{k_z^2}{2C_{AB}^2}\right)}{\int d^3k \psi(k) \exp(-B(pp)k_t^2) \exp\left(-\frac{k_z^2}{2C_{pp}^2}\right)} \right|^2 \quad (1)$$

up to nuclear effects in the parton distribution functions.

Note that if one defines the survival probability as the ratio of the differential cross section $\frac{d^2\sigma}{d^2p_t}$ for nuclear and nucleon targets their p_t dependence would be a factor $\exp\left(-\frac{B(AB)-B(pp)}{2}p_t^2\right)$. That means that the p_t dependence of J/Ψ suppression is due to the broadening of the transverse momentum distribution as a result of the final state interactions of the Q quarks in the nuclear medium.

In fig. 1 the result of eq. (1) is plotted versus the transverse momentum broadening of the J/Ψ 's: $\Delta p_t^2 = 2/B(pp) - 2/B(AB)$. E.g. $\Delta p_t^2 = 0.48$ GeV² was found at Fermilab energies in pAu . $C_{AB}^2 = C_{pp}^2$ is used as a first approximation. $S \approx 1$ for the J/Ψ . That means there is practically no change due to the broadening of the transverse momentum distribution. The parameters used for the calculation are explained in ref. [5]. As one can see we obtain even a slight enhancement for the Υ meson production. This model neglects a lot of effects that might occur in AB -collisions, but predicts that the J/Ψ is less suppressed in pA collisions at collider energies than at fixed target energies.

References

- [1] E. Eichten et al., Phys. Rev. **D21** (1980), 203
- [2] W. Buchmüller and S. Tye Phys. Rev. **D24** (1981) 132
- [3] M.J. Leitch et al., Phys. Rev. Lett. **72** (1994) 2542
- [4] G.T. Bodwin, Phys. Rev. **D31**(1985) 2616
- [5] L. Gerland et al., J. Phys. G in Print and eprint nucl-th/0009008

Shadowing Effects on Vector Boson Production*

R. Vogt (LBNL and UC Davis)

The Z^0 was proposed as an alternative reference process for quarkonium suppression at the LHC. There are two difficulties with using the Z^0 as a baseline for quarkonium suppression: the large mass differences, $m_{Z^0} \gg m_\Upsilon, m_{J/\psi}$, and the difference in production mechanisms, predominantly $q\bar{q}$ for the Z^0 and gg for quarkonium. Both these differences are important as far as nuclear effects are concerned. However, the differences that reduce the value of the Z^0 as a baseline process are the same that make it an interesting object of study itself—the Z^0 provides a unique opportunity to study quark shadowing at high Q^2 . Therefore, we examine the possible effects of shadowing on Z^0 production as well as W^+ and W^- production which are also quark dominated. The impact parameter dependence of the shadowing effect will also be shown.

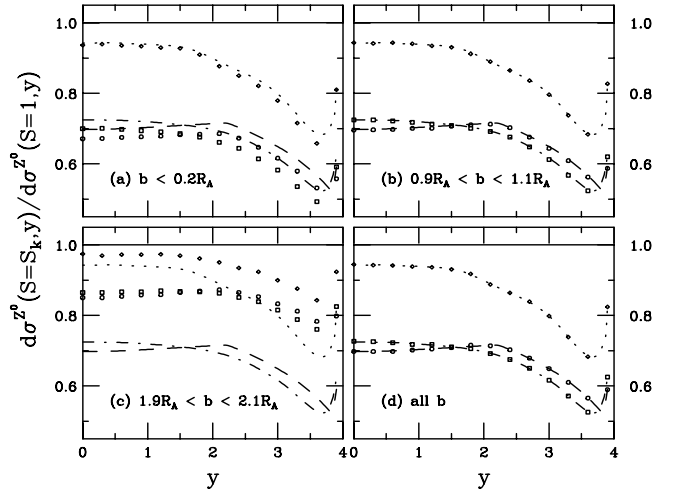
The electroweak production and decay channels of the massive vector bosons make them excellent candidates for shadowing studies since no hadronic final-state rescattering is possible. The Z^0 itself, with a 3.37% branching ratio to lepton pairs, will be easily observable by reconstructing the peak. Full reconstruction of the leptonic W^\pm decays, $W^\pm \rightarrow l^\pm \nu$, is not possible due to the missing energy given to the undetected neutrino but charged leptons with momenta greater than 40 GeV should be prominent. This technique has been used at the Tevatron to measure the asymmetry between W^+ and W^- production through their lepton decays since this asymmetry is sensitive to the ratio f_d^p/f_u^p at intermediate values of x and high Q^2 . If the charged leptons from W^\pm decays can be identified in heavy ion collisions, such asymmetry measurements may also be employed at the LHC to reduce systematics and obtain a more meaningful determination of the Q^2 dependence of quark shadowing in the nucleus.

The table gives the total cross sections in the CMS and ALICE central acceptances $|y| < 2.4$ and $|y| < 1$ respectively for no shadowing and with three shadowing parameterizations. The cross sections are larger than the virtual photon mediated Drell-Yan cross sections at lower masses. The results, given for Pb+Pb collisions, are integrated over impact parameter in units of nb/nucleon pair.

Detector	σ_1 (nb)	σ_{S_1} (nb)	σ_{S_2} (nb)	σ_{S_3} (nb)
Z^0				
CMS	15.41	10.87	10.96	14.26
ALICE	6.22	4.35	4.49	5.86
W^+				
CMS	20.85	14.39	14.54	18.93
ALICE	8.13	5.52	5.73	7.44
W^-				
CMS	21.84	15.08	15.26	19.83
ALICE	8.35	5.66	5.89	7.64

The figure compares the ratios of Z^0 production in Pb+Pb

collisions with three shadowing parameterizations to Pb+Pb collisions with no shadowing as a function of rapidity. The isospin effects wash out the differences between the W^+ and W^- distributions in the ratios so that the results are essentially identical for the two charged vector bosons. Therefore the ratios are shown only for the W^+ . The results are shown for several impact parameter bins, the most central bin, $b < 0.2R_A$, an intermediate impact parameter bin around $b \sim R_A$, and a peripheral bin around $b \sim 2R_A$. It is clear that by neglecting the impact parameter dependence of shadowing, one may make an overestimate of the effect in peripheral collisions, an important point if using the Z^0 as a baseline in different transverse energy bins. Note also that the integration over all impact parameters is equivalent to the average shadowing.



Once the basic nuclear shadowing effects on vector boson production have been understood, they can perhaps be used to study other medium effects in heavy ion collisions by comparing the leptonic and hadronic decay channels. The hadronic decays of the vector bosons, $\sim 70\%$ of all decays of each boson, may be more difficult to interpret. While the width of the Z^0 decay to l^+l^- is not expected to be modified in the quark-gluon plasma, the Z^0 has a 2.49 GeV total width and will decay in any quark-gluon plasma to two jets through $Z^0 \rightarrow q\bar{q} \rightarrow \text{jet} + \text{jet}$ in ~ 0.1 fm. Therefore, the decay jets could be modified in the medium which may still be progressing toward thermalization and will be subject to rescattering and jet quenching. Thus a comparison of a reconstructed Z^0 in the dilepton channel where no nuclear effects are expected since leptons do not interact strongly and medium-modified jets should result in a broader width for the $q\bar{q}$ channel than the l^+l^- channel. In addition, the Z^0 could be used to tag jets through the $q\bar{q} \rightarrow Z^0 g$ and $gq \rightarrow Z^0 q$ channels to study the jet properties in the quark-gluon plasma.

*Condensed from GSI-Preprint 2000-49, hep-ph/0011242.

Probing chiral dynamics by charged-pion correlations*

Jørgen Randrup (LBNL)

High-energy nuclear collisions are expected to produce transient systems within which chiral symmetry is approximately restored and the matter is partially deconfined. The identification and exploration of such a novel matter phase is a major experimental goal and the efforts have intensified with the recent commissioning of the Relativistic Heavy Ion Collider at BNL.

Through the past decade, it has been speculated that the rapid expansion of the collision zone, after an approximate restoration of chiral symmetry has occurred, may produce long-wavelength isospin-polarized agitations of the pionic field, commonly referred to as disoriented chiral condensates (DCC), which in turn should lead to anomalies in the resulting pion multiplicity distribution. However, the experimental search for the phenomenon has been hampered by the lack of signatures that are practically observable.

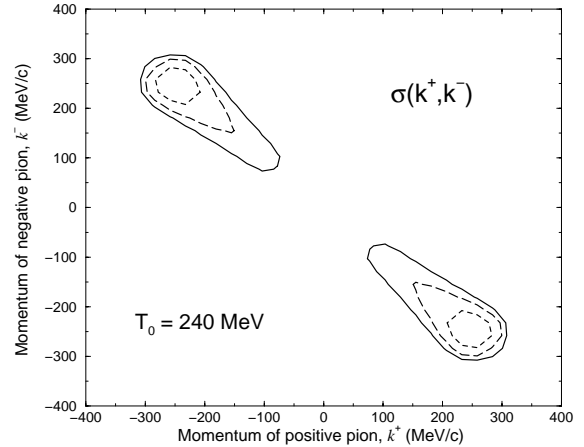
The present work identifies a novel observable that may be particularly suitable as an indicator of the DCC phenomenon, namely the approximate back-to-back correlation between oppositely charged soft pions.

The pionic degrees of freedom experience a rapidly changing environment that can be approximately accounted for by an in-medium effective mass depending both on the degree of agitation and on the chiral order parameter. Since the system is steadily cooling down while the order parameter reverts from its initial small value to its large vacuum value in a non-equilibrium fashion, the effective pion mass has then a correspondingly intricate evolution, displaying an overall decay towards the free mass overlaid by the effect of the rather regular oscillations by the relaxing order parameter. This time modulation of the effective mass may lead to parametric amplification those soft pionic modes with an energy near half the σ mass.

The effect is brought out most clearly in the simple case where the environment, and hence the effective mass, is spatially uniform, as is approximately the case in the interior of the collision zone. It is then obvious that although the time dependence of the mass may generate considerable agitation, this agency cannot add any net momentum. Thus the any pions produced by the mechanism must be formed pairwise and moving in opposite directions. Furthermore, by a similar reasoning, the time dependence of the mass does not add any change, so the produced pairs must be oppositely charged. Thus, the particles generated by an arbitrary time dependence in a uniform medium are charge-conjugate back-to-back pairs. This basic feature may be exploited as a probe of the chiral dynamics.

When the environment has a spatial dependence, as is more realistic, the pions experience forces that tend to erode the clear back-to-back correlation pattern. We have examined this effect with a quantum-field treatment of a one-dimensional sce-

nario, using a mass function that emulates the profiles obtained in more elaborate numerical simulations with the linear σ model. The resulting two-body correlation function for charge-conjugate pions is shown in the figure. The characteristic correlation structure is seen to be rather robust and so there is reason to hope that this signature may be experimentally observable.



Of course, this “signal” is partially obscured or eroded by a number of other processes and thus any attempt to extract it from the experimental data must take careful account of such “background” contributions.

One important issue concerns the possible presence of other agencies that may lead to a similar signal and thus forge the DCC signature. While there are many physically different sources of charge-conjugate pion pairs, fortunately only few lead to strong back-to-back correlations. Particularly important is the decay $\rho(770) \rightarrow \pi^+\pi^-$ but due to the high ρ mass, at least one of the pions has a momentum above 360 MeV/c which is somewhat above the upper limit of the expected effect ($k_{\max} \approx 300$ MeV/c). Moreover, although $\eta(550)$ and $\omega(780)$ may both contribute soft $\pi^+\pi^-$ pairs, these all arise in three-body decays and thus they are only rather weakly correlated and so they should not pose a serious problem.

In conclusion, then, we suggest that the data now being taken at RHIC be analyzed for indications of the described signature in the large-angle correlation of soft charge-conjugate pion pairs. It may also be worthwhile to scrutinize existing SPS data for this signal. If indeed identified, this signal may offer a means for probing the degree of chiral restoration achieved and the subsequent DCC dynamics.

* Condensed from nucl-th/0012020.

Mean-Field Instability of Trapped Ultracold Fermi Gases

R. Roth and H. Feldmeier (GSI)

The success in cooling a cloud of fermionic ^{40}K atoms, kept in a magnetic trap, to temperatures significantly below the Fermi energy [1,2] opened a unique possibility to study the properties of dilute degenerate Fermi gases experimentally. One long-term goal is the observation of a BCS phase transition in these systems. The mechanism to create Cooper pairs relies on an attractive interaction between the particles. At the same time these attractive interactions can cause a mean-field collapse of the metastable dilute Fermi gas towards high densities. Obviously a necessary prerequisite to reach the BCS transition is the stability of the normal Fermi gas.

We investigate the mean-field instability of the trapped Fermi gas in the framework of density functional theory. The energy density of the interacting multi-component Fermi gas is constructed in a mean-field picture using the Thomas-Fermi approximation. The interaction between the atoms is described by the s- and p-wave terms of the Effective Contact Interaction (ECI) [3,4], which depends on the s- and p-wave scattering length, a_0 and a_1 , resp., as well as on the s-wave effective volume b_0 . The ECI is constructed such that the exact two-body energy spectrum is reproduced by the expectation values of the ECI in mean-field type states.

The energy density of a single-component Fermi gas trapped in an external potential $U(\vec{x})$ reads

$$\mathcal{E}_1[\kappa(\vec{x})] = \frac{U(\vec{x})}{6\pi^2} \kappa^3(\vec{x}) + \frac{1}{20\pi^2 m} \kappa^5(\vec{x}) + \frac{a_1^3}{30\pi^3 m} \kappa^8(\vec{x}),$$

where $\kappa(\vec{x}) = \sqrt[3]{6\pi^2 \rho(\vec{x})}$ denotes the local Fermi momentum and a_1 the p-wave scattering length. The first term originates from the external potential, the second one from the kinetic energy, and the third term from the p-wave interaction. The s-wave part of the interaction does not contribute in a system of identical fermions due to the Pauli principle.

For attractive p-wave interactions, i.e., negative p-wave scattering length $a_1 < 0$, the highest power of $\kappa(\vec{x})$ in the energy density has a negative coefficient. This implies that there is a maximum density up to which the system is stable. Beyond this density the energy decreases for growing density and the system collapses towards a high density configuration. For fixed particle number N we obtain the following local condition for the stability of the single-component Fermi gas [3,4]

$$-a_1 \kappa(\vec{x}) \leq \sqrt[3]{3\pi}/2.$$

If this stability condition is violated anywhere in the trap then the system will collapse.

The energy density of a two-component Fermi gas, where we assume equal local Fermi momenta $\kappa(\vec{x}) = \kappa_1(\vec{x}) = \kappa_2(\vec{x})$ for both components, reads

$$\begin{aligned} \mathcal{E}_2[\kappa(\vec{x})] = & \frac{U(\vec{x})}{3\pi^2} \kappa^3(\vec{x}) + \frac{1}{10\pi^2 m} \kappa^5(\vec{x}) \\ & + \frac{a_0}{9\pi^3 m} \kappa^6(\vec{x}) + \frac{\tilde{a}_1^3}{10\pi^3 m} \kappa^8(\vec{x}) \end{aligned}$$

with $\tilde{a}_1^3 = a_1^3 + b_0/3$. In this case both, s- and p-wave interactions contribute and influence the stability of the system. We obtain the following stability condition for the two-component Fermi gas [3,4]

$$-a_0 \kappa(\vec{x}) - 2[\tilde{a}_1 \kappa(\vec{x})]^3 \leq \pi/2.$$

For practical purposes this stability condition can be rephrased in terms of an upper limit in the number of particles $N = N_1 = N_2$ assuming a parabolic trapping potential with mean oscillator length $\ell = 1/\sqrt{m\omega}$ [3,4]. Figure 1 shows the logarithm of the maximum particle number of each component as a function of the s- and p-wave scattering length in units of the mean oscillator length.

Attractive s-wave as well as attractive p-wave interactions can cause a mean-field collapse. If both components are attractive then their combined action decreases the maximum allowed density or particle number for the stable configuration. If one component is attractive and the other repulsive then the repulsive one stabilizes the system, i.e., increases N_{\max} . New phenomena appear in the case of attractive s-wave and repulsive p-wave interactions. If the p-wave scattering length exceeds about 1/3 of the s-wave scattering length (compare Fig. 1) the p-wave repulsion prevents a collapse completely, i.e., $N_{\max} \rightarrow \infty$. For p-wave repulsions slightly too weak to cause this absolute stabilization a novel high-density phase appears in the center of the trap if N_{\max} is exceeded.

We conclude that p-wave interactions have an important influence on the stability and may thus be helpful on the way to Cooper pairing in trapped ultracold Fermi gases.

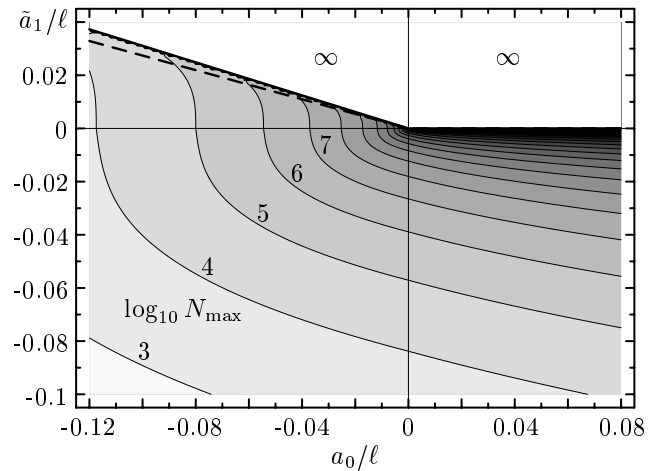


Fig. 1: Contour plot of the logarithm of the maximum particle number N_{\max} in a two-component Fermi gas as function of the s- and p-wave scattering lengths, a_0/ℓ and \tilde{a}_1/ℓ , where ℓ is the mean oscillator length of the trap.

- [1] B. DeMarco, D.S. Jin; Science 285 (1999) 1703.
- [2] B. DeMarco, S.B. Papp, D.S. Jin; e-print: cond-mat/0101445.
- [3] R. Roth, H. Feldmeier; e-print: cond-mat/0102416.
- [4] R. Roth, H. Feldmeier; J. Phys. B 33 (2000) 787.

see also: <http://theory.gsi.de/~trap/>

Parity Violation effects in highly-charged ions

I. Bednyakov, G. Plunien, G. Soff, Technische Universität Dresden
 L.N. Labzowsky, St. Petersburg State University,
 A.V. Nefiodov, St.Petersburg Nuclear Physics Institute,

Parity-nonconserving (PNC) atomic effects originate from the electroweak interaction of atomic electrons with the nucleus via Z -boson exchange. Comparing experimental results with theoretical predictions of the standard model allows to search for "new physics" beyond the standard model (e.g., a second Z -boson or new fermions) [1].

In the case of neutral atoms here is the discrepancy between theoretical and experimental results for PNC effects in the case of neutral atoms that might be explained by the uncertainties in the calculations caused by the inter-electronic interactions, correlation effects etc.

In highly-charged ions (HCI), on the other hand, the binding to the nucleus dominates by far the electron-electron interaction. The spin-independent part of an effective weak interaction Hamiltonian mediated by a Z -boson exchange is given by

$$\hat{H}_W(\mathbf{r}) = -\frac{G_F}{2\sqrt{2}} Q_W \rho_N(\mathbf{r}) \gamma_5, \quad (1)$$

where G_F is the Fermi constant, $\rho_N(r)$ is the nuclear density and γ_5 is the Dirac matrix. Due to this effective Hamiltonian states with opposite parity will be admixed. The transition amplitudes of a given atomic processes can be expressed as:

$$A = A_0 + i\eta A_1, \quad (2)$$

where A_0 denotes the amplitude of the basic process and A_1 is the amplitude being related to parity violation.

Electroweak-radiative corrections were considered both for neutral atoms (e.g. see Ref. [2] and also for hydrogen-like ions [3]. The consideration of these radiative corrections becomes necessary because they can contribute up to 10% of the total magnitude of PNC effects.

For experiments, a promising situation occurs in He-like ions due to the near-degeneracy of two levels with opposite parities, 2^1S_0 and 2^3P_0 near $Z = 64$ (Gd^{62+}) as well as close to $Z = 92$ (U^{90+}). The situation has been analyzed in Gd^{62+} and Eu^{61+} . In particular we propose a quenching-type experiment with an interference of hyperfine- and weak-quenched transitions [4].

A typical situation for parity violation in atoms concerns the $M1$ transition with an admixture of the $E1$ transition. The one-photon hyperfine-quenched transition $2^1S_0 \rightarrow 1^1S_0$, via emission of a magnetic photon ($M1$), is due to the hyperfine mixing of the 2^1S_0 and 2^3S_1 levels. The weak interaction of electrons opens another one-photon decay channel $2^1S_0 \rightarrow 1^1S_0$, via the $E1$ emission through the mixing of the 2^1S_0 and 2^3P_1 levels by the operator \hat{H}_W . As a result, the total amplitude A in Eq. (2) appears as a mixture of the basic $M1$ amplitude $A_0 \equiv A_s$ and of the additional $E1$ amplitude $A_1 \equiv A_p$. The corresponding transitions rates are W_s and W_p , respectively. The weak mixing coefficient η is determined by

$$i\eta\Delta_0 = \langle 2^3P_0 | \hat{H}_W | 2^1S_0 \rangle, \quad (3)$$

where $\Delta_0 = E_{2^1S_0} - E_{2^3P_0}$. The theoretical predictions

Nucl.	$W_s(\text{s}^{-1})$	$W_p(\text{s}^{-1})$	η
$^{151}_{63}\text{Eu}$	0.68×10^8	0.11×10^{14}	0.33×10^{-6}
$^{155}_{64}\text{Gd}$	0.58×10^6	0.75×10^{11}	0.91×10^{-6}

for these quantities in europium and gadolinium are listed in the Table. Due to the admixture of states of opposite parity, in a polarized-beam experiment a small asymmetry in the number of emitted photons per direction should become visible, expressed by

$$dW(\mathbf{n}) = \frac{W_s}{4\pi} [1 + \varepsilon (\boldsymbol{\zeta} \cdot \mathbf{n})] d\Omega \quad (4)$$

where \mathbf{n} indicates the direction of the photon emission and $\boldsymbol{\zeta}$ is the unit vector in direction of the polarization of the ion. The coefficient of asymmetry is given by $\varepsilon = 3\lambda_0\eta R/(I+1)$ with $R = \sqrt{W_p/W_s}$. Here $\lambda_0 \leq 1$ denotes the degree of polarization.

The total asymmetry effect turns out to be $\varepsilon \simeq 0.37\lambda_0 \times 10^{-3}$ for Gd^{62+} , which is unusually large for parity-violation effects, but the lifetime of the 2^1S_0 level is about one order of magnitude smaller than the hyperfine-quenched 2^3P_0 lifetime. This implies a strong background in experiments with Gd^{62+} .

In Eu^{61+} the weak asymmetry effect reduces to $\varepsilon \simeq 0.11\lambda_0 \times 10^{-3}$, but the 2^1S_0 level lives significantly longer than the hyperfine-quenched 2^3P_0 level.

Since photons being observed in this experiment originate from single-photon decays of the hyperfine- and weak-quenched $F = I$ state, the success of the experiment will depend crucially on the production of a significant degree of polarization for this state of the He-ion. This is a task to be achieved experimentally in order to exploit the advantages of highly-charged ion investigations for parity-violation effects.

References

- [1] G. Soff, I. Bednyakov, T. Beier, F. Erler, I. Goidenko, U. Jentschura, L. N. Labzowsky, A. Nefiodov, G. Plunien, R. Schützhold, and S. Zschocke. "Effects of QED and beyond from the atomic binding energy" (APAC2000 Conference), "Hyperfine Interactions"
- [2] B. W. Lynn and P. G. H. Sandars, J. Phys. B **27**, 1469 (1994).
- [3] I. Bednyakov, L. Labzowsky, G. Plunien, G. Soff, and V. Karasiev, Phys. Rev. A **61**, 012103 (1999).
- [4] L. N. Labzowsky, A. V. Nefiodov, G. Plunien, G. Soff, R. Marrus, and D. Liesen. *preprint 2000* "Parity-violation effect in heliumlike gadolinium and europium"

Divergence of Perturbation Theory and Resummation

Ulrich Jentschura and Gerhard Soff

TECHNISCHE UNIVERSITÄT DRESDEN, 01062 DRESDEN

Current determinations of fundamental constants [1] and the comparison of theory and experiment in high-precision experiments are based on perturbative expansions which can at best be regarded as divergent, asymptotic series in the coupling constant [2]. The first terms of the series decrease in absolute magnitude, before the factorial growth of the perturbative coefficients overcompensates the additional coupling factors of higher orders in perturbation theory, and the perturbation series ultimately diverges. Dyson's related argument [3] has given rise to much discussion and confusion, until recent explicit 30-loop calculations of perturbation series pertaining to ϕ^3 and Yukawa theories have firmly established the factorially divergent character of the perturbative expansion [4]. These considerations naturally lead to the question of how complete, nonperturbative results can be obtained from a finite number of perturbative coefficients, and how the nonperturbative result is related to the partial sums of the perturbation series.

We have investigated this problem [5] in connection to the Euler-Heisenberg-Schwinger effective Lagrangian which describes the quantum electrodynamic corrections to Maxwell's equations. The forward scattering amplitude of the vacuum ground state is described by a factorially divergent asymptotic series, $S_B \propto \text{const.} \times g_B \sum_{n=0}^{\infty} c_n g_B^n$. The expansion coefficients

$$c_n = \frac{(-1)^{n+1} 4^n |\mathcal{B}_{2n+4}|}{(2n+4)(2n+3)(2n+2)},$$

where \mathcal{B}_{2n+4} is a Bernoulli number and g_B is the coupling, display an alternating sign pattern and grow factorially in absolute magnitude. The process by which a finite, nonperturbative result is ascribed to a divergent perturbation series is known as *resummation*. The resummation to the complete nonperturbative result for S_B is accomplished by employing the delta transformation,

$$\delta_n^{(0)}(\beta, s_0) = \frac{\sum_{j=0}^n (-1)^j \binom{n}{j} \frac{(\beta+j)_{n-1}}{(\beta+n)_{n-1}} \frac{s_j}{a_{j+1}}}{\sum_{j=0}^n (-1)^j \binom{n}{j} \frac{(\beta+j)_{n-1}}{(\beta+n)_{n-1}} \frac{1}{a_{j+1}}},$$

where $s_n = \sum_{k=0}^n a_k$ is the partial sum of the input series and $a_j = c_j g^j$ is the j th term in the perturbation series; $(a)_m = \Gamma(a+m)/\Gamma(a)$ is a Pochhammer symbol. It has been observed that the delta transformation can be used under rather general assumptions for the extrapolation of the perturbation series, i.e. the prediction of unknown perturbative coefficients, and various applications to phenomenologically important quantum field theoretic perturbation series have been presented in [5,6]. In many cases, the delta transformation leads to better results than Padé approximants which have been discussed abundantly in the literature (see e.g. [7]).

A perturbation series often misses physically important physical effects when interpreted "at face value". For example, the perturbative expansion describing the energy shift of hydrogenic levels in an electric field (known as the Stark effect) has purely real coefficients, whereas the complete energy eigenvalue (more precisely, pseudoeigenvalue or resonance) also has an imaginary component. The imaginary part of the resonance, which describes the autoionization width, can be obtained from the purely real perturbation series by a transformation which can be characterized as a generalized Borel summation [8,9]. First, the factorial growth of the perturbation series is divided out by calculating the Borel transform, and the perturbation series $f(g) = \sum_n c_n g^n$ is replaced by its Borel transform $\mathcal{B}(g) = \sum_n c_n g^n / n!$. Then, the autoionization width is obtained by integrating the Borel transform in the complex plane along integration contours specified in [9,10]. The same resummation procedure can be used to obtain the quantum electrodynamic pair production amplitude for the case of an electric field background; the pair-production amplitude is related to the imaginary part of the effective action [10].

Recently, techniques have been investigated to accelerate the convergence of resummation procedures in order to obtain results even at large coupling, which are paradoxically based on the weak-coupling perturbative expansions [11]. The extrapolation from the weak-coupling limit to the regime of strongly coupled systems by analytic continuation of the perturbation series via Borel or delta transformations has wide applicability.

References

- [1] P. J. Mohr and B. N. Taylor, Rev. Mod. Phys. **72**, 351 (2000).
- [2] J. Zinn-Justin, *Quantum Field Theory and Critical Phenomena*, 3rd ed. (Clarendon Press, Oxford, 1996).
- [3] F. J. Dyson, Phys. Rev. **85**, 631 (1952).
- [4] D. Broadhurst and D. Kreimer, Phys. Lett. B **475**, 63 (2000).
- [5] U. D. Jentschura, J. Becher, E. J. Weniger, and G. Soff, Phys. Rev. Lett. **85**, 2446 (2000).
- [6] U. D. Jentschura, E. J. Weniger, and G. Soff, J. Phys. G **26**, 1545 (2000).
- [7] M. A. Samuel, J. Ellis, and M. Karliner, Phys. Rev. Lett. **74**, 4380 (1995).
- [8] V. Franceschini, V. Grecchi, and H. J. Silverstone, Phys. Rev. A **32**, 1338 (1985).
- [9] U. D. Jentschura, e-print physics/0010038 (Phys. Rev. A, in press).
- [10] U. D. Jentschura, Phys. Rev. D **62**, 076001 (2000).
- [11] U. D. Jentschura and G. Soff, J. Phys. A **34**, 1451 (2001).

The g factor of an electron bound in hydrogenlike ions - status of the theoretical predictions

Thomas Beier, *Gesellschaft für Schwerionenforschung, Darmstadt, Germany*

For only few fundamental physical quantities experiment [1] and theory [2] agree that well as for the g factor of the free electron. It can therefore be considered as a precision test of quantum electrodynamics (QED) for free particles. To test QED also in the presence of strong electric fields, measurements on the g factor of an electron bound in a hydrogenlike system are one possible way. In $^{12}\text{C}^{5+}$, a value of $g = 2.001\,041\,596(5)$ was measured [3] which has to be compared to the theoretical prediction of $g = 2.001\,041\,591(7)$ [4]. This measurement is therefore the most stringent comparison of QED theory and experiment in any system heavier than hydrogen up to now. The major uncertainty of the experimental value results from the mass ratio $m_e/m_{^{12}\text{C}^{5+}}$, taken from [5], and an only slight improvement in the theoretical precision would allow to determine the electron mass more accurately. Here, the current limits to theory are presented and discussed.

The value given in [4] includes the g factor of the free electron including all QED corrections to that value, and in addition the corrections due to the binding to a heavy nucleus:

1. the binding correction itself which can be characterized as a transition from the spin quantum number to the total angular-momentum quantum number that is the only observable in a central field. It describes the deviation of g from the Dirac value of 2 for the free electron and is given by $g_j = (2/3)[1 + 2\sqrt{1 - (Z\alpha)^2}]$ for the 1s state. This applies only to point-like nuclei. For extended nuclei, the wave function of the electron is slightly modified.
2. The finite nuclear-size correction which takes into account the extension of the nucleus is about 4×10^{-10} for carbon but amounts up to 1×10^{-3} for uranium where the uncertainty of the nuclear radius itself affects the prediction already on the 10^{-7} level.
3. The not-infinite nuclear mass causes the nucleus to move itself when orbited by the electron. A correct relativistic treatment has to consider nuclear recoil to all orders in the coupling constant $Z\alpha$ where Z is the charge of the nucleus. The exact form of this correction is not yet known and an existing expansion in $Z\alpha$ [6,7] yields reliable results only for light systems. For carbon it amounts to 87.5×10^{-9} with an estimated uncertainty of 1 % because of the expansion. This uncertainty should be considered to be 10 % of the value already for calcium. The complete relativistic recoil correction was calculated only for the Lamb shift up to now [8] and it seems to be much more complex for the g factor and the hyperfine structure splitting.
4. Another quantity connected with nuclear properties is that of nuclear polarization, i.e., the virtual excitation of nuclear degrees of freedom by exchange of at least two virtual photons with the electron. For the g factor, no investigations were carried out up to now. The works of G. Plu-

nien and G. Soff [9] deal with the influence on the Lamb shift in the approximation of Coulomb-photon exchange, and only recently the problem of transverse-photon exchange which is crucial for magnetic interactions was considered at least for the Lamb shift case [10]. However, we expect this effect to be even weaker than for the Lamb shift because the typical matrix element for g factor measurements is $\langle r \rangle$, compared to $\langle 1/r \rangle$ for the Lamb shift, and therefore the inner parts of the electronic wave function that contribute most to the nuclear polarization are less pronounced. It should be mentioned that this is *not* the case for the hyperfine structure splitting where the typical matrix element is given by $\langle 1/r^2 \rangle$. In that case, however, the effect is screened by other nuclear uncertainties (for a recent overview see [11]).

5. The most interesting quantities related to the g factor are the bound-state QED corrections. Those of first order in (α/π) (i.e. one virtual photon line in the corresponding Feynman diagram) are depicted in Fig. 1. They were eval-

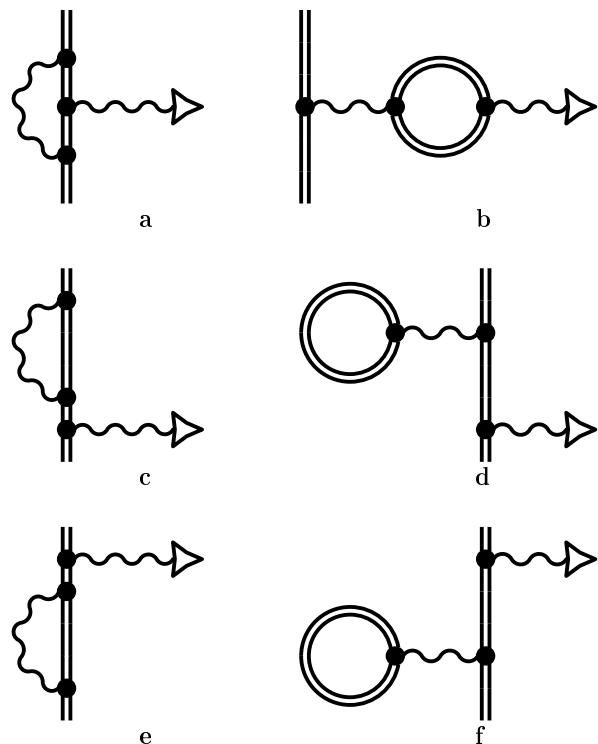


Fig. 1. Feynman diagrams representing the QED contributions of order (α/π) to the g factor of a bound electron. The wavy lines denote photons, which mediate the interaction with the external magnetic field represented by a triangle. In each diagram there is also one virtual photon. The solid double line indicates the electron and on the right side also virtual leptons in the electron-positron loops. The diagrams on the left are the self-energy-like corrections, those on the right the vacuum-polarization-like corrections. For the free electron, only the diagram similar to diagram a contributes.

uated in detail to all orders in $Z\alpha$ in [4]. They contain also the contribution to the g factor of the free electron of the same order, given by $\alpha/\pi \approx 2.323 \times 10^{-3}$. For comparison, the effect of binding in C^{5+} amounts only to 8.442×10^{-7} . In uranium the binding effect is 3×10^{-3} and therefore in particular heavy systems form an excellent base for investigations of bound-state QED.

The QED corrections of second order in (α/π) were never investigated beyond the first term in the $Z\alpha$ expansion. It can be shown for *all* orders of (α/π) that the leading term of the corresponding $Z\alpha$ expansion is given by $2 \times A^{(n)} \times (Z\alpha)^2/6$ where $A^{(n)}$ is the expansion coefficient for the n th power of (α/π) in the series for $g_{\text{free}}/2$ [12], i.e., $A^{(1)} = 1/2$. The next term in the $Z\alpha$ expansion is at least of the order $(Z\alpha)^4$, and therefore the $Z\alpha$ expansion allows to estimate the bound-state $(\alpha/\pi)^2$ contributions with an uncertainty of about 50 % for the case of carbon. This uncertainty increases rapidly for increasing Z , and we expect the error to be at least 100 % in the case of calcium already, where the leading term of the expansion for the first order in (α/π) already deviates for about 70 % from the non-perturbative value. The whole set of 50 diagrams for the order $(\alpha/\pi)^2$ is shown in Fig. 2. For the order $(\alpha/\pi)^3$, the number of diagrams exceeds 500. The 50 diagrams shown in Fig. 2 can be obtained by fixing the magnetic interaction to each point of the 10 diagrams contributing to the Lamb shift of order α^2 in hydrogenlike atoms (e.g., [13]). The calculation is slightly more complex because for each diagram the magnetic interaction and one additional electron propagator with the corresponding integration has to be considered. As there are problems already for some of the Lamb-shift diagrams, an evaluation of the set shown in Fig. 2 can not be expected without considerable effort. In particular, the diagrams that contribute most to the g factor in lighter systems are those with two self-energy loops in the upper rows of Fig. 2, and unfortunately exactly their counterpart, the so-called two-loop self-energy graphs, cause the major problems in the recent calculations for the Lamb shift (e.g., [14] and references therein). The situation would be different in muonic atoms where the vacuum-polarization contributions are strongly enhanced compared to those from self-energy-like graphs. An additional experiment on a muonic system therefore could provide valuable additional information. However, in muonic systems the nuclear polarization can be expected to be as large as the QED corrections of order (α/π) .

All theoretical contributions to the g factor of the electron bound in hydrogenlike carbon are given in Table 1. Together with the experimental value, this leads to an independent new value for the electron mass [15], $m_e = 5.485\,799\,092 \times 10^{-3}$ u. A detailed discussion about the corresponding measurement and evaluation procedure is to be found elsewhere in this report [16].

We want to thank S. G. Karshenboim, K. Pachucki, V. M. Shabaev, and V. A. Yerokhin for valuable discussions.

- [1] R. S. Van Dyck Jr. *et al.*, PRL 59 (1987) 26.
- [2] A. Czarnecki and W. J. Marciano, Nuc. Phys. B (Proc. Suppl.) 76 (1999), 245.
- [3] H. Häffner *et al.*, PRL 85 (2000) 5308.

- [4] T. Beier *et al.*, PRA 62 (2000) 032510.
- [5] D. L. Farnham *et al.* PRL 75 (1995) 3598.
- [6] R. Faustov, Nuovo Cimento LXIX A, No. 1 (1970) 37; Phys. Lett. 33B (1970), 422.
- [7] H. Grotch, PRA 2 (1970) 1605; H. Grotch and R. A. Hegstrom, PRA 4 (1971) 59.
- [8] V. M. Shabaev, PRA 57 (1998) 59; V. M. Shabaev *et al.*, PRA 57 (1998) 4235.
- [9] G. Plunien and G. Soff, PRA 51 (1995) 1119; PRA 53 (1996) 4614, and references therein.
- [10] N. Yamanaka *et al.*, Hyp. Int. 127 (2000) 297.
- [11] T. Beier, Phys. Rep. 339 (2000) 79.
- [12] A. Czarnecki *et al.*, Phys. Rev. A 63 (2001) 012509.
- [13] P. Mohr *et al.*, Phys. Rep. 293 (1998) 227.
- [14] V. A. Yerokhin, PRL 86 (2001) 1990, and refs. therein.
- [15] G. Werth *et al.*, Hyp. Int., in print.
- [16] W. Quint *et al.*, Contribution to this annual report.

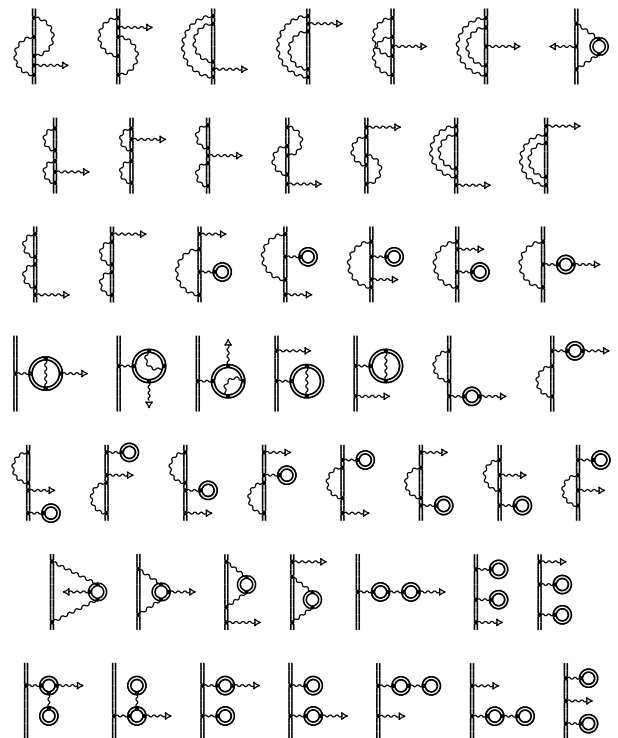


Fig. 2. Diagrams contributing to order $(\alpha/\pi)^2$ to the g factor of a bound electron. Only seven diagrams of this order have to be considered for the g factor of a free electron, similar to these of the first row.

Table 1. Known theoretical contributions to the g factor of an electron bound in the ground state of $^{12}C^{5+}$. All values are given in units of 10^{-9} . If no error is given, it is less than 0.5×10^{-10} . The error for the “total” value is a linear addition of the three errors given in order not to underestimate any systematic effect.

Contribution	numerical value (in 10^{-9})
binding	1 998 721 354.2
fin. nuc. size	0.4
recoil	87.5(9)
free QED, order (α/π) :	2 322 819.6
bound QED, order (α/π) :	844.3(12)
free QED, $(\alpha/\pi)^2$ to $(\alpha/\pi)^4$	-3 515.1
bound QED, $(\alpha/\pi)^2$ $(Z\alpha)^2$	-1.1(5)
total:	2 001 041 589.8(26)

Interelectronic-interaction effect on the radiative recombination of an electron with a heavy He-like ion

V.A. Yerokhin ^{a,b,c}, V.M. Shabaev ^{a,b,c}, T. Beier ^b, and J. Eichler ^c

^a St.Petersburg State University, St.Petersburg, Russia

^b Gesellschaft für Schwerionenforschung (GSI), Darmstadt, Germany

^c Hahn-Meitner Institut Berlin, Germany

In energetic atomic collisions between highly charged high- Z ions and low- Z target atoms, radiative electron capture (REC) is one of the most important reaction channels. In the limit of a loosely bound target electron, REC is identical with radiative recombination (RR). Reactions of this type have been extensively studied in recent years for heavy highly charged projectiles up to bare uranium. The relativistic theory of REC in the one-electron approximation is well established at present ([1] and references therein), and results of numerical calculations are in excellent agreement with experiment [2]. While radiative recombination of an electron with a bare nucleus is well understood theoretically, the process involving an ion with several electrons is complicated by the interelectronic interaction. The REC process into the L-shell of He-like uranium was measured in [3].

We systematically investigated the interelectronic-interaction effect on radiative recombination of an electron with a heavy He-like ion. Here, the number of electrons ($N=3$) is much smaller than the nuclear charge number Z and therefore their mutual interaction is by a factor $1/Z$ smaller than that with the Coulomb field of the nucleus. To zeroth approximation, the interelectronic-interaction can be neglected and thus the process is equivalent to RR of an electron with a bare nucleus, studied thoroughly in [1]. Here, we investigated the correction of first order in $1/Z$ due to the interelectronic interaction.

We consider RR of an electron with a definite momentum and polarization with a heavy He-like atom in the ground state located at the origin of the coordinate frame. The final state of the system is a Li-like ion in the state $(1s)^2v$, where v denotes a valence electron. The first-order (in $1/Z$) interelectronic-interaction correction to the process under consideration can be represented by a set of Feynman diagrams shown in Fig. 1. Here, the operator

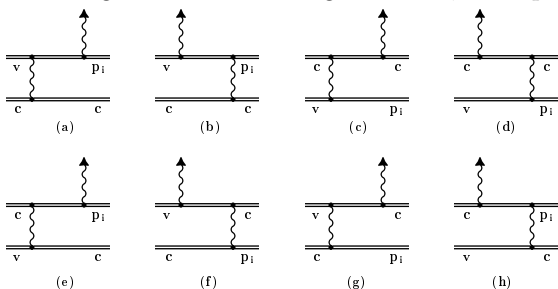


Fig. 1. Feynman diagrams representing the interelectronic-interaction corrections of first order in $1/Z$ to radiative recombination of an electron with a He-like atom. \mathbf{p}_i denotes the incoming electron in the continuum spectrum, \mathbf{v} and \mathbf{c} indicate the valence and the core electrons, respectively. The line terminated by a triangle represents the emitted photon.

Table 1. Zeroth-order total cross section $\sigma^{(0)}$ and the first-order interelectronic-interaction correction in different evaluations, in barns. $\sigma_{\text{zeff}}^{(1)}$ denotes the interelectronic-interaction correction calculated in the effective-nuclear-charge approximation with parameter $Z_{\text{eff}} = 90.3$, $\sigma_{\text{scr}}^{(1)}$ corresponds to the screening-potential approximation, $\sigma_{\text{int}}^{(1)}$ indicates the results of the rigorous relativistic treatment.

E [MeV/u]	$\sigma^{(0)}$	$\sigma_{\text{zeff}}^{(1)}$	$\sigma_{\text{scr}}^{(1)}$	$\sigma_{\text{int}}^{(1)}$
10	504.65	-17.390	-19.635	-21.392
2s _{1/2} 100	41.203	-1.880	-1.393	-2.055
700	2.457	-0.1768	-0.0979	-0.1051
10	656.95	-38.523	-34.978	-35.396
2p _{1/2} 100	33.041	-2.975	-2.535	-3.088
700	1.065	-0.1336	-0.1022	-0.0861
10	854.82	-38.620	-39.671	-40.008
2p _{3/2} 100	31.489	-2.259	-2.275	-2.896
700	0.622	-0.0600	-0.0568	-0.0489

of the photon emission and the operator of the electron-electron interaction are combined in all possible ways. We evaluate these diagrams directly, including the summation over the whole spectrum of the Dirac equation and the full electron-electron interaction that consists of the Coulomb, Breit and retarded parts. The details of the derivation are given in [4]. Here, we present the results of the evaluation.

The numerical results for the interelectronic-interaction correction to the total RR cross section of an electron with He-like uranium are presented in Table 1. The calculation is carried out for projectile energies of 10-700 MeV per nuclear mass unit. The results of the rigorous relativistic treatment are compared with the calculations based on an effective-nuclear-charge approximation and on the screening-potential approximation (for a discussion cf. [5]). The comparison shows a decreasing accuracy of the approximate methods for increasing projectile energy. On average, the screening-potential approximation is found to be more reliable than the effective-nuclear-charge approximation. Its typical deviation from the rigorous treatment is about 10 – 20 % of the interelectronic-interaction correction, i.e., about 1 – 2 % of the cross section of the process. Therefore, fully relativistic calculations are needed to obtain an accuracy better than a few percent of the cross section of the process.

We want to thank Th. Stöhlker for valuable discussions. Financial support by DFG and RFBR is gratefully acknowledged.

- [1] J. Eichler and W. Meyerhof, *Relativistic Atomic Collisions*, Academic Press, San Diego, 1995.
- [2] Th. Stöhlker *et al.*, Phys. Rev. Lett. 82 (1999) 3232.
- [3] Th. Stöhlker *et al.*, Phys. Rev. Lett. 73 (1994) 3520.
- [4] V. A. Yerokhin *et al.*, Phys. Rev. A 62 (2000) 042712.
- [5] V. A. Yerokhin *et al.*, Hyp. Int, in print.

Resonant Transfer and Excitation for H- and He-like U-Ions

Zoltán Harman, Stephan Zakowicz, Matthias Gail, Norbert Grün, Werner Scheid
Institut für Theoretische Physik, Justus-Liebig-Universität Giessen

We present calculations for the angular distribution of photons emitted after KLL-RTE (Resonant Transfer and Excitation) in collisions of U^{91+} - and U^{90+} -ions with hydrogen atoms. Measurements with H-like projectiles were recently performed by Ma et al. at GSI and are currently being evaluated [1]. In the past, a similar process has been studied both experimentally [2] and theoretically [3], in which graphite was used as target. However, the width of the Compton profile of the electron bound in the H-atom is smaller than in graphite, resulting in a better resolution of the resonance groups in the cross sections.

The electron bound in the hydrogen atom can be regarded as quasifree. Therefore, the RTE cross section can be calculated by using the cross section of dielectronic recombination (DR). In DR, a free electron is captured by the projectile with the simultaneous excitation of a bound electron, followed by the emission of a photon. Doubly-excited states embedded in the one electron continuum give rise to resonances in the cross sections. With perturbation theory we obtain the following expression for the differential cross section in the rest frame of the projectile ion:

$$\frac{d\sigma_{i \rightarrow d \rightarrow f}^{DR}}{d\Omega_k} = \frac{2\pi}{F_i} \frac{1}{2(2J_i + 1)} \sum_{M_f \lambda} \sum_{M_d} \sum_{M_i m_s} |\langle \Psi_d; J_d M_d | V_{capt.} | \Psi_i; J_i M_i, p_e m_s \rangle|^2 \times \frac{|\langle \Psi_f; J_f M_f, \mathbf{k} \lambda | H_{er} | \Psi_d; J_d M_d \rangle|^2}{(E - E_d)^2 + \Gamma_d^2/4} \rho_f.$$

This formula makes use of the isolated resonance approximation, in which interference effects between the intermediate states are neglected. The first matrix element describes the resonant capture of the free electron, where the operator $V_{capt.}$ is the sum of the Coulomb- and Breit-interaction operators. The second matrix element describes the radiative transition. The differential cross section can be expressed by means of the total cross section:

$$\frac{d\sigma_{i \rightarrow d \rightarrow f}^{DR}}{d\Omega_k} = \frac{\sigma_{i \rightarrow d \rightarrow f}^{DR}}{4\pi} (1 + \beta P_2(\cos \theta)),$$

where θ denotes the angle of emission of the photon with respect to the direction of the incoming electron. The anisotropy parameter β depends on the matrix elements for resonant capture and on the total angular momenta of the intermediate and final states.

In order to obtain the cross section for RTE in the impulse approximation, the cross section for DR is convoluted with the probability density of the target electron in momentum space:

$$\frac{d^2 \sigma_{RTE}}{d\Omega d\omega} = \int d^3 q' \frac{d\sigma_{DR}(\mathbf{q})}{d\Omega} |\phi_i(\mathbf{q}')|^2 \delta(\omega + E_f - e_i - E_i).$$

Here, $\phi_i(\mathbf{q}')$ denotes the Fourier transform of the wave function of the target electron in the target frame. The δ -function ensures the conservation of energy.

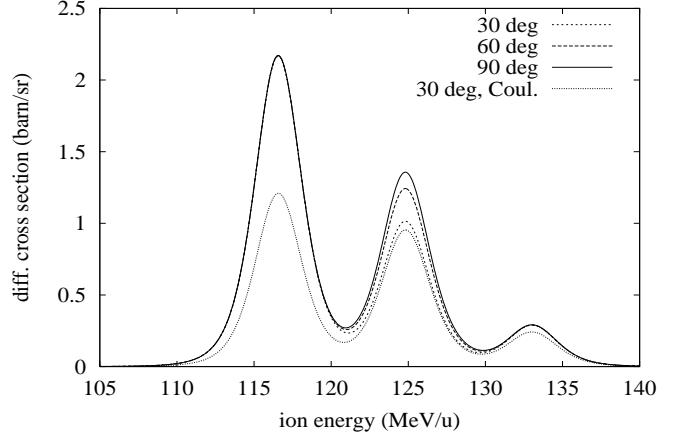


Figure 1: Differential cross sections for KLL-RTE in U^{91+} in the projectile frame at the angles $\theta = 30^\circ$, 60° and 90° .

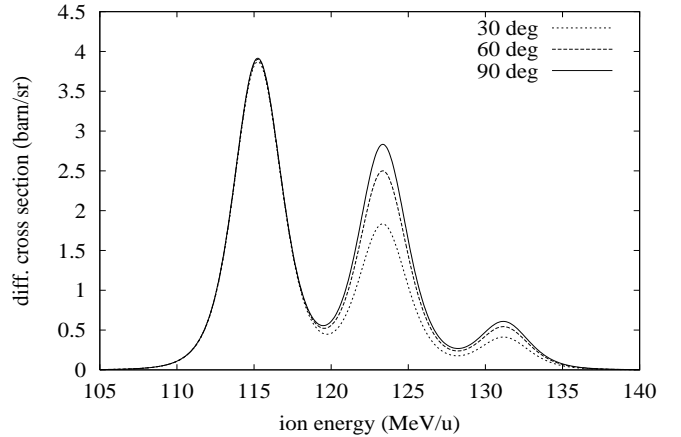


Figure 2: Differential cross sections for KLL-RTE in U^{90+} at the same angles.

Fig. 1 shows differential cross sections in the projectile system at different angles for U^{91+} -ions scattered on hydrogen atoms. The radiation has a strong angular dependence for energies in the range of the $KL_{1/2}L_{3/2}$ resonance group, while it is nearly isotropic for the other two resonance groups $KL_{1/2}L_{1/2}$ and $KL_{3/2}L_{3/2}$. The lowest curve was obtained by neglecting the effects of the Breit interaction.

The case of U^{90+} -ions is shown in Fig. 2. The cross section is anisotropic in the $KL_{1/2}L_{3/2}$ and $KL_{3/2}L_{3/2}$ groups. Also the cross sections are larger than the ones for the H-like projectile ions.

References

- [1] X. Ma et al., this report (2001)
- [2] T. Kandler et al., *Phys. Lett. A* **204** 274 (1995)
- [3] M. Gail et al., *J. Phys. B* **31** 4645 (1998)

Hyperfine Splitting of Hydrogenlike Thallium

M. Tomaselli ^{a,b}, T. Kühl ^b, W. Nörtershäuser ^b, D. Marx ^b, S. Borneis ^b, A. Dax ^b, H. Wang ^b,
and S. Fritzsche ^c

^a University of Darmstadt, ^b GSI Darmstadt, ^c University of Kassel

The investigation of hydrogenlike highly-charged ions is of interest for nuclear as well as for atomic physics. Measuring the ground-state hyperfine structure (HFS) splittings of these ions is a sensitive method to explore QED in extremely strong electric and magnetic fields and nuclear contributions to the electron energy. However, for a theoretical interpretation of the results it is necessary to separate the different contributions. Nuclear models have to provide charge and magnetization distributions of nuclei, which lead to the Breit-Rabi and the Bohr-Weisskopf effect, respectively, and corrections to the electron energy have to be calculated with QED. Interest was first focussed on the isotopes $^{207}\text{Pb}^{81+}$ and $^{205}\text{Bi}^{82+}$, where the theoretical description is simplified since they differ only by one nucleon from doubly-magic ^{208}Pb . The hyperfine structure of these isotopes was measured at GSI with laser spectroscopy at the ESR [1]. More recently, the hyperfine structure of $^{165}\text{Ho}^{66+}$, $^{185}\text{Re}^{74+}$, and $^{187}\text{Re}^{74+}$ was obtained by passive photon-emission spectroscopy in a high-energy electron-beam ion trap (SuperEBIT) at Livermore [2]. Similar experiments are presently under preparation to determine the HFS of thallium isotopes [3].

Previously, we applied the Dynamic Correlation Model (DCM) [4] to the hydrogenlike ions $^{207}\text{Pb}^{81+}$, $^{205}\text{Bi}^{82+}$, $^{165}\text{Ho}^{66+}$, and $^{185,187}\text{Re}^{74+}$ to derive the nuclear part in the HFS and combined the results with QED corrections [5]. The calculated hyperfine splittings are summarized in Table 1 and compared with other theoretical expectations [6, 7, 8] and experimental data. It turned out that the pure DCM results agree well with the experimental data, while adding the QED corrections led to a systematic deviation between theory and experiment. This is in contrast to the good description of nuclear properties by the dynamic correlation model and has motivated the application of the DCM to predict the HFS of the hydrogenlike thallium isotopes $^{203,205,207}\text{Tl}^{80+}$. The results are also included in Table 1. Besides, these calculations may guide future experiments at the GSI storage ring since an accurate *a priori* knowledge of the HFS transition frequency is required to avoid prohibitive large scan ranges.

In the DCM three terms contribute to the HFS: The first term is due to the single-hole magnetization, the second term was introduced in perturbative theory and describes spin-flip excitations [9], and the third term allows for collective correlation effects in the nucleus [5], it corresponds to higher-order perturbation diagrams. Taking these three terms into account the calculations accurately reproduce the experimental HFS. The systematic discrepancy to experimental data, which is observed after adding the QED corrections, might be the result of a double counting effect: The DCM calculations include “de facto” virtual mesons, which can decay into e^+e^- pairs, and these might be considered in radiative corrections as well. Another possibility is that the nuclear correlations, which are not taken into

account in QED calculations, have a distinct influence on the radiative corrections. Hence, the central question is how to compare the DCM terms and the radiative corrections of Refs. [10, 11]. The importance of this problem is evident: In the extreme single-particle model, QED and nuclear-magnetization corrections for high- Z atoms are of the same order of magnitude. Thus, the feasibility of testing the QED corrections depends strongly on the accuracy of the model used to evaluate the nuclear magnetization.

Table 1: Wavelengths of transitions between the ground state HFS components in hydrogenlike ions as calculated in the DCM and after combination with QED corrections taken from [11]. For comparison other theoretical and experimental data is given. All values in nm.

Ion	Theory			Exp.
	DCM	+QED	Other	
$^{165}\text{Ho}^{66+}$	572.71	575.44	572.5 [7] 563.9 [8]	572.79(15)[2]
$^{185}\text{Re}^{74+}$	455.96	458.36	451.0 [7] 448.6 [8]	456.05(30)[2]
$^{187}\text{Re}^{74+}$	451.69	454.06	-	451.69(30)[2]
$^{207}\text{Pb}^{81+}$	1019.1	1024.76	1020.5 [7] 1017.0 [8]	1019.7(2) [1]
$^{209}\text{Bi}^{82+}$	243.91	245.26	243.0 [7] 241.2 [8]	243.87(2) [1]
$^{203}\text{Tl}^{80+}$	385.89	388.01	383.98[6] 384.0 [7] 382.2 [8]	-
$^{205}\text{Tl}^{80+}$	382.79	384.89	380.22[6] 380.2 [7] 378.6 [8]	-
$^{207}\text{Tl}^{80+}$	377.68	379.74	-	-

References

- [1] I. Klaft *et al.*, Phys. Rev. Lett. **73**, 2425 (1993); P. Seelig *et al.*, Phys. Rev. Lett. **81**, 4824 (1998).
- [2] J. R. Crespo Lopez-Urrutia *et al.*, Phys. Rev. Lett. **77**, 826 (1996); Phys. Rev. A **57**, 879 (1998).
- [3] P. Beiersdorfer, private communication (2000).
- [4] M. Tomaselli, Ann. Phys. **205**, 362 (1991).
- [5] M. Tomaselli *et al.*, Phys. Rev. C **51** 2989 (1995); Phys. Rev. C **58**, 1524 (1998).
- [6] M.G.H. Gustavsson *et al.*, Hyperfine Interactions **127**, 437 (2000).
- [7] V.M. Shabaev *et al.*, Phys. Rev. A **56**, 252 (1997).
- [8] V.M. Shabaev, J. Phys. B **27**, 5825 (1994).
- [9] M. LeBellac, Nucl. Phys. **40**, 645 (1963).
- [10] S.M. Schneider *et al.*, Phys. Rev. A **50**, 118 (1994); H. Person *et al.*, Phys. Rev. Lett. **76**, 1433 (1996).
- [11] P. Sunergren *et al.* Phys. Rev. A **58**, 1055 (1998).

Asymptotic energy dependence of projectile inner-shell excitation cross sections in relativistic ion-atom collisions

Dorin Cezar Ionescu^{1,3} and Thomas Stöhlker^{1,2}

¹ Atomic Physics Division, Gesellschaft für Schwerionenforschung, D-64291 Darmstadt

² Institut für Kernphysik, J.W. Goethe Universität Frankfurt, D-60486 Frankfurt am Main

³ Institut für Theoretische Physik, Technische Universität Dresden, D-01062 Dresden

In recent years atomic collisions with ions moving with velocities close to the velocity of light have become experimentally feasible. While in the first place we are interested in a basic understanding of atomic phenomena for their own sake, a precise knowledge of the cross sections for collision processes is needed for certain aspects of the design and operation of accelerators. As an example, Coulomb excitation of electrons which is essential for stopping power investigations, is also an important production process for characteristic projectile photons in ion-atom encounters.

In particular, Coulomb excitation of heavy projectile ions enable the investigation of the influence of relativistic bound state wave functions on the dynamics in relativistic ion-atom collisions. In addition, such studies provide detailed information on the effects associated with the Liénard-Wiechert interaction between the active electron and the target nucleus [1]. Thus, with increasing energy spin-flip mediated transitions were shown to become quite important above roughly 100 MeV/u such that contributions associated with the velocity dependent (magnetic) part of the time dependent interaction are quite relevant. In contrast to ionization where measured total cross sections are available for highly-charged ions up to uranium for more than one decade, it was only recently that detailed experimental data on the K -shell excitation of high- Z projectile ions were reported [1, 2].

In the present investigation we elucidate further details of the mechanisms associated with the Coulomb excitation of high- Z_P projectiles by considering the asymptotic energy dependence of the relevant cross sections. Specifically, we extend our previous results into the extreme relativistic energy domain with energies of hundreds of GeV/u. The numerical calculations are complemented by an analytic representation of the asymptotic energy dependence of cross sections which brings additional insight. The projectile ion is chosen as the origin of the coordinate system such that the target provides the time dependent perturbation mediating the transition.

In Figure 1 we show the energy dependence of reduced cross sections σ/Z_T^2 for exciting a K -shell electron in hydrogen-like gold colliding with an atomic target with charge number Z_T . The cross sections are divided by Z_T^2 which is the scaling behavior in lowest-order perturbation theory. We consider the ($\text{Ly-}\alpha_1$) transition of a $1s_{1/2}$ spin-up electron ($\mu_i = 1/2$) to the $2p_{3/2}$ ($\mu_f = \pm 1/2, \pm 3/2$) states of the projectile ion (Au^{78+}). The upper curve (Σ) is associated with the total $\text{Ly-}\alpha_1$ cross section, the dashed (short-dashed) curve corresponds to the transition with $\Delta\mu = \mu_f - \mu_i = +1$ (spin-flip), and the dotted (dott-dashed) curve is related to $\Delta\mu = +2$ (0).

The present numerical results demonstrate that cross

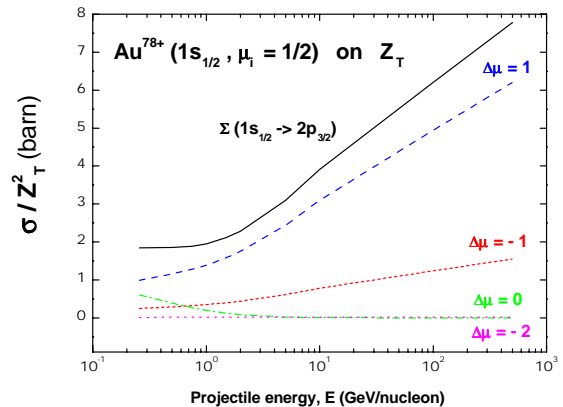


Figure 1: Reduced cross sections σ/Z_T^2 for projectile excitation as functions of the laboratory energy.

sections associated with transitions where the magnetic quantum number changes by one unit ($\Delta\mu = \pm 1$) increase with increasing energy roughly as $\ln E$ in the region above 1 GeV/u. In contrast, the cross sections associated with the other types of transitions ($\Delta\mu = 0, 2$) decrease with increasing collision energy, and approach zero in the asymptotic energy region. Note that the inclusion of screening would lead to different energy dependence [3]. As a result, the cross section for the unscreened $\text{Ly-}\alpha_1$ transition is provided solely by the $\Delta\mu = \pm 1$ transitions for collision energies in the GeV/u region and higher.

An interesting parallel can be made with a computationally simple treatment of the excitation process in the Fermi-Weizsäcker-Williams (FWW) approximation. There the actual electromagnetic field created by the moving ions is approximated by the field associated with a swarm of real photons. In addition, a free parameter which is related to the maximum photon energy is to be fixed (in some sense arbitrary), such that the domain of applicability of the method is often not clear. From Figure 1 one can see that above roughly 3 GeV/u only transitions with $\Delta\mu = \pm 1$ provide a nonzero contribution to the cross section. Thus, the present investigation provides a quantitative measure of the range that can be treated safely in a computationally simple FWW scheme.

References

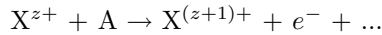
- [1] Th. Stöhlker et al., Phys. Rev. A **57**, 845 (1998); Phys. Lett. A **238**, 43 (1998).
- [2] T. Ludziejewski et al., Phys. Rev. A **61**, 052706-1 (2000).
- [3] A.H. Sorensen, Phys. Rev. A **58**, 2895 (1999).

Stripping of Fast Heavy Low-Charged Ions in Gases

V. Shevelko (GSI and P.N. Lebedev Institute, Moscow),
T. Stöhlker (GSI)

Electron loss and capture processes arising in collisions of heavy low-charged ions with atoms and ions are the main charge-changing reactions in heavy-ion driven inertial fusion (HIDIF) [1]. However, at present time, virtually no experimental and theoretical data are available for removal processes involving fast heavy low-charged ions.

In this work, the projectile-ionization (stripping) cross sections and beam lifetimes in reactions



have been calculated for ions $X = \text{Xe}, \text{Pb}, \text{Bi}, \text{U}$ ($z < 10$) colliding with neutral atoms $A = \text{H}, \text{He}, \text{Be}, \text{C}, \text{F}, \text{N}, \text{Ar}, \text{Xe}$ in the $E = 1 - 100 \text{ MeV/u}$ energy range. Calculations have been performed for *single*-electron stripping in the first-order perturbation theory using the LOSS computer code. The atomic structure of the target was taken into account in the form of its atomic form-factor $F(q)$ depending on the momentum transfer q .

For the case of ionization of Pb-like ions (Xe^{0+} , Bi^{1+} , ..., U^{10+}) and the energy range considered, a scaling law for stripping cross sections was obtained in the form:

$$\tilde{\sigma} = \sigma \cdot (I_P/Z_T)^{1.4}, \quad \tilde{E} = E/I_P, \quad (1)$$

where I_P is the *first* ionization potential of the projectile in eV, E is the beam energy in eV/u, and Z_T denotes the target nuclear charge. The scaled cross sections for Pb-like ions are displayed in Fig. 1 in comparison with available experimental data and other calculations (see [2] in detail); $1 \text{ Ry} = 13.606 \text{ eV}$.

Ion-beam lifetimes τ have been calculated with account for electron capture processes using the CAPTURE computer code. The values of τ are shown in Fig. 2. A small minimum for U^{28+} ions around 2 MeV/u is related to the influence of electron capture which for these ions prevails at energies $E < 10 \text{ MeV/u}$.

A comparison of the present calculations with experimental data [3]–[5], classical-trajectory Monte-Carlo (CTMC) calculations [6] and $Z_T^2 + Z_T$ scaling [7] shows the following peculiarities for the stripping processes of heavy low-charged ions in neutral targets:

1) the contribution from ionization of the projectile inner-shell electrons is very significant, and, in calculations, one has to account for 6–8 inner subshells,

2) at high energies, the stripping cross sections fall off approximately as $\sigma \sim E^{-1}$,

3) multiple-ionization processes seem to play a very important role and, according to [6], their contribution can reach up to 50 % to the total stripping cross section.

References

- [1] I. Hofmann, G. Plass (eds.): *The HIDIF-Study*, Report GSI-98-06, Darmstadt (1998)
- [2] I.Yu. Tolstikhina, V.P. Shevelko, Th. Stöhlker: Preprint GSI-2000-54, Darmstadt (2000)

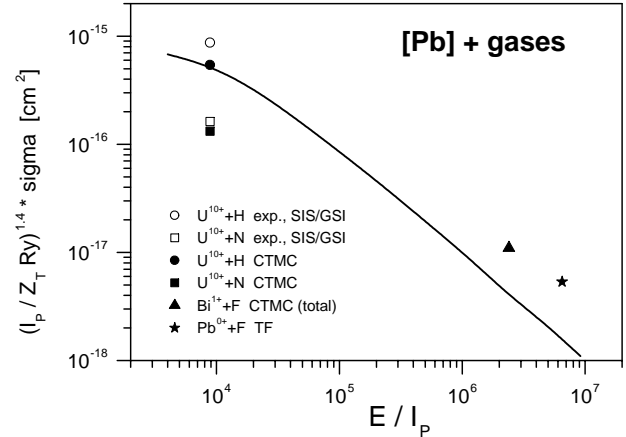


Figure 1: Scaled ionization cross sections of Pb-like ions colliding with neutral atoms, eq. (1). Solid curve – present result, symbols – experimental and theoretical data (see [2] in detail).

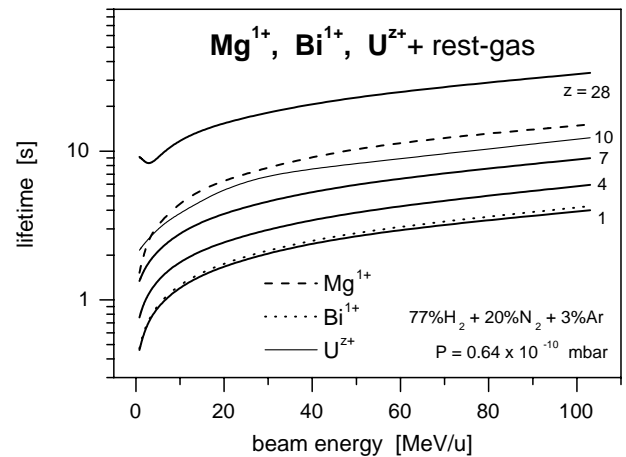


Figure 2: Beam lifetimes of ions colliding with a residual gas mixture and a gas pressure indicated in the figure – present result.

- [3] W. Erb: Report GSI-P-78, Darmstadt (1978)
- [4] B. Franzke: IEEE, NS-28, 2116 (1981)
- [5] K. Blasche et al.: GSI Scientific Report 1996, Darmstadt (1997), p. 159
- [6] R. Olson: Proc. HIF-2000, San Diego (Febr. 2000) (in press)
- [7] V.P. Shevelko et al.: Hyp. Int. **114**, 289 (1998); V.P. Shevelko et al.: NIM A **415**, 609 (1998)